

Copyright
by
Archawin Aroonsri
2014

**The Thesis Committee for Archawin Aroonsri
Certifies that this is the approved version of the following thesis:**

**Nanoparticle-Stabilized CO₂ Foam for Mobility Control
in CO₂ Enhanced Oil Recovery**

**APPROVED BY
SUPERVISING COMMITTEE:**

Supervisor:

Steven L. Bryant

Chun Huh

**Nanoparticle-Stabilized Supercritical CO₂ Foam for Mobility Control
in CO₂ Enhanced Oil Recovery**

by

Archawin Aroonsri, B.E.

Thesis

Presented to the Faculty of the Graduate School of

The University of Texas at Austin

in Partial Fulfillment

of the Requirements

for the Degree of

Master of Science in Engineering

The University of Texas at Austin

August 2014

Acknowledgements

First of all, I am pleased to acknowledge the Fulbright program and Chevron Thailand Exploration and Production, Ltd for granting me a scholarship to pursue my graduate study in the United States of America. My gratitude is extended to The U.S Department of Energy's National Energy Technology Laboratory (DOE-NETL) grant DE-DE0005917 for the full financial support on this research. However, this work would not be possible without the nanoparticles from 3M Company and Nissan Chemical Company.

I would like to offer my sincerest thanks to Professor Steven Bryant, my research supervisor, for his patient guidance and support throughout this research. My best appreciation would also be expressed to Professor Chun Huh., my co-supervisor, for many great advices and his enthusiastic encouragement. I am also thankful to Professor Keith Johnston, Andrew Worthen and Valentina Prigiobbe for their useful inputs and helpful discussions at the weekly group meetings. In addition, I would like to thank Glen Baum, lab supervisor, for helping me solve many problems with lab equipment and Gary Miscoe for providing me cores and transducer calibrations. Special thanks to Sophia Ortiz for her constant and prompt support on many paperwork and procurements.

Lastly, but most importantly, I would like to thank my family for their love, encouragement and unwavering support throughout my study. Additionally, my honest thank goes to all my friends here and at home, especially Pongpak Taksaudom, who has always been a wonderful and caring companion during my time in the US.

Abstract

Nanoparticle-Stabilized Supercritical CO₂ Foam for Mobility Control in CO₂ Enhanced Oil Recovery

Archawin Aroonsri, M.S.E.

The University of Texas at Austin, 2014

Supervisor: Steven L. Bryant

Foam has been used as a mobility control technique in CO₂ flooding to improve volumetric sweep efficiency. Stabilizing CO₂ foam with nanoparticle instead of surfactant has some notable advantages. Nanoparticle-stabilized foam is very stable because a large adsorption energy is required to bring nanoparticles to the bubble interfaces. As a solid, nanoparticle can potentially withstand the high temperature in the reservoir, providing a robust foam stability for an extended period of time. The ability of nanoparticles to generate foam only above a threshold shear rate is promising as foam can be engineered to form only in the high permeability zone. These nanoparticles are hundreds of times smaller than pore throats and thus can travel in the reservoir without plugging the pore throats.

Surface-modified silica nanoparticle was found to stabilize CO₂-in-water foam at temperature up to 80 °C and salinity as high as 7.2 wt%. The foam was generated through the co-injection of aqueous nanoparticle dispersion and CO₂ into consolidated rock cores, primarily sandstones, with and without an induced fracture in the core. A critical shear rate for foam generation was found to exist in both matrix and fracture, however, this critical

rate varied with the experiment conditions. The effects of experimental parameters on the critical shear rate and foam apparent viscosity were also investigated. Additionally, the flow distribution calculation in fractured sandstone cores revealed a diversion of flow from fracture toward matrix once foam was generated, suggesting conformance control potential in fractured reservoirs.

In order to study foam rheology, high-permeability beadpack was installed upstream of the core to serve as a foam generator. This allows the foam mobility to be measured solely while being transported through the core, without the complicating effect of transient foam generation in the core. The injection of the pre-generated foam into the core at residual oil condition was found to reduce the residual oil saturation to the same level as CO₂ flood, however, with the advantage of mobility control. The ‘coalescence-regeneration’ mechanism of foam transport in porous media possibly allowed the foam’s CO₂ to contact and mobilize the residual oil. The injection of the foam slug followed by a slug of only CO₂ was also tested, showing similar viscosification as the continuous foam injection, however, required less nanoparticles.

Table of Contents

List of Tables	xi
List of Figures	xiii
Chapter 1 Introduction	1
Chapter 2 Literature Review	3
2.1 Carbon Dioxide Foam for Enhanced Oil Recovery	3
2.2 Particle-Stabilized Emulsion/Foams	6
2.3 Silica Nanoparticle-Stabilized CO ₂ Foam in Porous Media	9
2.4 Foam generation and propagation in Porous media	11
Chapter 3 Experimental Materials, Equipment and Methods	16
3.1 Materials Used	16
3.1.1 PEG-coated 5 nm Silica Nanoparticles (3M)	16
3.1.2 EOR-5xs Silica Nanoparticles (Nissan Chemical)	16
3.1.3 Surfactant	16
3.1.4 Carbon Dioxide (CO ₂)	17
3.1.5 De-ionized Water (DI water)	17
3.1.6 Sodium Chloride (NaCl)	17
3.1.7 Calcium Chloride (CaCl ₂)	17
3.1.8 Boise Sandstone Cores	17
3.1.9 Berea Sandstone Cores	18
3.1.10 Indiana Limestone Cores	18
3.1.11 Fluorinated Ethylene Propylene (FEP) Shrink Wrap Tubing	19
3.1.12 Decane	19
3.2 Equipment	19
3.2.1 Core Holder	19
3.2.2 Nanoparticle Injection Pump	21
3.2.3 CO ₂ Accumulator and Injection System	21
3.2.4 Beadpack Column	22
3.2.5 Temperature Control Devices – Water Bath and Oven	22

3.2.6 View Cell	22
3.2.7 Waste Accumulator.....	23
3.2.8 Back Pressure Regulator (BPR).....	23
3.2.9 Pressure Transducers and Data Acquisition Module	24
3.2.10 Capillary Tubing	24
3.2.11 Decane Accumulator.....	24
3.2.12 Fluid Sample Collecting System.....	24
3.3 Experiment setup and methods	25
3.3.1 Co-injection Foam Generation Experiments	25
3.3.1.1 Co-injection experiments with liquid CO ₂ (room temperature experiment)	26
3.3.1.2 Co-injection experiments with supercritical CO ₂ (elevated temperature experiment)	37
3.3.2 Pre-generated Foam Coreflood Experiments.....	41
3.3.2.1 Rheology measurement of foam flowing in sandstone matrix using the branching manifold.....	41
3.3.2.2 Oil recovery using nanoparticle-stabilized CO ₂ foam	47
3.4 Data Analysis	55
3.4.1 Matrix Permeability	55
3.4.2 Core Apparent Viscosity.....	55
3.4.3 Mobility Reduction Factor (MRF).....	56
3.4.4 Shear Rate through the Matrix	57
3.4.5 Capillary Tube Apparent Viscosity	57
3.4.6 Shear Rate through the Capillary Tube.....	58
3.4.7 Net Confining Pressure	58
3.4.8 Fracture Permeability and Aperture Size	58
3.4.9 Fracture Shear Rate.....	60
3.4.10 Flow Decoupling Calculation for Fractured Cores.....	61
3.4.11 Oil Saturation Estimation (Weight Difference Method).....	64
3.4.12 Determining Pore Volume (PV) and Porosity of Rock Cores ..	65

Chapter 4 Results and Discussions	66
4.1 Foam Generation experiments by co-injection method	66
4.1.2 Foam Generation Experiments with Liquid CO ₂	75
4.1.2.1 Experiments in very high permeability Boise sandstone cores (~2000 mD)	75
4.1.2.2 Experiments in fractured Boise sandstone cores	84
4.1.2.3 Experiments in fractured and unfractured Berea sandstone cores (~200 mD)	87
4.1.2.4 Experiments in Indiana limestone cores (7 mD).....	93
4.1.3 Foam Generation Experiments with Supercritical CO ₂	96
4.1.3.1 Experiments in very high permeability Boise sandstone cores (~3000 mD)	96
4.1.3.2 Experiments in high permeability Berea sandstone cores (~200 mD).....	113
4.1.4 Discussion on the Influences of the Key Parameters in Foam Generation.....	117
4.1.4.1 Critical shear rate for foam generation and the effect of shear rate.....	117
4.1.4.2 Effect of foam quality (CO ₂ volume fraction)	117
4.1.4.3 Effect of salinity (salt concentration).....	121
4.1.4.4 Effect of temperature	122
4.1.4.5 Effect of matrix permeability.....	123
4.1.4.6 Effect of nanoparticle concentration	124
4.1.4.7 Matrix system versus fracture system.....	124
4.1.4.8 Effect of fracture permeability.....	125
4.2 Pre-generated Foam Coreflood Experiments.....	126
4.2.1 Rheology Measurement of Foam Flowing in Sandstone Matrix Using the Branching Manifold.....	126
4.2.2 Oil Recovery Experiment in Sandstone Cores with Pre-generated Foam.	134
Chapter 5 Conclusions and Recommendations.....	146
5.1 Conclusions.....	146

5.2 Future Work	149
5.2.1 Long-range, Low-shear Foam Transport	149
5.2.2 Synergy Effect Between Nanoparticles and Surfactants	149
5.2.3 Foam Texture Analysis Using Microscope View Cell	150
5.2.4 Supercritical CO ₂ foam in a Fractured Core	150
5.2.5 Foam Rheology Measurement	150
Appendix	151
A. Coreflood Experiments	151
Boise sandstone coreflood BS1 (3230 mD)	151
Boise sandstone coreflood BS2 (2250 mD)	154
Boise sandstone coreflood BS3 (3000 mD)	157
Boise sandstone coreflood BS4 (3360 mD)	159
Berea sandstone coreflood BRS1 (220 mD)	161
Berea sandstone coreflood BRS2 (170 mD)	162
References	163

List of Tables

Table 4-1 Matrix types and petrophysical properties of rock core used in foam generation experiment.....	66
Table 4-2 Summary of foam generation experiment in unfractured matrix core. The entries in first column indicate the core material (B, BS = Boise, BR, BRS =Berea, IL = Indiana limestone), core number and injection stage (total flow rates were varied sequentially in a typical experiment). *Apparent viscosity reported in experiments BR 4/1-2 measured in downstream capillary viscometer. ** Experiment BS 2/11-17 contain 0.04 wt% LAPB surfactant in the aqueous phase.....	67
Table 4-3 Summary of view cells observation of foam experiment in Boise sandstone core B4, B5 and B6.....	79
Table 4-4 Properties of fractured Boise sandstone core F1 and F2 (Hariz, 2012).	84
Table 4-5 Decoupling flow in matrix from flow in fracture of core F1. The number in bold indicate the condition where the critical shear rate (either in matrix or fracture) was exceeded.	86
Table 4-6 Decoupling flow in matrix from flow in fracture of core F2. The number in bold indicate the condition where the critical shear rate (either in matrix or fracture) was exceeded.	87
Table 4-7 Summary of view cell observation during supercritical CO ₂ foam experiment in Boise sandstone core at foam quality of 0.57 and 0.75. These experiments were carried out at 2000 psi and 50 °C, using 1 wt% EOR-5xs nanoparticle dispersion in 2 wt% NaCl brine. The black belts observed at the low shear rates were the reflection from CO ₂ -water interface.	100

Table 4-8 Summary of view cell observation during supercritical CO ₂ foam experiment in Boise sandstone core at foam quality of 0.5. These experiments were carried out at 2200 psi and 80 °C, using several type of aqueous phase recipe.....	102
Table 4-9 Summary of view cell observation during supercritical CO ₂ foam experiment in Boise sandstone core at foam quality of 0.5. These experiments were carried out at 2200 psi and 80 °C, using 0.04 wt% LAPB in 4 wt% NaCl with and without nanoparticle.....	103
Table 4-10 Summary of view cell observation of foam generation experiment at various particle concentration.....	112
Table 4-11 Summary of view cell observation during supercritical CO ₂ foam experiment in Berea sandstone core at 2200 psi, however at different temperature and salinity. The view cell was being filled from the side in the top row, instead was filled from the top in the second row.	116
Table 4-12 Summary of coreflood results in Boise sandstone core (820 mD) at residual oil saturation. Experiment were conducted at 2000 psia and room temperature (23 °C). Use EOR-5xs nanoparticle (Nissan Chemical), constant injection rate at 6 ml/min, giving flow velocity $u = 56$ ft/day.	138
Table 4-13 Summary of coreflood results in decane-saturated Boise sandstone core (3200 mD). Experiment were conducted at 2000 psia and room temperature (23 °C). Use EOR-5xs nanoparticle (Nissan Chemical) and a constant injection rate at 6 ml/min, giving flow velocity $u = 56$ ft/day.	144

List of Figures

Figure 2-1 Displacement front for different mobility ratios and injected pore volumes until breakthrough. Quarter of a five-spot (Habermann, 1960).	4
Figure 2-2 Surfactant concentration decreases gas relative permeability in sandstone core greatly but does not change brine relative permeability. (Friedmann et al. 1991)	5
Figure 2-3 Effect of particles wettability and contact angle on the structure of the foam. (Adapted from Binks (2002) according to Johnston and da Rocha (2009))	8
Figure 2-4 Schematic showing (A) no-foam (B) continuous-gas foam and (C) discontinuous-gas foam (Lee and Kam, 2013).	12
Figure 2-5 Schematic showing lamellae creation by leave-behind. (Rossen, 1995)	14
Figure 2-6 Schematic showing snap-off in a pore throat. (Rossen, 1995).....	14
Figure 2-7 Schematic of lamellae division. (Rossen, 1995).	14
Figure 3-1 Equipment setup for co-injection foam generation experiment	20
Figure 3-2 Schematic of core vacuum system	28
Figure 3-3 Schematic of core holder confining fluid system.....	30
Figure 3-4 A schematic of the CO ₂ accumulator and recharging system	36
Figure 3-5 CO ₂ density versus temperature at some specific operating pressure. Water density at 2200 psia (blue dots) was also plotted for comparison (all data from NIST, 2011).....	37
Figure 3-6 CO ₂ viscosity versus temperature at some specific operating pressure. Water density at 2200 psia (blue dots) was also plotted for comparison (all data from NIST, 2011).....	38

Figure 3-7 CO₂ – water interfacial tension versus temperature at 1741 psi and 2525 psia. The dash lines show the effect of salt concentration on interfacial tension (Bachu and Bennion, 2008).....38

Figure 3-8 Schematic of modified co-injection system with beadpack foam generator and the branching system.....43

Figure 3-9 A schematic of modified coreflood system for decane injection (drainage) and waterflooding (imbibition).....50

Figure 3-10 A schematic of modified co-injection system for enhanced oil recovery experiment.....54

Figure 3-11 A schematic of fractured core cross-section showing fracture width (W) and height (H).....59

Figure 3-12 Relationship between core apparent viscosity and matrix shear rate, determined from unfractured Boise sandstone coreflood data at 23 °C and 2000 psi (Hariz, 2012). Foam was generated through co-injection of 1 wt% 5 nm PEG-coated nanoparticle dispersion in DI water and CO₂ at the phase ratio of 1:1. The correlation was established for core apparent viscosity above the critical shear rate for foam generation of 460 s⁻¹.62

Figure 4-1 Apparent viscosity measured across core B4 in the baseline experiment (DI water + CO₂) plotted against pore volumes injected. The experiment was performed at 2000 psia and 23 °C, using volumetric phase ratio of 1:1.76

Figure 4-2 Apparent viscosity measured across core B4 in foam experiment (1wt% 3M PEG-coated nanoparticle in DI water + CO₂) plotted against pore volumes injected. The experiment was performed at 2000 psia and 23 °C, using volumetric phase ratio of 1:1 (foam quality of 0.5). Core MRF were calculated based on baseline apparent viscosity of 1.69 cP.....77

Figure 4-3 Core MRF versus core shear rate measured in core B4 (purple dots, this work), plotted in comparison with the experiment data from Hariz (2012). Open symbols indicate no foam visible in view cell; filled symbols indicate visible foam. All experiments performed at 2000 psia and 23 °C, using 1 wt% 3M PEG-coated nanoparticle in DI water and foam quality of 0.5.78

Figure 4-4 plot of core MRF vs. core shear rate, showing influence of foam quality Q and salinity on foam generation. Open symbols indicate no foam visible in view cell; filled symbols indicate visible foam. All experiments performed at 2000 psia and 23 °C, using 1 wt% 3M PEG-coated nanoparticle dispersion. Salinity and foam quality were varied.78

Figure 4-5 Apparent viscosity measured across the Boise core B5 and 3 intermediate sections (through pressure taps) in the baseline experiment (2 wt% NaCl brine + CO₂). The experiment was performed at 2000 psia and 23 °C, using volumetric phase ratio of 2:1.....82

Figure 4-6 Apparent viscosity measured across the Boise core B5 and 3 intermediate sections (through pressure taps) in foam experiment (1wt% 3M PEG-coated nanoparticle in 2 wt% NaCl brine + CO₂). The experiment was performed at 2000 psia and 23 °C, using volumetric phase ratio of 2:1. (foam quality of 0.67)83

Figure 4-7 Apparent viscosity measured across the Boise core B6 and 3 intermediate sections (through pressure taps) in foam experiment (1wt% 3M PEG-coated nanoparticle in 2 wt% NaCl brine + CO₂). The experiment was performed at 2000 psia and 23 °C, using volumetric phase ratio of 4:1. (foam quality of 0.8)83

Figure 4-8 Core apparent viscosity vs. fracture shear rate from the two foam experiments in fractured Boise sandstone coreflood under the same experiment condition. Fracture apertures for cores F1 and F2 were 104 microns and 65 microns, respectively. Dash lines are core-average value (combined matrix and fracture flow). The solid lines show the estimated shear rate and viscosity in the fracture.....86

Figure 4-9 Apparent viscosity measured across core Berea 3 and its intermediate sections (through pressure taps) in foam experiment (1wt% 3M PEG-coated nanoparticle in 2 wt% NaCl brine + CO₂). The experiment was performed at 2000 psia and 23 °C, using volumetric phase ratio of 1:1.88

Figure 4-10 Apparent viscosity measured in the capillary tube downstream of an unfractured Berea sandstone. 1 wt% PEG-coated silica in 2 wt% NaCl brine and CO₂ were co-injected using phase ratio of 1:1 at 2000 psia and 23 °C. The foam generation threshold falls between shear rates of 244 s⁻¹ and 366 s⁻¹.....90

Figure 4-11 Apparent viscosity vs. fracture shear rate obtained from a fractured Berea sandstone coreflood. Fracture gap size was 165 microns. 1 wt% PEG-coated silica in 2 wt% NaCl brine and CO₂ were co-injected using phase ratio of 1:1 at 2000 psia and 23 °C. Critical shear rate was estimated to be 3400 s⁻¹. Open symbols indicate no foam visible in view cell; filled symbols indicate visible foam.....91

Figure 4-12 Apparent viscosity measured across fractured Berea core (B2F) and its intermediate sections (through pressure taps) in the baseline experiment (2 wt% NaCl brine + CO₂). The experiment was performed at 2000 psia and 23 °C, using volumetric phase ratio of 1:1. Pressure drops in the upstream, middle and downstream sections were smaller than measuring range, thus cannot be observed.92

Figure 4-13 Apparent viscosity measured across fractured Berea core (B2F) and its intermediate sections (through pressure taps) in foam experiment (1wt% 3M PEG-coated nanoparticle in 2 wt% NaCl brine + CO₂). The experiment was performed at 2000 psia and 23 °C, using volumetric phase ratio of 1:1.....92

Figure 4-14 Apparent viscosity measured across Indiana limestone core (IL1) in foam experiment (1 wt% 3M PEG-coated nanoparticle in 2 wt% NaCl brine + CO₂). The experiment was performed at 1500 psia and 23 °C, using volumetric phase ratio of 1:1 (foam quality of 0.5).94

Figure 4-15 Core apparent viscosity versus core shear rate measured in Indiana limestone core. The experiment was performed at 1500 psia and 23 °C, using 1wt% 3M PEG-coated nanoparticle in DI water and foam quality of 0.5.....95

Figure 4-16 Apparent viscosity measured across Boise sandstone core vs. shear rate in foam experiment at 50 °C and 2000 psia. The experiment was performed using 1 wt% EOR-5xs nanoparticle in 2 wt% NaCl brine at foam quality of 0.57. Open symbols indicate no foam visible in view cell; filled symbols indicate visible foam. Baseline apparent viscosity was also plotted in black as a reference.....97

Figure 4-17 Apparent viscosity measured across Boise sandstone core vs. shear rate in foam experiment at 50 °C and 2000 psia. The experiment was performed using 1wt% EOR-5xs nanoparticle in 2 wt% NaCl brine at foam quality of 0.75. Open symbols indicate no foam visible in view cell; filled symbols indicate visible foam. Baseline apparent viscosity was also plotted in black as a reference.....98

Figure 4-18 Pressure drop measured across Boise sandstone core vs. shear rate in foam experiment at 80 °C and 2000 psia. The experiment was performed using 1 wt% EOR-5xs nanoparticle in 2 wt% NaCl brine at foam quality of 0.75. Open symbols indicate no foam visible in view cell; filled symbols indicate visible foam. Baseline apparent viscosity was also plotted in black as a reference.....99

Figure 4-19 Core apparent viscosity measured across Boise sandstone core vs. shear rate in foam experiment at 80 °C and 2200 psia. The experiment was performed using 5 different mixes of the aqueous phase at foam quality of 0.5. Open symbols indicate no foam visible in view cell; filled symbols indicate visible foam. Baseline apparent viscosity was also plotted in black as a reference.....101

Figure 4-20 Core apparent viscosity measured across Boise sandstone core vs. shear rate in foam experiment at 80 °C and 2200 psia. The experiment was performed using the dispersion of 1wt% EOR-5xs nanoparticle in 1 wt%, 2 wt% and 4 wt% NaCl brine with foam quality of 0.5. Baseline apparent viscosity was also plotted in black as a reference. Open symbols indicate no foam visible in view cell; filled symbols indicate visible foam.107

Figure 4-21 Core apparent viscosity measured across Boise sandstone core vs. shear rate in foam experiment at 57 °C and 2200 psia. The experiment was performed using the dispersion of EOR-5xs nanoparticle at 0.1, 0.5 and 1wt% in 7.2 wt% TDS brine with foam quality of 0.75. Baseline apparent viscosity was also plotted in black as a reference. Open symbols indicate no foam visible in view cell; filled symbols indicate visible foam.108

Figure 4-22 Apparent viscosity measured across Boise sandstone core and its intermediate sections in foam experiment (1 wt% EOR-5xs nanoparticle in 7.2 wt% TDS brine + CO₂). The experiment was performed at 2200 psia and 57 °C, using volumetric phase ratio of 3:1 (foam quality of 0.75). Shear thinning observed in the middle section.110

Figure 4-23 Core apparent viscosity measured across Berea sandstone core vs. shear rate in foam experiment at 80 °C and 2200 psia. The experiment was performed using 1 wt% EOR-5xs nanoparticle in 4 wt% NaCl brine at foam quality of 0.5. Open symbols indicate no foam visible in view cell; filled symbols indicate visible foam. Baseline apparent viscosity was also plotted in black as a reference.....113

Figure 4-24 Core apparent viscosity measured across Berea sandstone core vs. shear rate in foam experiment at 57 °C and 2200 psia. The experiment was performed using 1wt% EOR-5xs nanoparticle in 7.2 wt% TDS brine at foam quality of 0.75. Open symbols indicate no foam visible in view cell; filled symbols indicate visible foam. Baseline apparent viscosity was also plotted in black as a reference.....114

Figure 4-25 Core apparent viscosity measured across Boise sandstone core vs. foam quality, showing an optimum point around the quality of 0.5. The experiment was performed at 2000 psia using 1 wt% EOR-5xs nanoparticle in 2 wt% NaCl brine. Temperature were at 23 °C (blue) and 50 °C (red). The total injection rate was 10 ml/min (490 s⁻¹ in term of shear rate).120

Figure 4-26 Core apparent viscosity measured across Boise sandstone core vs. foam quality, showing an optimum point around the quality of 0.5. The experiment was performed at 80 °C and 2200 psia using 1 wt% EOR-5xs nanoparticle in 4 wt% NaCl brine. The total injection rate was 10 ml/min (490 s⁻¹ in term of shear rate).120

Figure 4-27 Core apparent viscosity measured across Berea sandstone core vs. foam quality, showing an optimum point around the quality of 0.5. The experiment was performed at 80 °C and 2200 psia using 1 wt% EOR-5xs nanoparticle in 4 wt% NaCl brine. The total injection rate was 6 ml/min (1190 s⁻¹ in term of shear rate).121

Figure 4-28 Pressure drop measured across the core and each intermediate sections of the baseline experiment in Boise sandstone (860 mD) core with the branching manifold (4 wt% NaCl brine + CO₂). The experiment was performed at 2000 psia and 23 °C, using foam quality of 0.75 (3:1). The injection rate was fixed at 20 ml/min, giving flow velocity $u = 187$ ft/day.

.....129

Figure 4-29 Pressure drop measured across the core and each intermediate sections of the pre-generated foam experiment in Boise sandstone core (860 mD) with the branching manifold (1 wt% EOR-5xs nanoparticle in 4 wt% NaCl + CO₂). The experiment was performed at 2000 psia and 23 °C, using foam quality of 0.75 (3:1). The injection rate was fixed at 20 ml/min, giving flow velocity $u = 187$ ft/day.....129

Figure 4-30 Apparent viscosity measured across each intermediate sections of the pre-generated foam experiment in Boise sandstone core (860 mD) at brine saturated condition (taken from the first portion of experiment result shown Figure 4-29, using (1 wt% EOR-5xs nanoparticle dispersion in 4 wt% NaCl brine). The experiment was performed at 2000 psia and 23 °C, using foam quality of 0.75 (3:1). The injection rate was fixed at 20 ml/min, giving flow velocity $u = 187$ ft/day.....130

Figure 4-31 Apparent viscosity measured across the core and each intermediate sections of co-injection experiment in Boise sandstone core (440 mD) using 1wt% EOR-5xs nanoparticle dispersion in 4 wt% NaCl brine. The experiment was performed at 2000 psia and 23 °C, using foam quality of 0.75 (3:1). The injection rate was fixed at 20 ml/min, giving flow velocity $u = 187$ ft/day.....132

Figure 4-32 Apparent viscosity measured across the core and each intermediate sections of pre-generated foam experiment in Boise sandstone core (440 mD) using 1wt% EOR-5xs nanoparticle dispersion in 4 wt% NaCl brine). The experiment was performed at 2000 psia and 23 °C, using foam quality of 0.75 (3:1). The injection rate was fixed at 20 ml/min, giving flow velocity $u = 187$ ft/day.....133

Figure 4-33 Apparent viscosity measured across each intermediate sections of the pre-generated foam experiment in Boise sandstone core at residual oil condition (1wt% EOR-5xs nanoparticle in 4 wt% NaCl + CO₂). Estimated decane saturation prior to foam injection was 30% (S_{or} to brine). The experiment was performed at 2000 psia and 23 °C, using foam quality of 0.75 (3:1). The injection rate was fixed at 20 ml/min, giving flow velocity $u = 187$ ft/day.....136

Figure 4-34 Apparent viscosity measured across each intermediate sections of the baseline experiment in Boise sandstone core at residual oil condition (4 wt% NaCl brine + CO₂). Estimated decane saturation prior to foam injection was 30% (S_{or} to brine). The experiment was performed at 2000 psia and 23 °C, using foam quality of 0.75 (3:1). The injection rate was fixed at 20 ml/min, giving flow velocity $u = 187$ ft/day.....137

Figure 4-35 Apparent viscosity measured across the core of the pre-generated foam experiment in Boise sandstone core at residual oil condition for four types of injection fluid(s): continuous foam flood, continuous CO₂ flood, continuous CO₂/brine flood and foam slug. These experiments were performed at 2000 psia, 23 °C and fixed total injection rate of 6 ml/min, giving flow velocity $u = 56$ ft/day.....138

Figure 4-36 View cell snapshots from continuous foam flood experiment, showing:
Initial condition filled with brine (A), oil bank arrival (B), continuous oil
flow (C, black arrow indicated the interface), foam breakthrough about
0.25 PVs after oil bank arrival (D) and the continuous foam flow where
steady state apparent viscosity was measured (E).140

Figure 4-37 View cell snapshots from foam slug injection experiment (case #4),
showing: flowing of decane-CO₂ bank in view cell (A), best visual
observation of foam after oil bank. (B, black arrow indicated bulk foam
at the view cell inlet) and continuous CO₂ flow period where steady state
apparent viscosity was measured (C).....142

Figure 4-38 Apparent viscosity measured across the core of pre-generated foam
experiment in decane-saturated Boise sandstone core. Three types of
injection experimented: continuous foam flood, CO₂ flood and CO₂/brine
flood. These experiment was performed at 2000 psia, 23 °C and fixed total
injection rate of 6 ml/min, giving flow velocity $u = 56$ ft/day. Decane
density at this experiment condition was 1.02 cP (data from NIST, 2011).
.....144

Figure A-1 Baseline apparent viscosity measured across the core BS1 versus pore
volume injected. The experiment was carried out using 2 wt% NaCl brine
and CO₂ at 2000 psi and 50 °C. Foam quality was fixed at 0.57. ...151

Figure A-2 Foam apparent viscosity measured across the core BS1 versus pore volume
injected. The experiment was carried out using 1 wt% EOR-5xs
nanoparticle dispersion in 2 wt% NaCl brine and CO₂ at 2000 psi and 50
°C. Foam quality was fixed at 0.57.151

Figure A-3 Baseline apparent viscosity measured across the core BS1 versus pore volume injected. The experiment was carried out using 2 wt% NaCl brine and CO₂ at 2000 psi and 50 °C. Foam quality was fixed at 0.75. ...152

Figure A-4 Foam apparent viscosity measured across the core BS1 versus pore volume injected. The experiment was carried out using 1 wt% EOR-5xs nanoparticle dispersion in 2 wt% NaCl brine and CO₂ at 2000 psi and 50 °C. Foam quality was fixed at 0.75.152

Figure A-5 Baseline apparent viscosity measured across the core BS1 versus pore volume injected. The experiment was carried out using 2 wt% NaCl brine and CO₂ at 2000 psi and 80 °C. Foam quality was fixed at 0.75. ...153

Figure A-6 Foam apparent viscosity measured across the core BS1 versus pore volume injected. The experiment was carried out using 1 wt% EOR-5xs nanoparticle dispersion in 2 wt% NaCl brine and CO₂ at 2000 psi and 80 °C. Foam quality was fixed at 0.75.153

Figure A-7 Baseline apparent viscosity measured across the core BS2 versus pore volume injected. The experiment was carried out using 2 wt% NaCl brine and CO₂ at 2200 psi and 80 °C. Foam quality was fixed at 0.5.154

Figure A-8 Foam apparent viscosity measured across the core BS2 versus pore volume injected. The experiment was carried out using 1 wt% EOR-5xs nanoparticle dispersion in 2 wt% NaCl brine and CO₂ at 2200 psi and 80 °C. Foam quality was fixed at 0.5.154

Figure A-9 Foam apparent viscosity measured across the core BS2 versus pore volume injected. The experiment was carried out using 5 wt% EOR-5xs nanoparticle dispersion in 2 wt% NaCl brine and CO₂ at 2200 psi and 80 °C. Foam quality was fixed at 0.5.155

Figure A-10 Foam apparent viscosity measured across the core BS2 versus pore volume injected. The experiment was carried out using 1 wt% EOR-5xs nanoparticle dispersion in 4 wt% NaCl brine and CO₂ at 2200 psi and 80 °C. Foam quality was fixed at 0.5.155

Figure A-11 Foam apparent viscosity measured across the core BS2 versus pore volume injected. The experiment was carried out using 1 wt% EOR-5xs nanoparticle dispersion + 0.04% LAPB surfactant in 4 wt% NaCl brine and CO₂ at 2200 psi and 80 °C. Foam quality was fixed at 0.5.156

Figure A-12 Foam apparent viscosity measured across the core BS2 versus pore volume injected. The experiment was carried out using 0.04% LAPB surfactant solution in 4 wt% NaCl brine and CO₂ at 2200 psi and 80 °C. Foam quality was fixed at 0.5. Experiment was ceased after 8 PV due to the plugging of view cell inlet line.156

Figure A-13 Baseline apparent viscosity measured across the core BS3 versus pore volume injected. The experiment was carried out using 2 wt% NaCl brine and CO₂ at 2200 psi and 80 °C. Foam quality was fixed at 0.5.157

Figure A-14 Foam apparent viscosity measured across the core BS2 versus pore volume injected. The experiment was carried out using 1 wt% EOR-5xs nanoparticle dispersion in 2 wt% NaCl brine and CO₂ at 2200 psi and 80 °C. Foam quality was fixed at 0.5.157

Figure A-15 Foam apparent viscosity measured across the core BS2 versus pore volume injected. The experiment was carried out using 1 wt% EOR-5xs nanoparticle dispersion in 3 wt% NaCl brine and CO₂ at 2200 psi and 80 °C. Foam quality was fixed at 0.5.158

Figure A-16 Foam apparent viscosity measured across the core BS2 versus pore volume injected. The experiment was carried out using 1 wt% EOR-5xs nanoparticle dispersion in 4 wt% NaCl brine and CO₂ at 2200 psi and 80 °C. Foam quality was fixed at 0.5.158

Figure A-17 Baseline apparent viscosity measured across the core BS4 versus pore volume injected. The experiment was carried out using 7.2 wt% TDS brine and CO₂ at 2200 psi and 57 °C. Foam quality was fixed at 0.75.159

Figure A-18 Foam apparent viscosity measured across the core BS4 versus pore volume injected. The experiment was carried out using 0.1 wt% EOR-5xs nanoparticle dispersion in 7.2 wt% TDS brine and CO₂ at 2200 psi and 57 °C. Foam quality was fixed at 0.75.159

Figure A-19 Foam apparent viscosity measured across the core BS4 versus pore volume injected. The experiment was carried out using 0.5 wt% EOR-5xs nanoparticle dispersion in 7.2 wt% TDS brine and CO₂ at 2200 psi and 57 °C. Foam quality was fixed at 0.75.160

Figure A-20 Foam apparent viscosity measured across the core BS4 versus pore volume injected. The experiment was carried out using 1 wt% EOR-5xs nanoparticle dispersion in 7.2 wt% TDS brine and CO₂ at 2200 psi and 57 °C. Foam quality was fixed at 0.75.160

Figure A-21 Baseline apparent viscosity measured across the core BRS1 versus pore volume injected. The experiment was carried out using 4 wt% NaCl brine and CO₂ at 2200 psi and 80 °C. Foam quality was fixed at 0.5.161

Figure A-22 Foam apparent viscosity measured across the core BRS1 versus pore volume injected. The experiment was carried out using 1 wt% EOR-5xs nanoparticle dispersion in 4 wt% NaCl brine and CO₂ at 2200 psi and 80 °C. Foam quality was fixed at 0.5.161

Figure A-23 Baseline apparent viscosity measured across the core BRS2 versus pore volume injected. The experiment was carried out using 7.2 wt% TDS brine and CO₂ at 2200 psi and 57 °C. Foam quality was fixed at 0.75.162

Figure A-24 Foam apparent viscosity measured across the core BRS2 versus pore volume injected. The experiment was carried out using 0.5 wt% EOR-5xs nanoparticle dispersion in 7.2 wt% TDS brine and CO₂ at 2200 psi and 57 °C. Foam quality was fixed at 0.75.162

Chapter 1 Introduction

For decades, foam has been a well-established mobility control concept in enhanced oil recovery (EOR) processes, primarily for the injection of CO₂ into the reservoir. Miscible CO₂ EOR can be very effective in the reservoir zones where CO₂ is able to contact the residual oil. However, the actual oil recovery from CO₂ flooding is usually lower than expected due to poor sweep efficiency. Large hydrocarbon zones were most of the time left behind due to the channeling of high mobility CO₂ in the reservoir. In addition to poor sweep efficiency, CO₂ channeling also poses an operational problem as the amount of CO₂ recycling drastically increases after early CO₂ breakthrough. The presence of foam in the reservoir decreases the mobility of CO₂ phase, creating a more uniform displacement front and mitigating CO₂ channeling problem.

Conventional foam, as widely used in the oil industry, is generated and stabilized with surfactants, the amphiphilic molecules that have an affinity both to CO₂ and water. These surfactants, while very effective as foaming agents even at very low concentration, lacks the capability to provide long-term foam stability when the reservoir temperature or salinity is high. The recent advances in nanotechnology revealed the ability of nanoparticles in stabilizing emulsions and foam with outstanding stability. Surface-modified silica nanoparticle was found to be able to stabilize CO₂-in-water foam (Espinosa 2010, Hariz 2012, Worthen 2012, 2013a) which promises a great potential for long-term extended-range mobility control in CO₂ EOR process. Although the behavior of foam in porous media was studied extensively, only limited study has been carried out on the behavior of nanoparticle-stabilized CO₂ foam in porous media. Therefore, this research sought to investigate the stability and transport of silica nanoparticle-stabilized CO₂ foam

in porous media, especially with supercritical CO₂ at high-temperature high-pressure conditions.

As the main focus was the development of nanoparticle-stabilized CO₂ foam for improved mobility control in CO₂ EOR process, the following objectives were pursued step-by-step with a series of experiments. First of all, this research aimed to test the ability of surfaced modified silica nanoparticle in stabilizing CO₂-in-water foam and the feasibility of in-situ foam generation in the consolidated rock. As explained in the Chapter 2, previous foam generation studies with nanoparticles were mostly performed in unconsolidated porous media. In this work, foam generation was studied in several types of the rock matrix, primarily sandstones, at various conditions that would be encountered in actual reservoirs. Second, the effects of key parameters on foam generation and rheology were also investigated. Several sensitivity studies were performed to quantify the effects of salinity, foam quality, critical shear rate for foam generation, etc. Third the in-situ rheology of nanoparticle stabilized foam flowing in the rock core was characterized. The apparent viscosity of the foam was measured at various matrix shear rates as it is the key to successful mobility control process. Last but not least, this work investigated the ability of nanoparticle-stabilized CO₂ foam in reducing residual oil saturation. Additionally, the stability and mobility of foam in the presence of the hydrocarbon phase, both mobile and immobile, was investigated.

The second chapter provided the background for this research and reviewed the past research on the subject to serve as a foundation for this thesis. The third chapter described the materials and methods used in conducting experiments. The results from the experiments were discussed in Chapter 4. The final chapter provided conclusions from the experiments as well as the recommendations for future works.

Chapter 2 Literature Review

2.1 CARBON DIOXIDE FOAM FOR ENHANCED OIL RECOVERY

For over 40 years, carbon dioxide (CO₂) flooding has been widely used as an enhance oil recovery (EOR) technique, producing around 280,000 barrels per day or about 5% of total US oil production in 2012 (Enick and Olsen, 2012). Recently, CO₂ EOR has become even more attractive and were likely to expand in the upcoming years due to high crude oil price and also as a way of utilizing the CO₂ available through advance in carbon capture and storage (CCS) technology (Enick et al., 2012). Although CO₂ flooding is proven to be domestically successful, improving its recovery efficiency is yet a challenge. One of the key problems is a poor sweep efficiency due to unfavorable (high) mobility ratio between CO₂ and water. The problem is even more prominent with the presence of natural fractures in the reservoir, providing high permeability conduits for CO₂ to bypass low permeability oil-bearing zones. Premature CO₂ breakthrough results in unnecessary cycling of CO₂.

Since making the mobility ratio more favorable has been the main objective of the earlier research and so is for this thesis research, the mobility ratio is first defined below. Mobility ratio (M) is the ratio between mobility of the displacing and the displaced fluid, defined as

$$M = \frac{\lambda_{Displacing\ fluid}}{\lambda_{Displaced\ fluid}} = \frac{\lambda_{CO_2}}{\lambda_{oil}} = \frac{k_r\ CO_2 / \mu_{CO_2}}{k_r\ oil / \mu_{oil}}$$

where λ is the mobility, k_r is the relative permeability and μ is the viscosity. At reservoir condition, CO₂ viscosity (~0.05 - 0.10 cP) is considerably lower than oil and brine viscosity, resulting in an unfavorable mobility ratio, i.e., much greater than 1. Reducing CO₂ mobility would lower the mobility ratio and improve sweep efficiency. The severity

of channeling would be less which help delay the CO₂ breakthrough as illustrated in Figure 2-1.

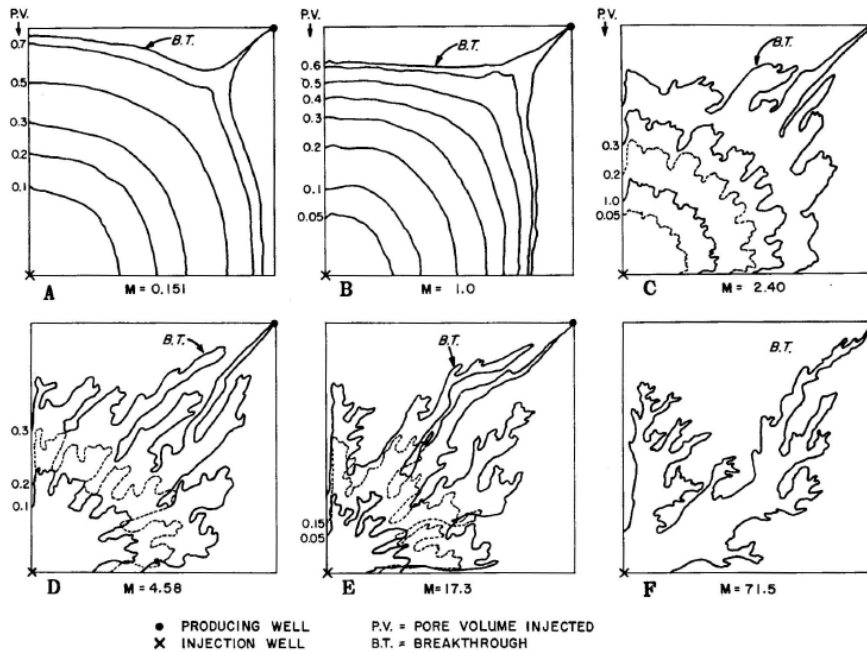


Figure 2-1 Displacement front for different mobility ratios and injected pore volumes until breakthrough. Quarter of a five-spot (Habermann, 1960).

To date, there have been many efforts to address CO₂ flood mobility control and conformance control problem. According to a review by Enick and Olsen (2012), CO₂ mobility control technique includes direct CO₂ thickening, water-alternating-gas (WAG) and CO₂ foam. Direct CO₂ thickening is a method to make CO₂ more viscous for which polymers or other viscosifying agents are mixed with CO₂. This technology, however, is still limited as it is not economically feasible. WAG is the most common and preferred mobility control method that has been used in the field for decades. Instead of increasing CO₂ viscosity, alternating injection of CO₂ and brine reduces the CO₂ saturation, causing

a reduction of CO₂ relative permeability (Bennion and Bachu, 2005). The use of CO₂ foam¹ was claimed to improve vertical sweep greatly, even more effectively than WAG (Li et al., 2010). Mobility control with CO₂ foam is through two mechanisms. First, the effective viscosity of CO₂ phase is increased drastically from the low viscosity of the CO₂ gas. While flowing through porous media, the presence of foam lamellae (thin liquid film separating CO₂ droplets) increases the drag force on the CO₂, creating significant resistance to flow. This additional resistance is accounted as an increase in apparent viscosity of the gas phase (Hirasaki and Lawson, 1985). Second, CO₂ foam reduces the CO₂ relative permeability by promoting gas trapping that limits CO₂ flow paths in the pore network. Although gas phase permeability decreases with higher trapped gas saturation, the water permeability was found to remain unchanged, as demonstrated in Figure 2-2 (Friedmann et al., 1991; Rossen and Renkema, 2007).

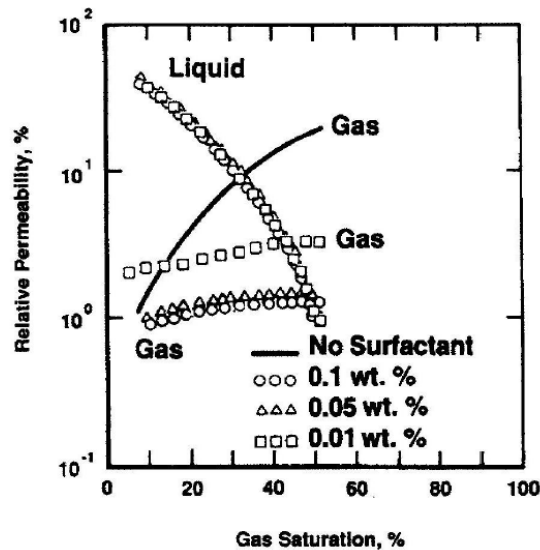


Figure 2-2 Surfactant concentration decreases gas relative permeability in sandstone core greatly but does not change brine relative permeability. (Friedmann et al. 1991)

¹ In this thesis, usage of the term “foam” refers to both liquid and supercritical CO₂ dispersed in water.

Conventionally, surfactant has been widely used to generate and stabilize CO₂ foam. Nevertheless, whether the use of surfactant-stabilized foam can successfully achieve mobility control depends on the long-term sustained generation of lamella in the porous media, due to its lack of long-term stability (Rossen, 1995). Inside the reservoir, stability of surfactant-stabilized foam suffers from surfactant loss due to adsorption onto the reservoir rock and the surfactant degradation under high reservoir temperature. The use of nanoparticle to stabilize CO₂ will potentially overcome these limitations of surfactant, and enhance long-term foam stability. As solid particles, nanoparticles are expected to withstand harsh reservoir conditions such as high temperature and high salinity, and also their surface treatment can make them to have low adsorption onto the reservoir rock. The characteristics of particle-stabilized foam are to be further discussed in the following section.

2.2 PARTICLE-STABILIZED EMULSION/FOAMS

Particle-stabilized emulsion, known as "Pickering Emulsion," is the type of emulsions that are stabilized by fine solid particles without the surfactant (Pickering, 1907). Once these solid particles are adsorbed onto the interface between the two phases, they will form the rigid barrier that prevents droplet coalescence (Binks, 2002). This mechanism leads to the outstanding stability, which spurs a great interest in utilizing such emulsions. An oil-in-water emulsion, which remained stable for several months, was found to be generated using silica nanoparticle (Zhang et al., 2010).

Emulsion stability is also affected by many factors including particle size, shape, concentration, surface wettability, and interactions between particles (Binks, 2002; Tambe and Sharma, 1994). The adsorption energy (E), defined as the energy required to detach particles from the fluid-fluid interface, is described with the equation below

$$E = \pi r^2 \gamma_{\alpha\beta} (1 \pm \cos\theta)^2$$

where r is the radius of the particle, $\gamma_{\alpha\beta}$ is the interfacial tension between the two fluid phases, and θ is the contact angle of particles at the fluid interface, as measured through the aqueous phase. For example, a 5 nm particle strongly held at $\theta = 90^\circ$ on the interface of CO₂-water foam would require approximately 130 kT of energy for the particle to be removed ($\gamma_{\text{CO}_2\text{-water}}$ is around 30 mN/m at 60 °C according to Bachu and Bennion (2008)). This high energy of detachment (or attachment) compared to the thermal energy (kT) makes the adsorption of particles onto the interface effectively irreversible. In contrast, surfactants only have the adsorption energy of several kT, allowing them to move relatively freely to and from the interface. Therefore, particles are considered to be more effective in stabilizing emulsion if their sizes are not too small, as the adsorption energy depends on the square of the particle radius (Binks, 2002).

The wettability of particles not only affects the foam/emulsion stability but also controls the foam/emulsion structure. A parameter that determines the internal phase and external phase of the emulsion is the hydrophilic-lipophilic balance (HLB). The same analogy can be applied on the structure of CO₂ foam by defining hydrophilic-CO₂-philic balance (HCB) according to the following equation (Worthen et al., 2013a):

$$\frac{1}{HCB} = \frac{A_{AC} - A_{AA} - A_{CC}}{A_{AW} - A_{AA} - A_{WW}}$$

where $A_{\alpha\beta}$ represent the interaction pair potential between α and β , with A stands for amphiphile, C for CO₂ and W for water. If the amphiphile-CO₂ interaction potential is stronger than that of amphiphile-water pair, the HCB is then smaller than one, and vice versa. For particles, however, wettability is usually characterized by measuring the contact angle (θ) that a particle makes with the interface. Hydrophilic particles, having $\theta < 90^\circ$ or $HCB > 1$, prefer the aqueous phase in which case the interface is concave toward CO₂

to form CO₂-in-water foam. On the contrary, hydrophobic (or CO₂-philic) particles, with $\theta > 90^\circ$ or HCB < 1 , favor the CO₂ phase and interface will bend about water to form water-in-CO₂ foam (Dickson et al., 2004; Johnston and da Rocha, 2009). The effect of the particle wettability on the structure of foam is illustrated in Figure 2-3.

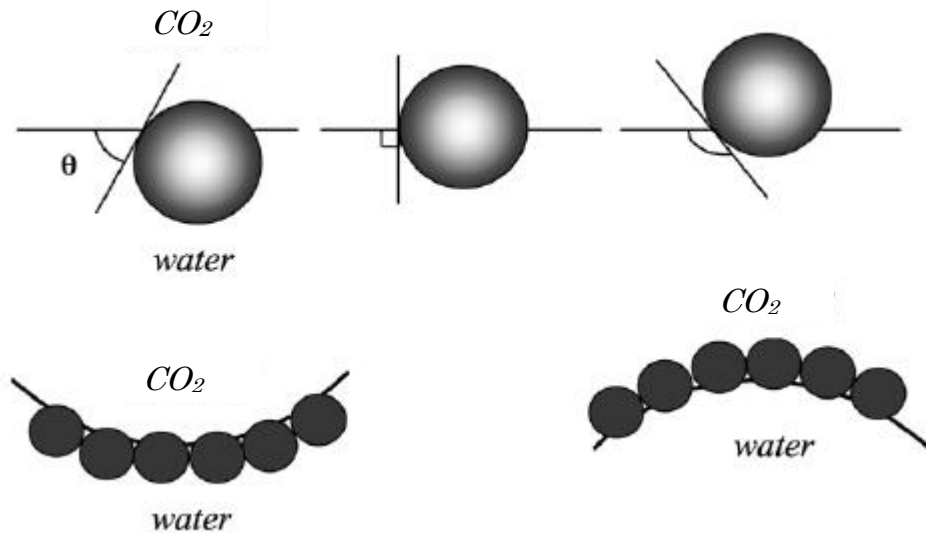


Figure 2-3 Effect of particles wettability and contact angle on the structure of the foam. (Adapted from Binks (2002) according to Johnston and da Rocha (2009))

In this study, we focus specifically on the use of colloidal silica nanoparticles in stabilizing CO₂ -water foam, mainly for porous media application. Even though the wettability of these particles was tuned by their surface modification, they are generally CO₂-in-water foams. The next section provides more details on these silica particles and their abilities in stabilizing foam. Key insights from the past research on the generation and transportation of silica nanoparticle stabilized foam in porous media will also be discussed.

2.3 SILICA NANOPARTICLE-STABILIZED CO₂ FOAM IN POROUS MEDIA

Colloidal silica nanoparticles are known to be able to effectively stabilize foam once enough mechanical energy is introduced to the mixture of the two fluids and the particles. Once adsorbed onto the interface, these particles promote foam stability by preventing the internal phase droplets from coalescing. When the silica nanoparticles without surface coating are dispersed in water, the silanol (SiOH) groups are generated on the silica surface (Binks et al., 2005). As a result, these bare silica nanoparticles are extremely water-wet. The wettability of the silica particle can be tailored to suit a specific combination of the two foaming fluids through surface modification. The surface modification process consists of covalently attaching onto the surface of the nanoparticle. One example is the polyethylene glycol (PEG) coated silica nanoparticles, provided by 3M, which were extensively studied by Espinosa et al. (2010), Worthen et al. (2012, 2013a), and Aroonsri et al. (2013), and which were found to stabilize CO₂-in-water foam for a wide range of conditions as described further later. Even with the surface treatment, these coated silica nanoparticles are still relatively hydrophilic and prefer to form foam with external aqueous phase. In addition, the PEG coating also provides a steric repulsive force, which improves their dispersion stability in the presence of salt. In contrast, bare silica are only stabilized electrostatically and will flocculate once salt is added.

The study from Espinosa et al. (2010) also showed that CO₂-in-water foam stabilized with the PEG coated silica nanoparticle have viscosity as high as 18 times that of the viscosity of the fluid mixture without nanoparticles. This foam was generated through co-injection of aqueous nanoparticle dispersion and CO₂ into the beadpack, filled with 180-micron spherical glass beads. In his study, effects of various parameters on the performance of the silica nanoparticle in foam generation were examined. These

parameters include shear rate, temperature, volumetric phase ratio, salinity, and particle concentration.

One of the key findings of Espinosa et al. (2010) was the existence of a threshold shear rate to generate foam described as ‘critical shear rate’. Below the critical shear rate, foam cannot be generated even with the co-injection through beadpack, consistent with the physical concept that a certain amount of mechanical energy is required to adsorb the particle onto the interface, as described above. At 1350 psi and 23 °C, critical shear rate for CO₂ foam generation were determined to be less than 720 s⁻¹ at his coreflood conditions. The critical shear rate was also found to increase with increasing temperature i.e., as 2750 s⁻¹, and 4000 s⁻¹ were required at 75 °C and 90 °C, respectively. The increase in shear rate requirement at elevated temperature is possibly explained by the destabilization of foam due to a decrease in CO₂ density, which in turn decreases the nanoparticle’s CO₂-philicity (Dickson et al., 2004). At high temperatures, the CO₂ density is significantly reduced from the density at room temperature and are only around one-fifth of water density at the same condition, resulting in high-density contrast that also promotes buoyancy forces.

Apart from foam generation in beadpack, stable CO₂ foam was also reported to be generated by co-injection through sandstone matrix (Boise sandstone and Berea sandstone) using PEG-coated silica nanoparticles. Aroonsri et al. (2013) demonstrated that the critical shear rate for foam generation also exists in the sandstone matrix and depends on various parameters, from medium type to experiment condition. The critical shear rate was determined to be 470 s⁻¹ for Boise sandstone and below 300 s⁻¹ for Berea sandstone at 2000 psi and room temperature.

The effect of other parameters on the performance of CO₂ foam was also investigated. Volumetric phase ratio (or foam quality, f_g) is defined as the volumetric ratio between the CO₂ phase and the aqueous phase of the injection stream at the experiment

condition. Mo et al. (2012) suggested that the foam with maximum flow resistance can be found at the foam quality between 40% and 60%. Aroonsri et al. (2013) reported that the optimum foam quality can be found at around 75%. In addition, increasing salinity also results in an increase in flow resistance in terms of increasing the foam's apparent viscosity.

The ability of coated silica nanoparticles in stabilizing CO₂-water foam open a bright future for foam mobility control in enhanced oil recovery and CO₂ sequestration. Nanoparticles are believed to be able to improve long-term foam stability to the new level that surfactant foam cannot achieve. In this thesis, the generation and propagation of silica nanoparticle-stabilized foam in porous media will be investigated. Using surfactant stabilized foam as an analog, the mechanisms of foam generation and transport in porous media were summarized in the following section.

2.4 FOAM GENERATION AND PROPAGATION IN POROUS MEDIA

Falls et al. (1988) and Rossen (1995) define the foam in porous media as “dispersion of gas in liquid such that the liquid phase is interconnected, and at least some of the gas flow paths are blocked by lamellae (thin liquid film).” Two types of foam were also described: (1) continuous gas foam (weak foam), with which there exists at least one unblocked flow path of CO₂ and (2) discontinuous gas foam (strong foam), with which all of the open CO₂ paths are blocked by lamellae (Figure 2-4). Unlike continuous gas foam with which the gas phase flow as a Newtonian fluid, gas phase in discontinuous gas foam does not move unless lamellae are being displaced. Putting these lamellae in motion requires a minimum pressure drop across the pore throat to be greater than the capillary resistance (Rossen, 1990). These lamellae provide flow resistance, which may be regarded as an increase in the apparent viscosity of the gas phase.

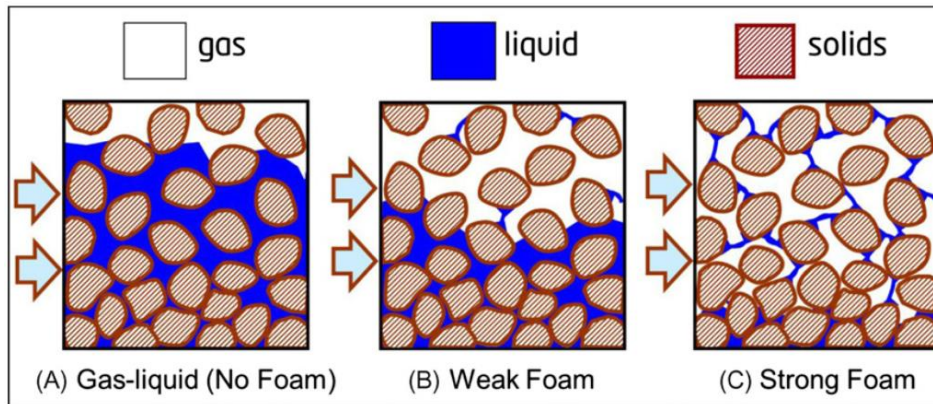


Figure 2-4 Schematic showing (A) no-foam (B) continuous-gas foam and (C) discontinuous-gas foam (Lee and Kam, 2013).

According to the extensive studies on surfactant-stabilized foam, in foam flow, lamellae are continually being created and destroyed regardless of whether the foam texture evolve or remain constant. However, there is no definitive evidence for such coalescence-regeneration behavior with the nanoparticle-stabilized foams, having a more rigid protection at the interface. Rossen (1995) and Kovscek and Radke (1994) had summarized the mechanisms by which lamellae are created in porous media into three main categories, as described below.

The first lamellae creation mechanism is “leave-behind” which only occurs during the drainage process, i.e., when gas saturation is rising. In a porous medium initially saturated with a surfactant solution, large numbers of lamellae are created in the pore throats by being ‘left behind’ after gas enters the pore bodies. As shown in Figure 2-5, assuming no lamellae break during the process, the leave-behind lamellae are simply those remaining in the uninvaded pore throats. Keep in mind that the schematic shown in Figure 2-5 is only two-dimensional and that the gas enters the paths arbitrarily in the schematic. In reality, a three-dimensional medium would result in a much larger number of lamellae

created, and the paths that the gas enter would alter by the locations of narrow and wide pore throats.

Second, lamellae can be created by “snap-off” as the capillary pressure fluctuates. Illustrated in Figure 2-6, a film of water first accumulates in the throat; then with decreasing capillary pressure, the film swells and bridges the throat, blocking gas flow and creating a new lamella. In order for snap-off to occur, the capillary pressure must first rise to a certain level so that gas can occupy the throat and then fall to a certain value depending on the throat geometry for the new lamella to be created. Capillary pressure can either fluctuate in space or time by a number of processes, e.g., imbibition on a macroscopic scale, fluctuation of individual bubble pressures of a flowing foam, pressure drop in the gas phase itself, etc.

Third, lamellae can also be created by “division” when a moving lamella enters a pore body with several pore throats. As shown in Figure 2-7, when transporting through the pore body, the lamella stretches across the pore body and creates a new lamella in each unblocked pore throat. Assuming no lamella break during the process unless a lamella passes through a pore throat, it can be observed in Figure 2-7, from left to right, that this process can create a large number of lamellae as long as there are some lamellae moving through the pore body (overcoming the capillary resistance). Again, the paths that the lamellae take in the schematic shown in Figure 2-7 are arbitrary. In reality, the lamellae would take the least resistant path through the medium.

Apart from the three mechanisms mentioned above, Rossen (1995) also suggested a foam can be created by evolution of gas within the liquid phase. However, the phenomenon only occurs when enough gas is, chemically or physically, produced from the liquid phase at reservoir conditions.

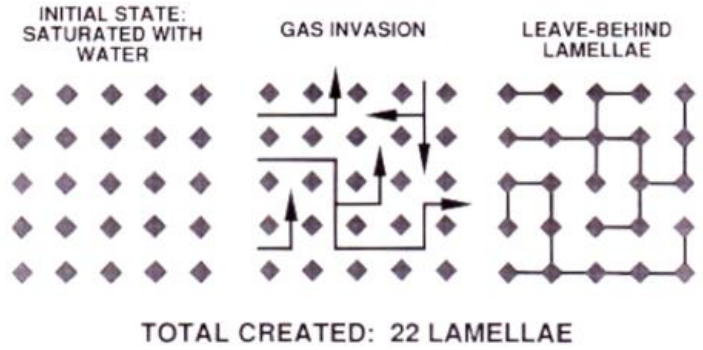


Figure 2-5 Schematic showing lamellae creation by leave-behind. (Rossen, 1995)



Figure 2-6 Schematic showing snap-off in a pore throat. (Rossen, 1995).

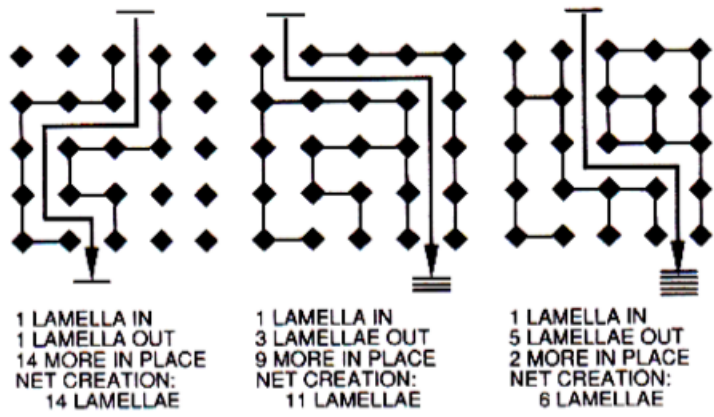


Figure 2-7 Schematic of lamellae division. (Rossen, 1995).

In addition to foam generation, the propagation of foam in porous media is also the key to mobility-control foam process. Foam propagation, or “growth of the region of low gas permeability,” is thought to be the movement of the bubbles for discontinuous gas foam. However, propagation of continuous gas foam is controlled by the propagation of the foaming agent itself - i.e. surfactant and nanoparticles (Rossen, 1995). For the propagation of the pre-generated foam, Ettinger and Radke (1992), based on surfactant foam, reported that fine texture pre-generated foam rapidly become coarser once enter consolidated rock. Also, the new texture seems to be controlled by the porous medium and flow rated and relatively insensitive to the original texture. In contrast, Friedmann and Jensen (1986) claimed that mobility and propagation of the pre-generated foam in porous media are indeed influenced by the initial foam texture. Sufficiently coarse foam was found to collapse within a short distance travelled in the rock core.

The theories and laboratory observations summarized in this section were based on surfactant-stabilized foam, which should provide a good basis for further study of nanoparticle-stabilized foam. However, it should be noted that some process can be different due to the different nature of foaming agent. Although the study of surfactant foam has been well established, the topic nanoparticle stabilized foam is relatively new. This thesis hoped to fill this gap by further study generation and transport of silica nanoparticle stabilized foam in porous media.

Chapter 3 Experimental Materials, Equipment, and Methods

This chapter first described the nanoparticles and other materials used in conducting experiments presented in this thesis. The chapter then continued to describe the laboratory equipment, experiment setup, followed by step-by-step experiment procedures. Two main types of experiments were carried out: co-injection foam generation experiment and pre-generated foam coreflood experiment. Data analysis methods and governing equations were also discussed.

3.1 MATERIALS USED

3.1.1 PEG-coated 5 nm Silica Nanoparticles (3M)

PEG-coated silica nanoparticles were received by courtesy of Dr J. Baran from 3M Co., St. Paul, MN. as a dispersion of 19.3 wt% concentration. This hydrophilic nanoparticle has a silica core of 5 nm diameter with PEG chains grafted onto the surface.

3.1.2 EOR-5xs Silica Nanoparticles (Nissan Chemical)

EOR-5xs nanoparticle was another type of nanoparticle which had been used in coreflood experiments. These nanoparticles, produced by Nissan Chemical Company, consist of a 5 nm silica core and the proprietary surface coating. It was received as an aqueous dispersion of 20 wt% concentration.

3.1.3 Surfactant

Rhodia Mackham DAB-ULS surfactant, at a very low concentration, was mixed with nanoparticle dispersion to test the synergy effect in the supercritical CO₂ foam generation experiments. The original surfactant solution contains lauramidopropyl betaine (LAPB) surfactant at 35 wt% concentration.

3.1.4 Carbon Dioxide (CO₂)

Industrial grade carbon dioxide (>99% purity) was procured from Matheson Tri-Gas Inc. (Basking Ridge, NJ). The liquid carbon dioxide was delivered in a cylinder at 800 psia and was compressed into the accumulator at 2000 psia using a pneumatic compressor before use.

3.1.5 De-ionized Water (DI water)

De-ionized water, used to dilute nanoparticle dispersion to desired concentration, was produced from Barnstead Nanopure II filtration system.

3.1.6 Sodium Chloride (NaCl)

Sodium chloride was added to the aqueous phase in order to preserve core permeability and study the sensitivity of foam generation to salinity. Laboratory grade sodium chloride was obtained from Fisher Scientific.

3.1.7 Calcium Chloride (CaCl₂)

In some of the experiments, calcium chloride, in addition to sodium chloride, was also introduced to the aqueous phase, mimicking the presence of Ca²⁺ divalent cations in the formation brine. Laboratory grade calcium chloride was obtained from Fisher Scientific.

3.1.8 Boise Sandstone Cores

Boise sandstone was the main porous media of choice for coreflood experiments due to its high permeability, low clay content. Boise sandstone used in this thesis had porosity of approximately 30% and permeability ranging from 1 to 3 Darcy, allowing a wide range of flow velocity to be tested. The low clay content also minimized the permeability reduction during experiment due to clay swelling. In a preparation for coreflood experiment, Boise sandstone was cut into a cylindrical core of 1 inch diameter

and either 6 inches or 12 inches long. Next, sandstone core was wrapped with PTFE tape and shrink wrap tubing to avoid flow along the core wall and reduce the amount of carbon dioxide contacting rubber sleeve. The core was then vacuumed and then saturated with brine as an initial condition before the coreflood was carried out. After each coreflood, the initial condition was restored by injecting 10 PVs of brine at high pressure to remove any remaining carbon dioxide gas in the core.

3.1.9 Berea Sandstone Cores

Berea sandstone was the second type of water-wet porous media tested in co-injection foam generation experiments. Berea sandstone used in this thesis had porosity of approximately 21%, permeability around 200 mD, and relatively larger clay content. Its lower permeability permits the study of the effect of matrix permeability. Similar to Boise sandstone core, the same procedure was employed to prepare a Berea sandstone core. However, at least 2 wt% concentration of NaCl in the aqueous phase was recommended to avoid permeability damage from clay swelling.

3.1.10 Indiana Limestone Cores

Indiana limestone was also used in co-injection foam generation experiments to test the feasibility of nanoparticle-stabilized foam generation in low permeability matrix. This Indiana limestone, obtained from Kocurek Industries Inc.(Caldwell, TX), had matrix porosity of approximately 18% and permeability around 5-10 mD, further extending the range of matrix permeability investigated in this thesis. Indiana limestone was also chosen due to its superior strength (compare to other types of limestone) which allowed the possibility of further experiments with fractured cores. Similar to sandstone cores, the same procedure was employed to prepare a limestone core. However, the vacuum time for this

lower permeability Indiana limestone was doubled of that for sandstones, to ensure that most of trapped air was removed.

3.1.11 Fluorinated Ethylene Propylene (FEP) Shrink Wrap Tubing

Heat-shrink tubing (1-inch diameter), made of a co-polymer, was obtained from Geophysical Supply Company (Houston, TX). The tube was used to wrap the core, protecting the core holder rubber sleeve from carbon dioxide damage as well as holding the metal spacer when a 6-inch core was used.

3.1.12 Decane

Decane was used to represent hydrocarbon phase in oil recovery experiments with CO₂ foam. At the condition of the experiment, decane and CO₂ were miscible, forming only single phase. This allowed the effect of miscible CO₂ flood to be tested. Decane was purchased from Fisher Scientific, having >99% purity.

3.2 EQUIPMENT

A schematic of the apparatus used for foam generation and transport experiments was shown in Figure 3-1. The components of the apparatus were described in this section. Section 3.3 described how experiments were conducted in the apparatus.

3.2.1 Core Holder

Core holder used in the coreflood experiments was the Hassler type core holder with five intermediate pressure taps, manufactured by Phoenix Instruments Inc. (serial number UTPT-HAS-1x12-5k-27). It was designed to handle a 1-inch diameter core sample with the length up to 12 inches. In our setup, the core holder was mounted vertically on a steel frame inside the oven. At room temperature, the allowable working pressure was rated at 5000 psia.

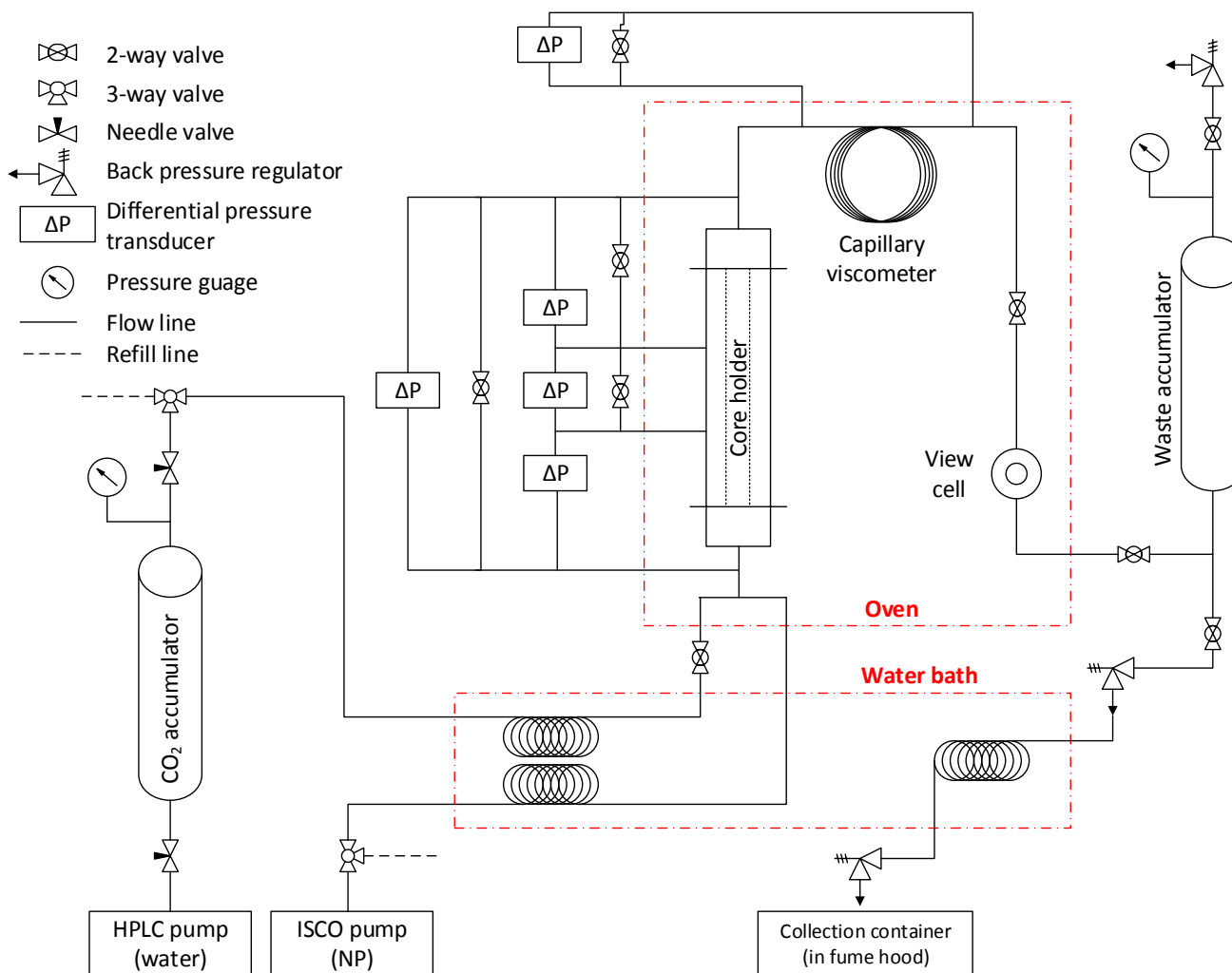


Figure 3-1 Equipment setup for co-injection foam generation experiment

Inside the core holder was a rubber sleeve that provided the seal around the core, prohibiting flow along the outer surface of the core. AFLAS 80 Durometer was chosen as the material for rubber sleeve (as well as O-rings) due to its superior resistance to rapid depressurization of dissolved CO₂ than the Viton type material. In order to establish seal around the core, Enerpac P-392 hand pump was utilized to inject hydraulic oil into the annulus between the core holder and the rubber sleeves, providing a confining pressure that could be read off the installed pressure gauge. To ensure a tighter seal, a segment of both platens of the core holders was also machined down, therefore, these platens could be inserted into the shrink-wrapped tubing.

In order to accommodate a sandstone core shorter than 6 inches in length, spacers were used. These spacers were 3-inch cylinders of 1-inch diameter with 1/8-inch diameter hole bored through the center. The surface of both ends of the spacers was also grooved to promote evenly distributed fluid flow across the core face.

3.2.2 Nanoparticle Injection Pump

Teledyne ISCO 500D syringe pump was used to inject brine or aqueous dispersion of nanoparticle. The pump had the maximum capacity of 500 ml and maximum working pressure of 3750 psi. For the purpose of this thesis, the pump was operated in a constant flow rate mode.

3.2.3 CO₂ Accumulator and Injection System

A 3,000-ml floating-piston accumulator donated by Occidental Petroleum was used as high-pressure liquid CO₂ storage (2000 psi). The piston provided seal that separated the accumulator vessel into two parts: the upper CO₂ storage compartment and the lower side driving water compartments. As used in the core holder, the recommended material for O-ring seals was also AFLAS rubber due to its superior CO₂ resistance.

To charge the CO₂ accumulator, a Haskel ASF-B32 pneumatic compressor was used to compress low-pressure liquid CO₂ from the cylinder into the top compartment. CO₂ was then displaced from the accumulator by injecting water into the bottom compartment using model 1500 HPLC dual piston pump. This HPLC pump had a maximum flow rate of 12 ml/min with maximum pressure rated at 6000 psi. It also had a self-flushing system to maintain smooth operation. Flushing fluid, which required frequent replacement, was a solution of 80% DI water and 20% isopropanol.

3.2.4 Beadpack Column

A high-pressure column (HiP, Erie, PA) was filled with 180 μm spherical glass beads and was used as a beadpack. The HiP column had an ID of 0.386 cm and was 10.2 cm long. Pieces of mesh were placed at both ends of the beadpack to prevent glass beads from exiting into the flow system.

3.2.5 Temperature Control Devices – Water Bath and Oven

For supercritical CO₂ experiments, injected CO₂ and water were pre-heated by submerging the coiled injection lines in the water bath. The injection lines were then routed to the 24 cu-ft Blue M oven where the core holder was set up. The oven was used to maintain desired experiment temperature as well as provide secure housing for the high-pressure coreflood system.

3.2.6 View Cell

The high-pressure vessel with 1.5 cm diameter window was installed downstream of the core holder allowing foam and its texture to be observed. The window glass was made of sapphire by Swiss Jewel Company, having a diameter of 1 inch and a thickness of 3/8 inches.

3.2.7 Waste Accumulator

A 500-ml floating-piston accumulator was used to collect the experiment effluent at the outlet of the system. The accumulator was pre-loaded with DI water and connected to the back pressure regulator. The effluent drove the piston and displaced DI water through the pressure regulator, maintaining a steady back pressure. This setup also prevented the CO₂ and nanoparticle dispersion from contacting and damaging the back pressure regulator as well as the pressure gauge.

3.2.8 Back Pressure Regulator (BPR)

The pressure of the fluids flowing through the core was maintained at the desired set point using a spring loaded back pressure relief valve (Swagelok model SS-4R3A). The operating pressure range could be changed by the switching the load spring of different stiffness. The exact set point could then be fine-tuned by tightening the spring cap. It was recommended that the back pressure relief valve be used together with the waste accumulator setup for best performance (Figure 3-1).

In the case where properties of the effluent as a function of time were required, waste accumulator was removed to allow liquid effluent to be collected with the fractional fluid collector. A back pressure regulator, therefore, needed to be connected directly to the outlet of the coreflow system. In contrast to a smooth single phase DI water flow, two phases (CO₂ and water) effluent caused a significant fluctuation in backpressure while flowing through the relief valve. To minimize the back pressure fluctuation, two back pressure relief valve, set at 1000 psi apart, were connected in series with a 10-ft section of coiled tubing in between. The coiled tubing was submerged in the water bath at 80 °C, allowing the CO₂ to change gradually from the liquid state to the gas state (via supercritical state).

3.2.9 Pressure Transducers and Data Acquisition Module

A total of five Rosemount differential pressure transducers (model 3051CD5A22A1A) were set up to measure the pressure drop across the beadpack, core holder, and across 3 sections of core through intermediate pressure taps. These pressure transducers could withstand a maximum working pressure of 3600 psia and could measure differential pressure as high as 2000 psig.

3.2.10 Capillary Tubing

In foam generation experiments with liquid CO₂, a coil of 10-ft capillary tubing with an internal diameter of 0.03 inches (1/16 inches OD) was used in measuring the apparent viscosity of fluid mixtures downstream of the core. Pressure drop was measured across the capillary tube and used in the apparent viscosity calculation. In pre-generated foam experiment, the coils of 5-ft and 20-ft capillary tubings (with the same ID) were also installed parallel to the core holder, as parts of the branching manifold system described in Section 3.3.2.1 (Figure 3-8). Together with a set of valves, these capillary tubes allowed the foam flow rate through core to be varied while the flow rate through the foam generation section (the beadpack) was held constant, enabling the study of foam rheology.

3.2.11 Decane Accumulator

A 400 ml floating-piston accumulator was used as a decane container during the drainage process of CO₂ foam EOR experiments. The accumulator was filled with decane before being displaced by injected brine from ISCO pump.

3.2.12 Fluid Sample Collecting System

Fraction collector (ISCO retriever II) with plastic tubes was setup at the outlet of the coreflood system to collect liquid sample after the CO₂ was vented into the atmosphere.

3.3 EXPERIMENT SETUP AND METHODS

3.3.1 Co-injection Foam Generation Experiments

Co-injection coreflood experiments were carried out to investigate foaming ability of silica nanoparticles by direct co-injection of CO₂ and nanoparticle dispersion through the cores. The experiment first started with liquid CO₂ at room temperature and later performed with supercritical CO₂ at elevated temperature, simulating high-pressure high-temperature reservoir condition.

Shown in Figure 3-1, was the equipment setup for the co-injection foam generation experiments. Once the rock core was loaded into the core holder, the co-injection experiment started by pumping aqueous dispersion of nanoparticle from ISCO pump, while displacing the CO₂ out from the accumulator with injected DI water from HPLC pump. The two injected fluid mixed at the T-junction immediately upstream of the core holder then flowed into the core holder where an array of 4 differential pressure transducers was installed. The first three pressure transducers utilized the intermediate pressure taps along the core holder, that each of them individually measured core pressure drop in the 3 sections: upstream, middle, and downstream. The remaining pressure transducer was installed in parallel to the others, measuring the total pressure drop across the whole core (intermediate pressure measurement was only available in some of the experiments). After the effluent exited the core, it was routed to the coil of capillary tubes, where the pressure drop was also measured (only available in liquid CO₂ experiment). The effluent then continued to flow to the view cell, where the visual presence of foam (as well as its texture) was observed, before finally flowing to the waste accumulator. The pressure of the system was controlled using the back pressure regulator at the outlet side of waste accumulator

while the temperature was maintained at the desired set point using the water bath and the oven (indicated as red dashed line).

3.3.1.1 Co-injection experiments with liquid CO₂ (room temperature experiment)

This section provided detailed procedures of the experiments, from core preparation to depressurizing the system at the end of the experiment. After the core had been prepared and loaded into the core holder, core permeability was measured by injecting brine (or DI water) into the core at various rate and recording the steady-state pressure drop across the core. Once the core was characterized, the first co-injection was carried out with a desired overall flow rate and volumetric ratio of CO₂ phase to aqueous phase without nanoparticle in the aqueous phase to establish a baseline. The pressure drop was measured and the apparent viscosity of the CO₂/water mixture was recorded. After the baseline experiment, a core restoration process was performed: at least 8 pore volumes (PVs) of brine were injected into the core at 500 psi to remove the remaining CO₂ from the core and restore the brine-saturated initial condition. Next, foam generation experiment was performed by co-injecting aqueous nanoparticle dispersion and CO₂. After the experiment was finished, the core restoration process was again carried out before the permeability measurement was done to identify any possible formation damage, for example from nanoparticles retained in the core or geochemical reactions between rock grains and the CO₂-saturated brine. After each CO₂-water co-injection experiment, the system was vented, and the waste accumulator was reloaded. After several experiments, the CO₂ accumulator might also require a refill. The detailed procedures for each experiment stage were provided below.

Preparing the core: initially, the core was cut from the block into 1-inch diameter and 12 inches long cylinder. The new core was normally wetted from the cutting process, thus was then left in the oven at 100 °C for at least a day to dry out. Once the core was dry, it could be cut to the desired length with a hacksaw, and then filed on cut surfaced to restore its original texture. Next, the core was wrapped with PTFE tape and inserted into the shrink wrap tubing (For 6-inch core, spacers were also inserted into the shrink wrap). The core was then put into the oven at 200 °C in order for the shrink wrap tubing to activate. Once the wrapping process was completed, the dry weight of the wrapped core was measured. The core was placed in a sealed chamber and was vacuumed for a day. A schematic of the core vacuum system was shown in Figure 3-2. Next, the 3-way valve at the top of the chamber was switched to introduce the brine (or DI water) into the vacuumed chamber. Once the core was submerged under the brine, vacuum pump was restarted again to remove any remaining trapped air. Another 6 hours in the vacuum chamber was recommended before the saturated core was ready. A longer vacuum time should be allowed for core with low matrix permeability (i.e. Berea sandstone, Indiana limestone) to ensure complete removal of trapped air. The wet weight of the saturated core was also measured and compare with dry weight to determine pore volume and porosity of the core using the calculation shown in section 3.4.12.

In order to prepare the fractured core, the procedure proposed by Hariz (2012) was followed, using the load frame to fracture the core. Due to the size of load frame plate, the core length was limited to 6 inches or shorter. After the 6-inch core was cut, the core was wrapped with shrink wrap across the whole core body. The shrink wrap provided confining pressure which prevented the rock from crumbling while being fractured. After the wrapped core was then put under the load frame plate, load was applied at the rate of 1,000 psi/min. Once the core failed in tension, the pressure load must be relieved immediately to

avoid further crushing. After it was removed from the load frame, the shrink wrap tubing was cut to take the two side of the core apart. Using the PTFE tape, the two pieces of rock were then put together. The fractured core and two core holder spacers were then wrapped together in the heat shrink wrap tubing (like other 6 inches core). Two pieces of mesh with different sizes was placed in between the core and the spacers on both ends, preventing fine particles associated with the fracturing process from moving into other parts of the apparatus. Once the wrapped core was ready, the same vacuum and saturation process was applied before the core could be used in the experiment.

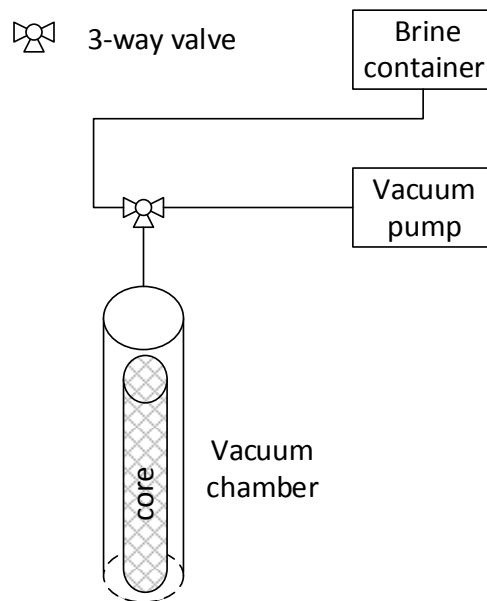


Figure 3-2 Schematic of core vacuum system

Loading a core into the core holder: once the core was prepared as described earlier, the following procedure was used to load the core into the core holder as well as connecting the intermediate pressure taps. Shown in Figure 3-3 was a schematic of the core holder confining fluid system.

1. Open the confining pressure relief valve at the top of the core holder to relax the rubber sleeve. Gently slide the wrapped core into the core holder rubber sleeve from the top. Do NOT force the core down into the sleeve as it may damage the sleeve or misplace the end cap, resulting in hydraulic oil leakage.
2. Connect the top platen to the core (put into the extended portion of the shrink wrap). Continue to push the core down the sleeve slowly until the other end of the core protrude from the bottom of the core holder.
3. Connect the bottom platen to the other end of the core (again put into the extended portion of the shrink wrap). Push the bottom platen and the core up, all the way back into the core holder. Turn it counter-clockwise until the clover-leaf bayonet is fastened into place. Also tighten the hand-screw at the bottom end cap.
4. Place the retainer on the top end cap and tighten the hand-screw to lock the core in place and apply axial confinement.
5. From the bottom, unscrew the second and the fourth pressure tap outlet fittings to reveal the small tubing through which the rubber sleeve was penetrated. Use the electric hand-drill to place a hole on the core through the small tubing. Tighten the pressure tap outlet fittings back into places.
6. Close the confining pressure relief valve at the top of the core holder. Apply at least 600 psi confining pressure by operating the hand pump.

7. Connect the inlet and outlet line with the “Quick-connect” fittings at both ends of the core holder. Start pumping aqueous phase from ISCO pump into the system at 1 ml/min. Ensure that there was no air anywhere in the injection line.
8. Wait until the aqueous phase start flowing from out from the pressure tap outlet (with drilled hole) before connecting the pressure transducers line. Before tightening the connection, make sure the transducer lines are completely filled with water for the best performance. The presence of air in the transducer lines will amplify the fluctuation in pressure measurement. Once the lines are connected, the system is ready for coreflood.

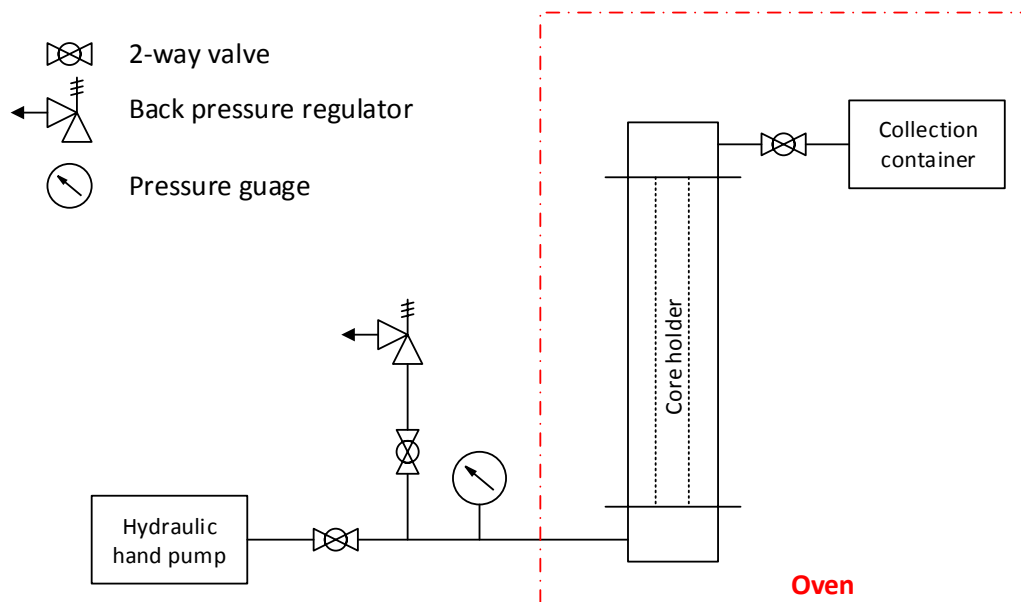


Figure 3-3 Schematic of core holder confining fluid system

Measuring core permeability: after a core was loaded into the core holder, the next step was to measure the permeability of the core. This step was very important as the permeability was to be used in the interpretation of apparent viscosity for both baseline and foam experiment. The permeability measurement was conducted by injecting brine into the core at several different flow rate while measuring pressure drop across the core. At each constant injection rate, it was recommended to inject at least 1 PV to ensure that a steady pressure drop was obtained. These steps were then repeated with a different flow rates until at least three or more data point was collected to ensure a good data quality. The pressure drop data across the core and its individual sections were recorded using LabVIEW software on the data acquisition desktop computer. Based on the collected pressure drop, injection rate data and core dimensions, the core permeability was calculated using Darcy's law. Once the permeability measurement was finished, there was no need to unload the core from the core holder as it was still at brine-saturation initial condition. The core was ready for the next co-injection experiment.

Co-injection through the core (with and without nanoparticle): the following procedure applied for both nanoparticle-free baseline experiment and nanoparticle stabilized foam experiment. Both baseline experiment and foam experiment were conducted using the identical experiment conditions in the same core. This enabled a direct evaluation of the effect of nanoparticle on the apparent viscosity of CO₂-aqueous phase mixture as it flowed through the rock. Although nanoparticle adsorption onto the rock matrix was minimal, it was important to perform the baseline experiment first to avoid the nanoparticle contamination in the core that would affect the baseline experiment. The detailed procedures for CO₂-aqueous phase co-injection were described below.

1. Check if the waste accumulator is reloaded and properly connected with the system and the back pressure regulator (BPR). ‘Quick-connect’ fitting was installed on both sides of the waste accumulator for convenience.
2. Ensure that the CO₂ accumulator contains enough CO₂ for the experiment. Refilled the CO₂ accumulator if required. Also, check if there is enough DI water in the reservoir to feed the HPLC pump during CO₂ injection.
3. Load the ISCO pump with brine (for baseline) or nanoparticle dispersion (for foam experiment). Ensure that both the ISCO pump cylinder and injection line are free of trapped air.
4. Make sure the confining pressure relief valve at the core holder is closed. Apply confining pressure by operating the hand pump. Always maintain the net confining pressure at 600 psi or above.
5. Start the aqueous injection at low flow rate, using a constant flow rate mode of the ISCO pump. Start recording pressure using LabVIEW software.
6. Tighten the screw-top of the BPR to hold the flow and let the pressure build-up. Adjust confining pressure accordingly as the system pressure increase. Slowly adjusted the BPR until the desired pressure is reached.
7. Once the system is at the desired pressure, let the flow continue for at least 1PV or until the pressure drop measurement stabilized.
8. While waiting for pressure drop to stabilized, open the two choke valves at the CO₂ accumulator and align the three-way valve toward the coreflood system. Start the HPLC pump on the CO₂ side and make sure the accumulator pressure is approximately 50 psi above the injection pressure to avoid liquid flow back into the CO₂ accumulator. Leave the CO₂ injection valve shut until ready for co-injection.

9. Introduce CO₂ into the system by opening the CO₂ injection valve. Operate the HPLC pump on constant injection rate mode.
10. Continue the co-injection until the CO₂ breakthrough in the view cell and the steady pressure drop is reached. The injection rate can then be changed while the CO₂ volumetric phase ratio is maintained.
11. Repeat this step 10 until the waste accumulator is completely filled. At this point, the pressure drop reading will fall to zero as there is no flow. Immediately stop both the ISCO pump and HPLC pump as well as shut-off the CO₂ injection valve to prevent over-pressurization.
12. Stop recording the data. The system can be vented using the procedure provided next.

Depressurizing the system: when a co-injection experiment was finished, a vast amount of high-pressure fluid mixture (mainly CO₂) must be carefully vented to prevent any damage to the equipment and more importantly to protect the working personnel from any possible health hazard. The below procedure was followed to depressurize the system.

1. Ensure all injection pump is stopped, and the CO₂ inlet valve is closed.
2. Make sure the vent-line BPRs are tightened, and the vent valve is closed. Check if the vent-line outlet and the container in the fume hood are secured.
3. Turn on the water bath. The heat from water bath will prevent the freezing and ice-clogging in the vent line as the CO₂ cools during depressurization.
4. Open the valve to core holder bypass line to minimize the pressure drop during depressurization as well as reduce the risk of damaging pressure transducers.

5. Open the valve at the T-junction in front of the waste accumulator to open access to vent-line. Open the vent valve and slowly unscrew the BPRs to start venting the system. The presence of two BPRs enables a more gradual expansion of the CO₂.
6. Depressurizing the system as slow as possible to allow the CO₂ to exsolve gradually from the rubber sleeve. Rapid decompression of the CO₂ will damage the rubber sleeve and O-rings.
7. As the system pressure decrease, release a small amount of confining fluid through the check-valve at the outlet of the hand-pump to relief some confining pressure. However, the net confining pressure must be maintained above 600 psi at all time to prevent leakage at the core holder.
8. Make sure both pressure reading at the ISCO pump and a mechanical gauge at the waste accumulator BPR show zero pressure. After the pressure is slowly brought down to atmospheric pressure, the confining pressure can then be completely relieved.
9. The waste accumulator can now be disconnected for cleaning and reloading. If the core is to be used further, the core restoration process is performed to remove the trapped CO₂. Otherwise, it's safe to remove the core.

Restoring the core to the initial condition: after the co-injection experiment, there was still some CO₂ trapped inside the core. In order to restore the brine-saturated initial condition, 8-10 PV of brine was injected into the core to displace and dissolve the remaining CO₂. This process was done through the vent line with tightened BPR to apply some back pressure. An increase in system pressure reduced the CO₂ volume and at the same time increased the solubility of CO₂ in water, accelerating the CO₂ displacement

process. The core pressure drop would slowly decrease (can be observed in real time in LabVIEW data acquisition program) as the core was being cleaned and finally saturated with brine. After the core was restored, it was recommended to perform permeability measurement to determine the change in permeability and any possible formation damage.

Refilling CO₂ Accumulator: as described earlier in the equipment section, the CO₂ accumulator was a pressure vessel with a floating piston that creates two separating chamber for displaced liquid CO₂ and displacing water. If the CO₂ level was low, this procedure was followed to recharge the CO₂ accumulator. A schematic of the CO₂ accumulator and recharging system was in Figure 3-4.

1. Drain the water out from the bottom chamber of the accumulator. To do so, disconnect the water injection line (running from HPLC pump) then slowly open the choke valve. The remaining CO₂ will expand and push the piston down, driving all the water out of the accumulator. Once the water flow stop, close the choke valve and connect the water line back.
2. Fully open the choke valve on CO₂ side of the accumulator and also align the 3-way valve toward the Haskel pneumatic compressor.
3. Open the air source valve, CO₂ tank valve and CO₂ regulator.
4. Operate the compressor by opening the valve at low pressure CO₂ feed line then immediately opening the valve at driving air feed line. The compressor will start compressing CO₂ into the top chamber of the accumulator.
5. Keep the compressor running until the pressure reaches around 1500 psia before shutting down the compressor by closing the two feed-line valves. Further compression of the CO₂ chamber can be done by injecting water into the bottom chamber with HPLC pump.

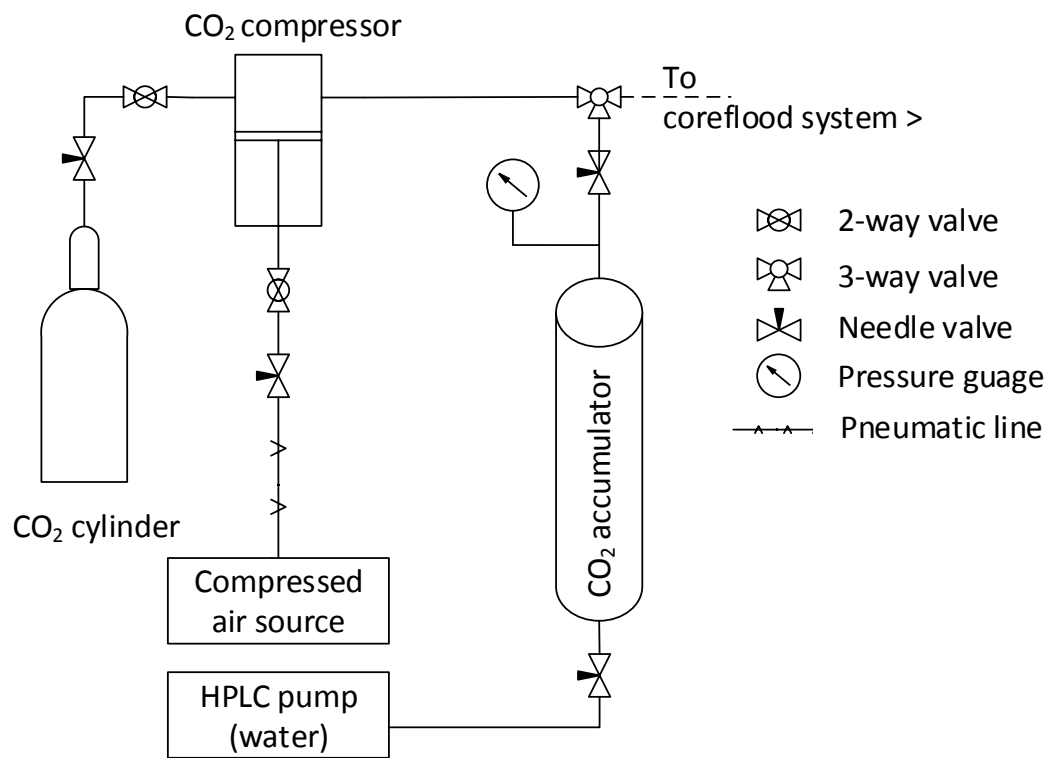


Figure 3-4 A schematic of the CO₂ accumulator and recharging system

3.3.1.2 Co-injection experiments with supercritical CO₂ (elevated temperature experiment)

As temperature increases, the properties of CO₂ changes as it evolves from the liquid state to the supercritical state. Figure 3-5 and Figure 3-6 showed the how CO₂ density and viscosity evolve with temperature, at specific pressure of interest. Water properties at 2000 psi were also plotted together on the chart as a reference. Figure 3-7 illustrated the interfacial tension between CO₂ and water at different temperature, pressure and salinity reported by Bachu and Bennion (2008).

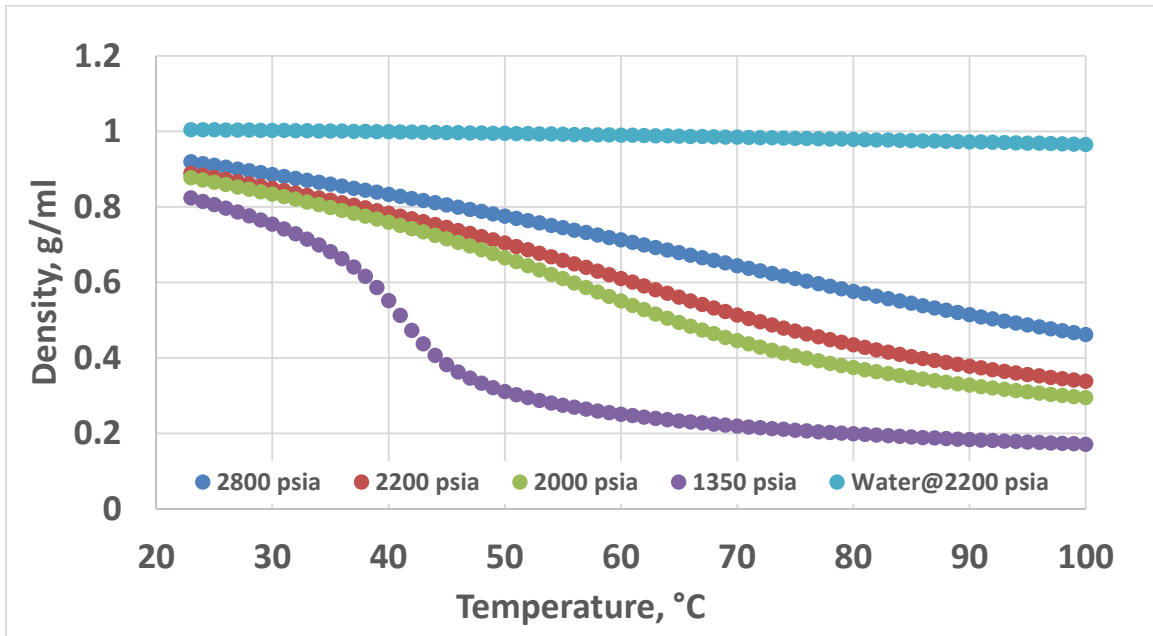


Figure 3-5 CO₂ density versus temperature at some specific operating pressure. Water density at 2200 psia (blue dots) was also plotted for comparison (all data from NIST, 2011).

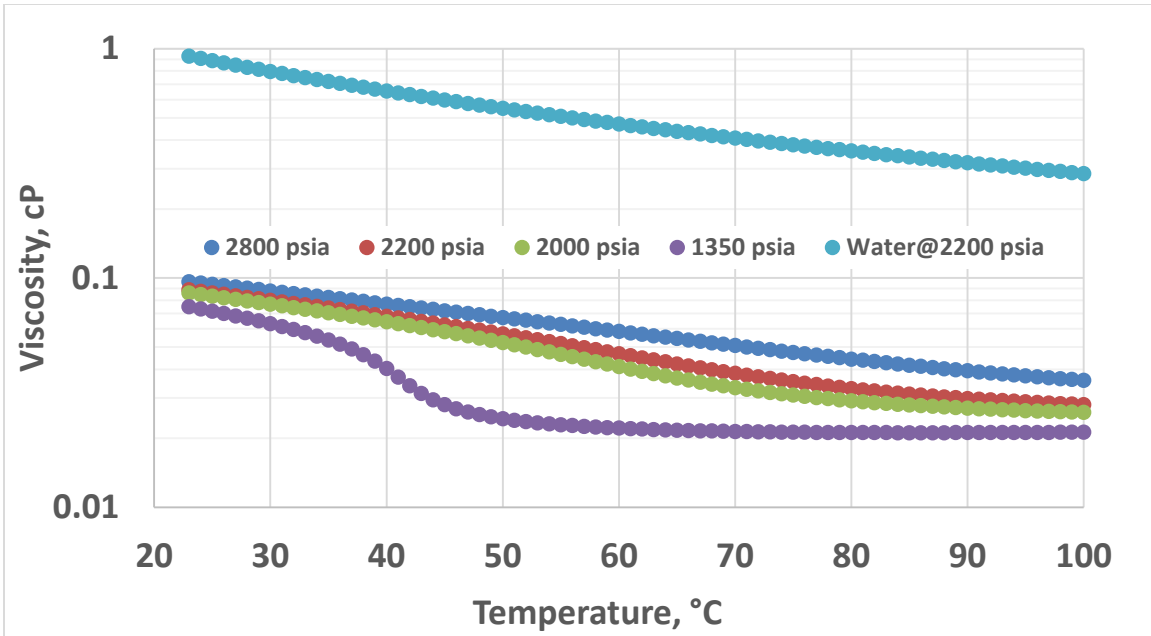


Figure 3-6 CO₂ viscosity versus temperature at some specific operating pressure. Water density at 2200 psia (blue dots) was also plotted for comparison (all data from NIST, 2011).

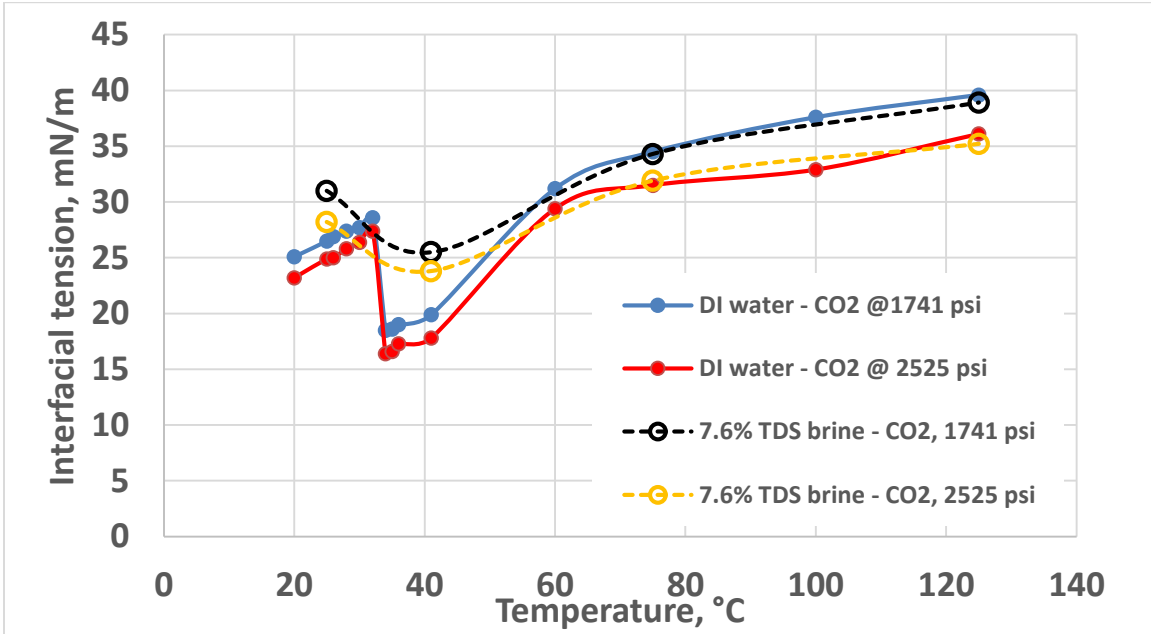


Figure 3-7 CO₂ – water interfacial tension versus temperature at 1741 psi and 2525 psi. The dash lines show the effect of salt concentration on interfacial tension (Bachu and Bennion, 2008).

In the experiments with supercritical CO₂, the same procedure as introduced earlier for liquid CO₂ experiment was employed. However, some additional steps were required before starting and after finishing the experiments as described below.

Injection rate calculation: unlike water, CO₂ density drop drastically as it expand at higher temperature. Foam quality (f_g) is the volumetric fraction of CO₂, in the CO₂/aqueous phase mixture, calculated at the condition of the experiment, thus the rate of CO₂ displacement from the accumulator need to be adjusted to account for the change in density between accumulator conditions and coreflood conditions. Since CO₂ accumulator was at ambient condition and was relatively large compared to total planned injected volume, the following equations were used to calculate CO₂ displacement rate at accumulator condition. However, adjustment was not required for aqueous phase injection rate as the change in water density was negligible.

$$Q_{CO_2} = f_g \cdot Q_{total} \cdot \frac{\rho_{CO_2,exp}}{\rho_{CO_2,accum}}$$

Q_{CO_2} = CO₂ displacement rate at accumulator condtion (cm³/min)

f_g = desired foam quality (volume fraction of CO₂)

Q_{total} = total injection rate at the experiment condition (cm³/min)

$\rho_{CO_2,exp}$ = CO₂ density at the experiment condition (g/cm³)

$\rho_{CO_2,acc}$ = CO₂ density at the accumulator condition (g/cm³)

Experiment setup pre-heat: Before starting the experiment, both water bath and the oven needed to be pre-heated to the desired temperature 30 minutes in advance. This allowed the core holder and the setup inside the oven to achieve the desired temperature. The following steps pre-heated the system.

1. Check for leaks in the high-pressure part of the apparatus. Make sure all the tube connection are properly secure.
2. Displace all the air out from the core holder annulus then close the confining pressure vent line valve at the top of the core holder.
3. Open the check valve located at the hand pump outlet to relieve the increasing hydraulic oil pressure from thermal expansion.
4. Close the oven door, turn on and set the temperature controller to desired set point.
5. Check water level in the water bath. Make sure all tubing are submerged. Turn on and change the temperature to desired set point.
6. Let the system heat up for 30 minute.
7. Close the check valve at the hand pump. Start applying confining pressure.
8. Start liquid injection pump and bring up the system pressure to the set point. Continue to increase the confining pressure and make sure the net confining pressure is within 600-800 psi (too much pressure will fracture the core).
9. Continue to inject the aqueous phase for at least 1 PV before introducing CO₂ into the system. Follow the rest of the co-injection experiment procedure as shown in the liquid CO₂ section. Always monitored the confining pressure. Release some if required.

After experiment cool-down: After finishing the experiment is finished, turn off the oven but keep the water bath running. Start venting the system using the same procedure as stated earlier for liquid CO₂. Always relieve some confining pressure as the system pressure reduces. Once the accumulator is empty, the water bath can be turned off and core restoration process can be initiated. Otherwise, leave the system for several hours to cool down before removing the core and cleaning up.

3.3.2 Pre-generated Foam Coreflood Experiments

In this type of experiment, foam was generated in the beadpack instead of direct co-injection of CO₂ and aqueous phase into the core. A beadpack, as referred to in this thesis, is a high-pressure column filled with 180 microns spherical glass beads. Due to the current practice of foam generation by direct co-injection of CO₂ and nanoparticle dispersion into core, the corresponding pressure drop measure across the core took into account two effects: flow resistance associated with foam generation, and transport of the generated foam (a distinction between these effects is drawn for nanoparticle-stabilized foams because of the large adhesion energy of nanoparticles, which suggests that foam bubbles could be quite stable once established.) Installing the beadpack foam generator upstream of the core holder allowed the two processes to be separated, thus enabling further study of foam rheology and its ability in recovering oil. Two types of the pre-generated foam were discussed in this section: (1) foam rheology measurement using the branching manifold and (2) oil recovery using nanoparticle-stabilized CO₂ foam. Experiment settings and methods for these experiments were provided below.

3.3.2.1 Rheology measurement of foam flowing in sandstone matrix using the branching manifold.

The aim of this experiment was to study the rheology of the pre-generated nanoparticle-stabilized CO₂ foam by measuring the apparent viscosity of foam travelling in the core for a range of velocity and shear rates. This data provided a viscosity-shear rate relationship of nanoparticle stabilized foam in a core, and thus indicated whether the foam exhibited shear thinning rheology. Although the pressure drop across the core does not include a contribution from foam generation in this setup, there still exists a challenge in the measurement of rheology in this setup. As the texture of generated foam changed with the shear rate and velocity, varying the total injection rate into beadpack would result in

the pre-generated foam with varying texture and viscosity. Thus the foam entering the core at one shear rate would not be identical to the foam entering the core at a different shear rate. In order to solve this problem, the new branching manifold was introduced so that constant flow rate through the foam-generating beadpack could be maintained while varying the flow rate through the rock core. The experiment setup and procedure were described below.

Figure 3-8 showed a schematic of the modified co-injection system with the branching manifold. Similar to the prior experiment setup for foam generation, the aqueous phase was injected from the ISCO pump while the CO₂ phase was displaced from the CO₂ accumulator using HPLC pump. The two fluids mixed at the T-junction and flowed into the beadpack where foam was being generated. Pressure drop across the beadpack was also monitored to see the consistency of generated foam. After leaving the beadpack, the pre-generated foam was routed to the branching manifold consisting of three valves and two capillary tubes having identical diameter but different length, 5ft and 20ft long, respectively. These capillary tubes were installed in parallel to the core holder providing alternative flow paths bypassing the core holder. By operating the three valves, some of the foam flow was diverted toward the capillary tubes, allowing control of foam flow rate through the core. Pressure drops across the entire branching system and 3 core sections were measured with the pressure transducers. These pressure drops were used in the interpretation of flow allocation between core and tube(s) and the calculation of foam apparent viscosity. After foam effluent exited the core, it flowed through the view cell for visual observation. The effluent then routed to the waste accumulator, having BPR installed at downstream to maintain system pressure. The oven was only used as housing for the setup since all of the experiment were carried out at ambient temperature. Similarly, the water bath was only operated during system depressurization to avoid line freezing.

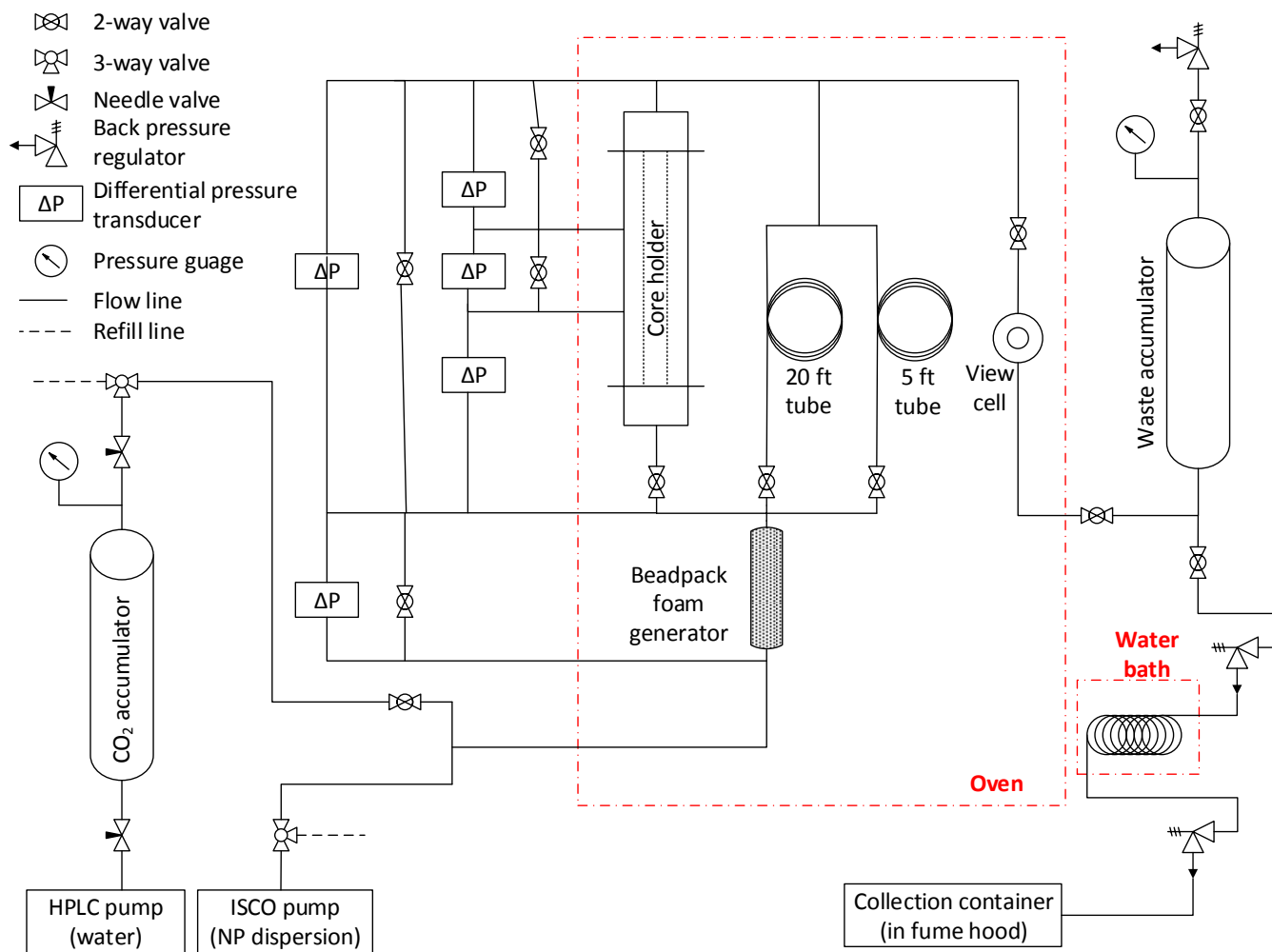


Figure 3-8 Schematic of modified co-injection system with beadpack foam generator and the branching system.

Preparing the beadpack: the foam generating beadpack was prepared using the procedure given below.

1. Clean the column and the two end caps. Leave them to dry.
2. Ball up the metal mesh and stuff them into the opening of both end caps to confine glass beads within the column.
3. Attach and tighten an end cap onto one side of the column. Start to fill the column with glass beads.
4. Knock on the side of the column several time while pouring the beads. This help ensure that the column is completely filled.
5. Attach and tighten the other end cap onto the column to secure the glass beads.

After the beadpack was prepared, its permeability was measured in the same manner as the permeability measurement in rock cores. It was recommended to check the permeability of the beadpack frequently. Pore plugging could cause a reduction in permeability during the leakage of beads results in a larger permeability of the beadpack column. In both cases, the column needed to be re-packed.

Pre-generated foam coreflood with branching manifold system: the procedure to conduct pre-generated foam experiment was very similar to the foam generation experiment, from loading the core to venting the system. However, there were some details on operating the branching manifold system which was the key of this experiment. Thus, the step-by-step procedure to perform the experiment was provided below.

1. Check if the waste accumulator is reloaded and properly connected with the system and the back pressure regulator (BPR). ‘Quick-connect’ fitting was installed on both sides of the waste accumulator for convenience.

2. Ensure that the CO₂ accumulator contains enough CO₂ for the experiment. Refilled the CO₂ accumulator if required. Also, check if there is enough DI water in the reservoir to feed the HPLC pump during CO₂ injection.
3. Load the ISCO pump with brine (for baseline) or nanoparticle dispersion (for foam experiment). Ensure that both the ISCO pump cylinder and injection line are free of trapped air.
4. Make sure the confining pressure relief valve at the core holder is closed. Apply confining pressure by operating the hand pump. Always maintain the net confining pressure at 600 psi or above.
5. At the branching manifold, open the core holder valve but leave the other two capillary tube valves closed.
6. Start the aqueous injection at low flow rate, using a constant flow rate mode of the ISCO pump. Start recording pressure using LabVIEW software.
7. Tighten the screw-top of the BPR to hold the flow and let the pressure build-up. Adjust confining pressure accordingly as the system pressure increase. Slowly adjust the BPR until the desired pressure is reached.
8. Once the system is at the desired pressure, let the flow continue until the pressure drop measurement stabilized.
9. While waiting for pressure drop to stabilize, open the two choke valves at the CO₂ accumulator and align the three-way valve toward the coreflood system. Start the HPLC pump on the CO₂ side and make sure the accumulator pressure is approximately 50 psi above the injection pressure to avoid liquid flow back into the CO₂ accumulator. Leave the CO₂ injection valve shut until ready for co-injection.

10. Introduce CO₂ into the system by opening the CO₂ injection valve. Operate the HPLC pump on constant injection rate mode. The rise of pressure drop in beadpack mark the arrival of CO₂ and the generation of the first foam.
11. Continue the co-injection until the CO₂ breakthrough in the view cell and the steady pressure drop across the core is reached.
12. Maintain the injection rate. Together with the opened core holder valve, open the 20 ft capillary tube valve to divert some foam flow. Keep the 5 ft capillary tube valve shut. Now the flow rate through core is reduced to the second measurement point. Wait until the pressure drop stabilized.
13. Maintain the injection rate. Together with the opened core holder valve, open the 5 ft capillary tube valve. Immediately close the 20 ft capillary tube valve. Now the flow rate through core is reduced to the third measurement point. Wait until the pressure drop stabilized.
14. If there's still enough volume left in the waste accumulator, open all three valves at the branching manifold to bring down the core flow rate to the fourth measurement point. Wait until the pressure drop stabilized.
15. When the waste accumulator is completely filled, the pressure drop reading will fall to zero as there is no flow. Immediately stop both the ISCO pump and HPLC pump as well as shut-off the CO₂ injection valve to prevent over-pressurization.
16. Stop data are recording. The system can be vented using the same procedure as provided in section 3.3.1 for foam generation experiment.

3.3.2.2 Oil recovery using nanoparticle-stabilized CO₂ foam

The purpose of this experiment was to test the ability of nanoparticle-stabilized CO₂ foam in enhanced oil recovery (EOR) and determine foam mobility in the presence of the hydrocarbon phase. Again, foam was pre-generated in the beadpack before being injected into the core containing residual oil and sometimes mobile oil. Decane was selected to represent hydrocarbon phase as it was miscible with CO₂ at the experiment condition. In addition to pre-generated foam experiment, the other types of injection (CO₂/brine, liquid CO₂, foam slug) were also performed in the core at residual oil condition. Experiment results of pre-generated foam injection and the others three injection schemes were compared in both mobility control and oil recovery aspects. The experiment procedures and equipment setup were described as follow.

Establishing residual oil condition in the core: Figure 3-9 showed a schematic of the system used for decane injection (drainage) and water flooding (imbibition) to create residual oil condition in the core. Decane was first measured and loaded into the accumulator before being displaced into core using the ISCO pump. The beadpack foam generator was removed to avoid decane contamination that would affect foam generation process. Decane effluent then continued to flow through the view cell before leaving the system through the BPR system. However, the waste accumulator was still attached to monitor the back pressure without exposing the pressure gauge to decane. Detailed procedure for decane injection was shown below.

1. Check if the waste accumulator is reloaded and properly connected with the system and the pressure gauge. ‘Quick-connect’ fitting was installed on both sides of the waste accumulator for convenience. The waste accumulator setup will be used for back pressure monitoring.

2. Fill the other accumulator with decane. Secure the accumulator on the stand then connect to two 'Quick-connect' fitting to coreflood system. Align the three-way valve at the ISCO pump toward decane accumulator. Also, open the outlet valve at the decane accumulator.
3. Load the ISCO pump with brine. Ensure that both the ISCO pump cylinder and injection line are free of trapped air.
4. Make sure the confining pressure relief valve at the core holder is closed. Apply confining pressure by operating the hand pump. Always maintain the net confining pressure at 600 psi or above.
5. Open the core holder valve but leave the core bypass valve and the two branching valves closed.
6. Start the ISCO pump to displace decane from the accumulator, using a constant flow rate mode. Start recording pressure using LabVIEW software.
7. Tighten the screw-top of the BPR to hold the flow and let the pressure build-up. Adjust confining pressure accordingly as the system pressure increase. Slowly adjusted the BPR until the desired pressure is reached.
8. Once the system is at the desired pressure, continue the injection for about 8PV or until the pressure drop measurement stabilized.
9. After finishing decane injection, stop the ISCO pump and close the decane accumulator outlet valve. Switch the three-way valves at ISCO pump to close position the refill the ISCO pump with brine.
10. Align the three-way valve at the ISCO pump toward the core holder and start injecting brine into core for about 8 PV. Wait until pressure drop stabilized that all mobile decane are displaced. The core is now at residual oil condition.

11. When finish the experiment, stop both the ISCO pump. Stop recording the data.
The system can be vented by slowly unscrew the BPRs until atmospheric pressure is reached.
12. Once the system is completely depressurized, the core is taken out from the core holder to measure the wet weight at residual oil condition. The wet weight is used to estimate the residual oil saturation in the core. The amount of decane coming out of the system is also measured.

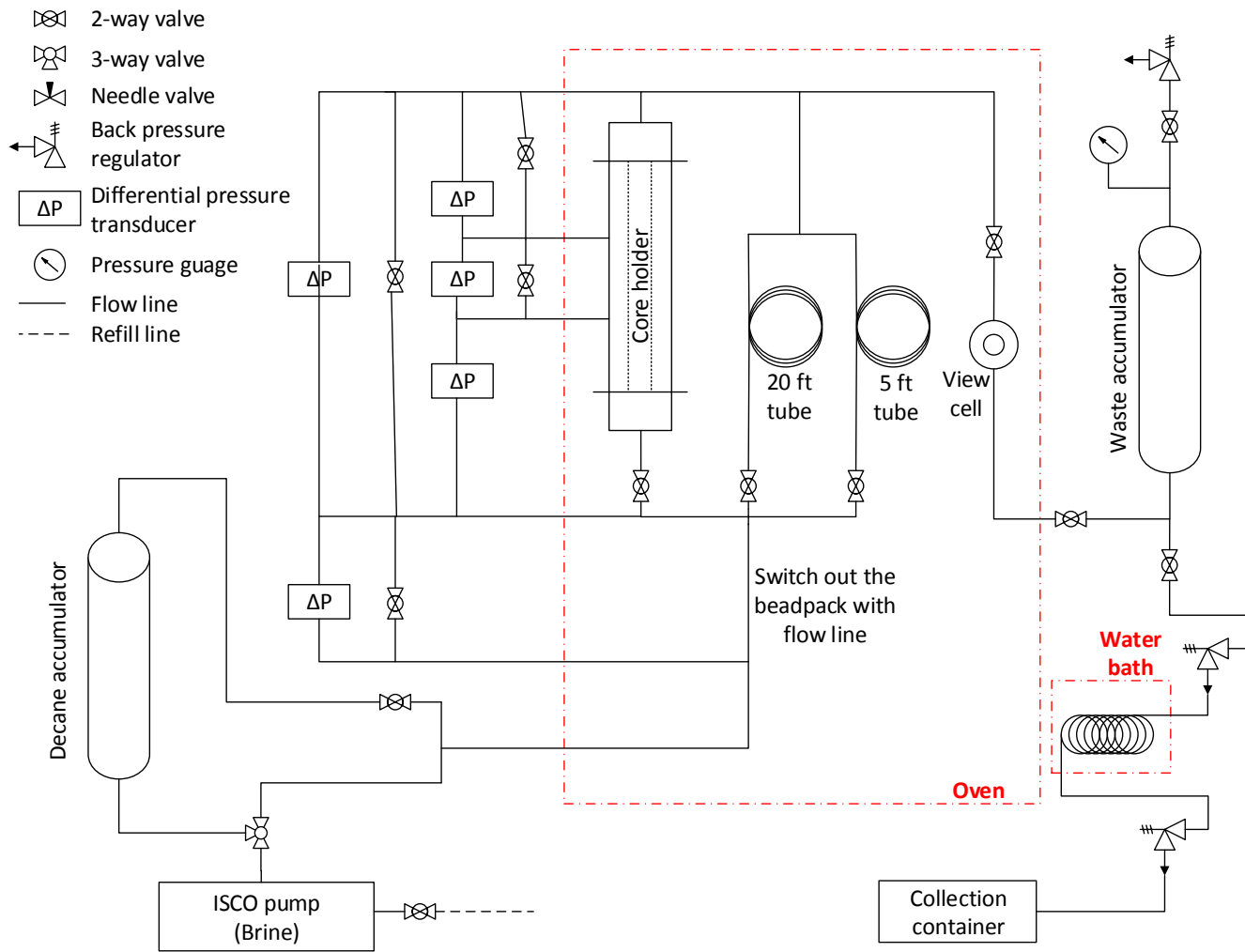


Figure 3-9 A schematic of modified coreflood system for decane injection (drainage) and waterflooding (imbibition).

Pre-generated foam EOR experiment: after the core was loaded back into the core holder. Pre-generated foam EOR experiment was performed. The experiment setup was similar to the pre-generated foam coreflood system presented earlier, however, with the addition of the fraction collector at the system outlet to collect liquid sample. As the effluent was vented continuously during flow, the multiphase flow of CO₂-brine-decane mixture through the BPR would cause a fluctuation in system pressure. Utilizing the two-BPR-in-series configuration, in conjunction with the water bath, helped alleviate the pressure fluctuation by avoiding immediate CO₂ phase change from liquid into gas. A schematic of pre-generated foam EOR coreflood system was shown in Figure 3-10. The following procedure below was used in conducting EOR coreflood experiment with pre-generated CO₂ foam. The beadpack preparation was given earlier in Section 3.3.2.1.

1. Check if the waste accumulator is reloaded and properly connected with the system and the pressure gauge. ‘Quick-connect’ fitting was installed on both sides of the waste accumulator for convenience. The waste accumulator setup will be used for back pressure monitoring.
2. Prepare the fraction collector at the outlet of the coreflood system.
3. Ensure that the CO₂ accumulator contains enough CO₂ for the experiment. Refill the CO₂ accumulator if required. Also, check if there is enough DI water in the reservoir to feed the HPLC pump during CO₂ injection.
4. Heat the water bath (containing double BPRs configuration) to approximately 80 °C.
5. Load the ISCO pump with brine (for CO₂/brine baseline) or nanoparticle dispersion (for foam experiment). Ensure that both the ISCO pump cylinder and injection line are free of trapped air.

6. Make sure the confining pressure relief valve at the core holder is closed. Apply confining pressure by operating the hand pump. Always maintain the net confining pressure at 600 psi or above.
7. Open the core holder valve but leave the core by-pass valve and the two branching valves closed.
8. Start the aqueous injection at low flow rate, using a constant flow rate mode of the ISCO pump. Start recording pressure using LabVIEW software.
9. Tighten the screw-top of the most downstream most BPR to hold the flow and let the pressure build-up to 1000 psi. Adjust confining pressure accordingly as the system pressure increase.
10. Tighten the second BPR and adjust until the desired pressure is reached. Once the system is at the desired pressure, let the flow continue until the pressure drop measurement stabilized. Always maintain at least 600 psi of net confining pressure.
11. While waiting for pressure drop to stabilized, open the two choke valves at the CO₂ accumulator and align the three-way valve toward the coreflood system. Start the HPLC pump on the CO₂ side and make sure the accumulator pressure is approximately 50 psi above the injection pressure to avoid liquid flow back into the CO₂ accumulator. Leave the CO₂ injection valve shut until ready for co-injection.
12. Introduce CO₂ into the system by opening the CO₂ injection valve. Operate the HPLC pump on constant injection rate mode. The rise of pressure drop across the beadpack mark the arrival of CO₂ and the generation of the first foam. Start collecting liquid sample using a fraction collector.

13. Once finish the experiment, stop both the ISCO pump and HPLC pump as well as shut-off the CO₂ injection valve.
14. Stop recording the data. Turn off the fraction collector. The system can be vented by slowly unscrew the BPRs until atmospheric pressure is reached.
15. Clean out all CO₂ from the core using core restoration method provided earlier. Take the core out and measure the wet weight to determine the remaining residual oil saturation.

Other types of EOR experiments: apart from pre-generated foam coreflood and the CO₂/brine injection baseline, two others types of injection were also performed to compare the mobility of injected fluids, as well as their oil recovery performance. The first one was liquid CO₂ injection (without aqueous phase injection). The procedure for CO₂ flood was very similar to pre-generated foam injection. However, only CO₂ was being injected into the core after the system pressure was brought up to the desired value through brine injection. The second type of experiment was foam slug injection where only several pore volume of foam was injected into the core before the aqueous injection was cut-off (by stopping the ISCO pump). The CO₂ injection continued, but with CO₂ injection rate increased to match the volumetric flow rate at which the slug of foam was injected. The rest of procedures, including core restoration and residual oil saturation measurement, were identical to the pre-generated foam injection experiment.

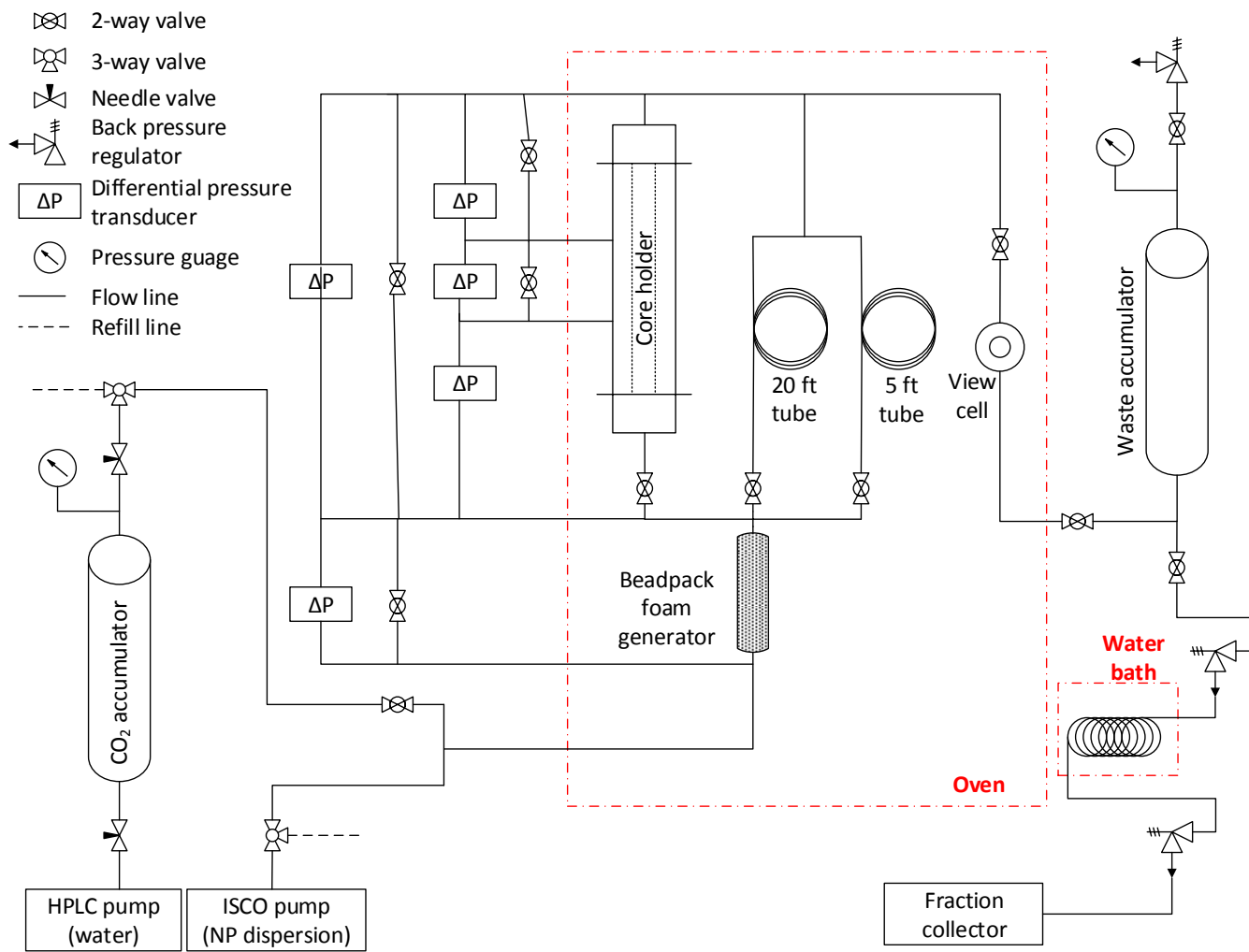


Figure 3-10 A schematic of modified co-injection system for enhanced oil recovery experiment.

3.4 DATA ANALYSIS

3.4.1 Matrix Permeability

The permeability of the core (and beadpack) used in experiments was calculated using Darcy's law:

$$k = \frac{Q\mu L}{A\Delta P}$$

k = permeability of the core (cm^2)

Q = volumetric flow rate (cm^3/s)

μ = viscosity of injected fluid ($Pa * s$)

L = length of core (cm)

A = cross sectional area of core (cm^2)

ΔP = pressure drop across core (Pa)

3.4.2 Core Apparent Viscosity

The apparent viscosity of the core was calculated using Darcy's law, considering foam as a phase:

$$\mu_{app,core} = \frac{kA\Delta P}{QL}$$

$\mu_{app,core}$ = foam apparent viscosity across the core ($Pa * s$)

k = permeability of the core (cm^2)

Q = volumetric flow rate (cm^3/s)

L = length of core (cm)

A = cross sectional area of core (cm^2)

ΔP = pressure drop across core (Pa)

3.4.3 Mobility Reduction Factor (MRF)

During co-injection of CO₂ and aqueous phases the pressure drop depends on relative permeabilities of each phase. Because this research was concerned only with the effect of nanoparticles, the contribution of phase relative permeabilities was not determined. Instead the effects of relative permeability change and apparent viscosity change were lumped together, and the term “mobility reduction factor” was used to describe the ratio of the pressure drop across the core for the foam experiment (aqueous phase contain nanoparticles) to that of the baseline experiment (aqueous phase does not contain nanoparticles). Because the apparent viscosity of the flowing fluids was proportional to pressure drop, the MRF was also equal to the ratio of apparent viscosities:

$$MRF = \frac{\Delta P_{foam}}{\Delta P_{baseline}} = \frac{\mu_{app,foam}}{\mu_{app,baseline}}$$

ΔP_{foam} = pressure drop across the core for the foam experiment (psia)

$\Delta P_{baseline}$ = pressure drop across the core for the baseline experiment (psia)

$\mu_{app,foam}$ = core apparent viscosity in the foam experiment (cP)

$\mu_{app,baseline}$ = core apparent viscosity in the baseline experiment (psia)

3.4.4 Shear Rate through the Matrix

The shear rate on the fluids flowing through a non-fractured core (and beadpack) was calculated using the following equation (Lake, 1989):

$$\dot{\gamma} = \frac{4Q}{(A\sqrt{8k\phi})}$$

$\dot{\gamma}$ = shear rate (s^{-1})

Q = volumetric flow rate (cm^3/s)

A = cross sectional flow area (cm^2)

k = permeability (cm^2)

ϕ = porosity (dimensionless)

3.4.5 Capillary Tube Apparent Viscosity

The apparent viscosity of the fluid flowing through the capillary tubing was determined using the Hagen-Poiseuille equation:

$$\mu_{app} = \frac{\pi\Delta P r^4}{8LQ}$$

μ_{app} = apparent viscosity ($Pa \cdot s$)

ΔP = pressure drop across capillary tubing (Pa)

r = inner radius of capillary tubing (cm)

L = length of capillary tubing (cm)

Q = volumetric flow rate (cm^3/s)

This equation is rigorous for laminar flow of a single phase Newtonian fluid. For typical experiment conditions in this thesis, the flow was laminar, but foam and baseline experiments always involved two fluids. Thus the term “apparent viscosity” was used.

3.4.6 Shear Rate through the Capillary Tube

Assuming single phase laminar flow, a wall shear rate in a circular capillary tube was defined as:

$$\dot{\gamma} = \frac{4Q}{\pi r^3}$$

$\dot{\gamma}$ = shear rate (s^{-1})

Q = volumetric flow rate (cm^3/s)

r = tubing radius (cm)

3.4.7 Net Confining Pressure

The net confining pressure is the difference between the pressure of the confining fluid and the pore pressure. In order to ensure a good seal around a core, it was recommended to maintain at least 600 psia of net confining pressure. The net confining pressure was defined as:

$$P_{net\ confining} = P_{confining} - P_{pore}$$

The confining pressure was read off the pressure gauge, located near the hydraulic oil hand pump. Pore pressure was estimated as followed.

$$P_{pore} = \frac{P_{in} + P_{exit}}{2}$$

3.4.8 Fracture Permeability and Aperture Size

Fracture, as referred to by Hariz (2012) and in this work, was treated as a rectangular slit whose width was infinitely larger than height. Figure 3-11 showed a schematic of fractured core cross-section, indicating fracture width (W) and height (H). Assuming a flow of single phase Newtonian fluid through a slit, a comparison of flow-through-slit equation and Darcy's law yielded a definition of fracture permeability given below for H measured in cm.

$$k_f[cm^2] = \frac{H^2}{12}$$

$$k_f[mD] = 8.44 \times 10^9 H^2$$

k_f = fracture permeability (cm^2 or mD)

H = fracture height or aperture size (cm)

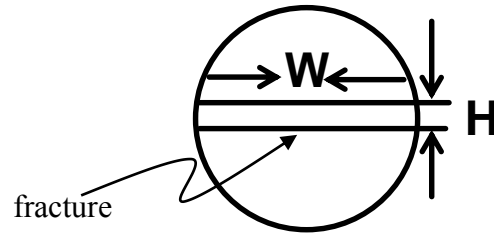


Figure 3-11 A schematic of fractured core cross-section showing fracture width (W) and height (H).

In the permeability measurement of a fractured core, the result was a combination of matrix permeability and fracture permeability. Assuming fluid was flowing through the matrix and through the fracture in parallel under the same pressure gradient, the core average permeability (\bar{k}) was given as:

$$\bar{k} = \frac{k_m * (A_c - A_f) + k_f A_f}{A_c}$$

\bar{k} = core average permeability permeability (cm^2)

k_m = matrix permeability (cm^2)

k_f = fracture permeability (cm^2)

A_f = core cross – sectional area (cm^2)

A_c = fracture cross – sectional area (cm^2)

The fracture cross-section was estimated as a rectangular slit having the area of WH . Substituting the fracture cross-sectional area (A_f) and the fracture permeability (k_f) into the core average permeability equation (\bar{k}), the following equation was obtained.

$$\bar{k} = \frac{12k_m \cdot (A_c - WH) + WH^3}{12A_c}$$

Based on the measured core average permeability (\bar{k}), matrix permeability (k_m), and core geometry, the fracture aperture size (H) was calculated and used to determine the fracture permeability (k_f). Once the fracture permeability was known, the fractions of flow in the matrix (F_m) and fracture (F_f) were determined using the following relations, respectively:

$$F_f = \frac{WH * k_f}{\bar{k} * A_{core}}$$

$$F_m = 1 - F_f$$

3.4.9 Fracture Shear Rate

Assuming a single phase laminar flow of a Newtonian fluid through a slit, a wall shear rate in fracture was calculated by the following equation (Son, 2007):

$$\dot{\gamma} = \frac{6Q}{WH^2}$$

$\dot{\gamma}$ = shear rate (s^{-1})

Q = volumetric flow rate (cm^3/s)

W = fracture width (cm)

H = fracture height or aperture size (cm)

3.4.10 Flow Decoupling Calculation for Fractured Cores

Although flow allocation between the matrix and fracture could be computed from pressure drop and total flow rate data in the case of flow of a single phase Newtonian fluid, the flow allocation calculation during foam flow was a challenge due to the foam generation threshold and the non-Newtonian nature of foam. At some specific injection rate, foam generation might have occurred in the matrix but not in the fracture, depending on flow allocation between matrix and fracture and whether the critical shear rate in each domain was reached. However, the availability of foam generation data in unfractured Boise sandstone core allowed the matrix flow to be estimated during the fractured Boise sandstone coreflood. The other information needed was the rheology of the foam. At the same experiment condition as fractured core coreflood, a relationship between core apparent viscosity and matrix shear rate was determined based on coreflood data from Hariz (2012) as shown in Figure 3-12. This coreflood data was obtained by co-injecting CO₂ and 1 wt% dispersion of 5 nm PEG-coated nanoparticle in DI water into Boise sandstone cores at 2000 psi and 23° C. As our foam generation experiments in fractured Boise sandstone cores were performed at identical experiment conditions as Hariz's, the viscosity correlation shown in Figure 3-12 was used to estimate the foam apparent viscosity in the matrix domain of our fractured Boise sandstone coreflood. Note that Hariz's data indicated shear-thickening foam rheology. As this apparent viscosity data also included the influence of foam generation, the shear-thickening behavior observed was due to the improvement of foam texture and the increase in lamellae density with the shear rate increment.

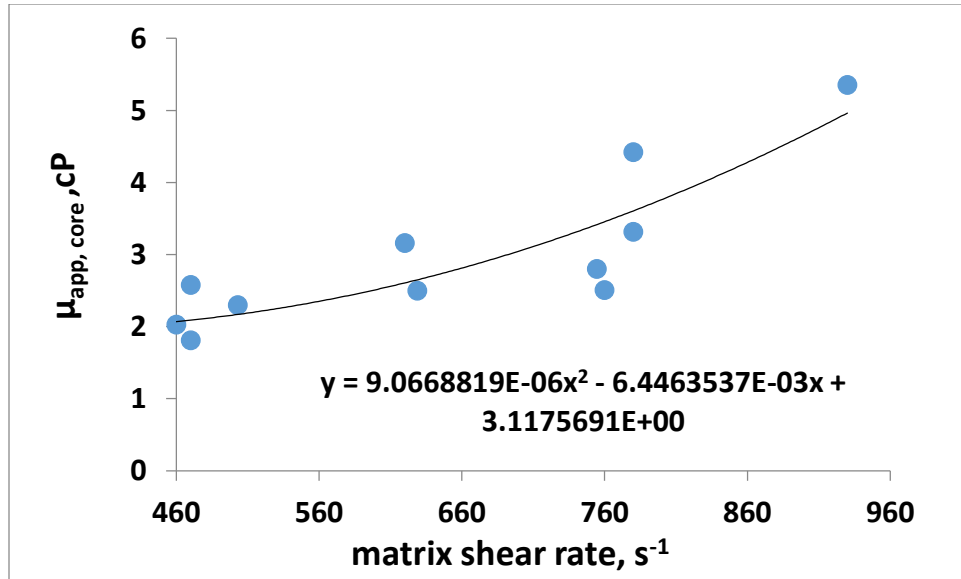


Figure 3-12 Relationship between core apparent viscosity and matrix shear rate, determined from unfractured Boise sandstone coreflood data at 23 °C and 2000 psi (Hariz, 2012). Foam was generated through co-injection of 1 wt% 5 nm PEG-coated nanoparticle dispersion in DI water and CO₂ at the phase ratio of 1:1. The correlation was established for core apparent viscosity above the critical shear rate for foam generation of 460 s⁻¹.

Because the permeabilities of matrix and fracture were known, the fracture apparent viscosity could be approximated under the simplifying assumption that there was no cross flow between fracture and matrix. Again, the fracture cross-section was estimated as a rectangular slit having the area of WH . Assuming that the mixture of CO₂ and nanoparticle dispersion was flowing as a single phase, the fluxes flowing into the fracture and into the matrix were calculated using the Darcy's equation below.

$$Q_t(1 - F_f) = \frac{k_m(A_c - WH)}{\mu_{m_{app}}} \left(\frac{\Delta P}{L} \right)$$

$$Q_t \cdot F_f = \frac{k_f WH}{\mu_{f_{app}}} \left(\frac{\Delta P}{L} \right)$$

Summing up the above two equations and re-arranging, we obtained,

$$\mu_{f_{app}} = \frac{k_f WH}{\left(\frac{\Delta P}{L}\right) - \frac{k_m(A_c - WH)}{\mu_{m_{app}}}}$$

$\mu_{f_{app}}$ = apparent viscosity in fracture (Pa · s)

$\mu_{m_{app}}$ = apparent viscosity in matrix (Pa · s)

Q_t = total volumetric flow rate (cm³/s)

ΔP = pressure drop across the core (Pa)

F_f = fraction of flow in the fracture (fraction)

k_m = matrix permeability (cm²)

k_f = fracture permeability (cm²)

W = fracture width (cm)

H = fracture aperture size (cm)

A_c = core cross – sectional area (cm²)

L = core length (cm)

To calculate $\mu_{f_{app}}$ from the equation above, we need to know $\mu_{m_{app}}$, which however was unknown being a function of the matrix shear rate, which in turn was proportional to the flow rate in matrix (i.e. $Q_t(1 - F_f)$). Below the critical shear rate in matrix, it was assumed that $\mu_{f_{app}}$ and $\mu_{m_{app}}$ were equal as no foam was generated. Above the critical shear rate, $\mu_{m_{app}}$ was determined from the correlation between the matrix apparent viscosity and the matrix shear rate as shown in Figure 3-12. The matrix shear rate, given by Lake (1989), was modified as follow:

$$\dot{\gamma}_{m_{eff}} = \frac{4Q_t(1 - F_f)}{(A_{Core} - WH)\sqrt{8K_m\phi_m}}$$

The iterative calculation of $\mu_{f_{app}}$ first started by assuming an initial value of F_f based on a single-phase Newtonian fluid flow. Then, based on the assumed F_f , flow could be allocated between the matrix and fracture domain. Next, $\mu_{m_{app}}$ and $\dot{\gamma}_{m_{eff}}$ were determined using the modified Darcy's and shear rate equations, respectively. In addition, $\mu_{m_{app}}$ was also calculated from the viscosity-shear rate correlation (Figure 3-12) at the obtained $\dot{\gamma}_{m_{eff}}$. If $\mu_{m_{app}}$ from the correlation did not agree with $\mu_{m_{app}}$ from the Darcy's equation, the new F_f was determined by substituting $\mu_{m_{app}}$ from the viscosity-shear rate correlation into the Darcy's equation for the matrix domain. The entire calculation was repeated with this new F_f and iterated until the two $\mu_{m_{app}}$ values agreed. The final F_f and $\mu_{m_{app}}$ were then used to calculate the fracture apparent viscosity ($\mu_{f_{app}}$) using the equation shown earlier. The table showing calculated results was given in Section 4.1.2.2.

3.4.11 Oil Saturation Estimation (Weight Difference Method)

In order to determine the saturation of the oil phase residing in the core, the wet weight of the core containing oil was compared to the original wet weight of the core at brine saturated condition. The weight difference was a result of the density difference between decane and brine and the change in saturation. The derivation of oil saturation from core weight was shown below:

$$W_{S_w=1} = W_{matrix} + PV \cdot \rho_w$$

$$W_{S_w=1-S_o} = W_{matrix} + PV \cdot (\rho_w \cdot (1 - S_o) + \rho_D \cdot (S_o))$$

$$W_{S_w=1} - W_{S_w=1-S_o} = PV \cdot S_o \cdot (\rho_w - \rho_D)$$

Thus,

$$S_o = \frac{(W_{S_w=1} - W_{S_w=1-S_o})}{PV \cdot (\rho_w - \rho_D)}$$

S_o = oil saturation (fraction)

$W_{S_w=1}$ = original core wet weight at brine saturated condition (g)

$W_{S_w=1-S_o}$ = wet weight of oil bearing core (g)

PV = pore volume (cm^3)

ρ_w = density of water (g/cm^3)

ρ_D = density of decane (g/cm^3)

3.4.12 Determining Pore Volume (PV) and Porosity of Rock Cores

The pore volume of rock cores as well as core porosity were determined by the difference in the core weight at different saturation conditions using the relationship below. The weight of core matrix was the dry weight of the core (before vacuumed) as the weight of trapped air is negligible.

$$PV = \frac{W_{S_w=1} - W_{matrix}}{\rho_w}$$

Thus,

$$\phi = \frac{PV}{AL}$$

PV = pore volume (cm^3)

$W_{S_w=1}$ = core wet weight at brine saturated condition (g)

W_{matrix} = core dry weight at zero water saturation condition (g)

ρ_w = density of water (g/cm^3)

ϕ = pore volume (cm^3)

A = cross – sectional area of the core (cm^2)

L = core length (cm)

Chapter 4 Results and Discussions

4.1 FOAM GENERATION EXPERIMENTS BY CO-INJECTION METHOD

The aim of the foam experiments described in this section was to investigate the ability of surface-modified silica nanoparticle in stabilizing CO₂-water foam at different condition as well as the shear rate threshold phenomena. These foam generation experiments were carried out in the rock cores using the co-injection method and the experiment setup described earlier in section 3.3.1. Nanoparticle dispersion and CO₂ were co-injected directly into the rock core where differential pressure drop across the core was measured. Pressure drop across the core is converted into apparent viscosity and also compared with the baseline experiment (same core, same fluids and injection rates but without nanoparticles) to infer mobility reduction factor (MRF).

To represent a wide variety of reservoir formations, various types of cores were used in these experiments, including both unfractured matrix and artificially fractured core (by means of loading until failure in tension in a load frame). The effect of matrix permeability on foam generation was also investigated using very high permeability Boise sandstone cores, high permeability Berea sandstone cores and the low permeability limestone cores. Table 4-1 listed the average petrophysical properties of each matrix type used in these experiments.

Table 4-1 Matrix types and petrophysical properties of rock core used in foam generation experiment.

Matrix type	Permeability	Avg. Porosity
Boise sandstone	1000 – 3000 mD	29%
Berea sandstone	150 – 250 mD	21%
Indiana limestone	5-10 mD	18%

Another key factor that possibly played an important role in foam generation was the properties of the CO₂ phase. Thus, the investigation in this section was divided into the following two main parts according to the state of carbon dioxide phase: liquid CO₂ experiments (at room temperature) and supercritical CO₂ experiments. Table 4-2 summarized the results and key parameters of the coreflood experiments. Any plots of apparent viscosity versus pore volume injected which were not presented in this section were given in the appendix.

Table 4-2 Summary of foam generation experiment in unfractured matrix core. The entries in first column indicate the core material (B, BS = Boise, BR, BRS = Berea, IL = Indiana limestone), core number and injection stage (total flow rates were varied sequentially in a typical experiment).

*Apparent viscosity reported in experiments BR 4/1-2 measured in downstream capillary viscometer.

** Experiment BS 2/11-17 contain 0.04 wt% LAPB surfactant in the aqueous phase.

Exp.	ϕ	K (mD)	T (°C)	P _{outlet} (psi)	NP type	%NP	Salt %TDS	Fg	Q (ml/min)	V _{sup} (ft/d)	Shear rate (s ⁻¹)	dP (psi)	Core μ_{app} (cP)	Foam in view cell
B 4/1	0.29	1940	23	2000	5 nm PEG (3M)	1	0	0.50	3	28	190	5.2	2.1	N
B 4/2	0.29	1940	23	2000	5 nm PEG (3M)	1	0	0.50	6	56	370	7.7	2.0	Y
B 4/3	0.29	1940	23	2000	5 nm PEG (3M)	1	0	0.50	8	75	500	9.6	2.2	Y
B 4/4	0.29	1940	23	2000	5 nm PEG (3M)	1	0	0.50	10	93	620	12.5	2.4	Y
B 4/5	0.29	1940	23	2000	5 nm PEG (3M)	1	0	0.50	12	112	740	15.5	2.7	Y
B 5/1	0.29	1576	23	2000	5 nm PEG (3M)	1	2	0.67	3	28	210	6.8	1.5	Y

Table 4-2 (continued)

Exp.	ϕ	K (mD)	T (°C)	P _{outlet} (psi)	NP type	%NP	Salt %TDS	Fg	Q (ml/min)	V _{sup} (ft/d)	Shear rate (s ⁻¹)	dP (psi)	Core μ_{app} (cP)	Foam in view cell
B 5/2	0.29	1576	23	2000	5 nm PEG (3M)	1	2	0.67	6	56	420	11.3	1.5	Y
B 5/3	0.29	1575	23	2000	5 nm PEG (3M)	1	2	0.67	9	84	620	16.3	1.6	Y
B 5/4	0.29	1576	23	2000	5 nm PEG (3M)	1	2	0.67	12	112	830	22.2	1.7	Y
B 6/1	0.29	1740	23	2000	5 nm PEG (3M)	1	2	0.80	3	28	200	6.3	1.3	N
B 6/2	0.29	1740	23	2000	5 nm PEG (3M)	1	2	0.80	6	56	400	10.9	1.6	Y
B 6/3	0.29	1740	23	2000	5 nm PEG (3M)	1	2	0.80	9	84	590	15.0	1.6	Y
B 6/4	0.29	1740	23	2000	5 nm PEG (3M)	1	2	0.80	12	112	790	19.3	1.6	Y
B 6/5	0.29	1740	23	2000	5 nm PEG (3M)	1	2	0.80	15	140	980	24.1	1.7	Y
B 4/1BL	0.29	1940	23	2000	none	0	0	0.50	3	28	190	4.3	1.7	N
B 4/2BL	0.29	1940	23	2000	none	0	0	0.50	6	56	370	6.4	1.7	N
B 4/3BL	0.29	1940	23	2000	none	0	0	0.50	8	75	500	7.9	1.7	N
B 4/4BL	0.29	1940	23	2000	none	0	0	0.50	10	93	620	9.5	1.7	N
B 4/5BL	0.29	1940	23	2000	none	0	0	0.50	12	112	740	10.5	1.7	N
B 5/1BL	0.29	1576	23	2000	none	0	2	0.67	3	28	210	6.6	1.5	N
B 5/2BL	0.29	1576	23	2000	none	0	2	0.67	6	56	420	10.6	1.4	N
B 5/3BL	0.29	1575	23	2000	none	0	2	0.67	9	84	620	13.9	1.4	N
B 5/4BL	0.29	1576	23	2000	none	0	2	0.67	12	112	830	17.8	1.3	N
B 6/1BL	0.29	1740	23	2000	none	0	2	0.80	3	28	200	6.2	1.3	N
B 6/2BL	0.29	1740	23	2000	none	0	2	0.80	6	56	400	9.7	1.3	N
B 6/3BL	0.29	1740	23	2000	none	0	2	0.80	9	84	590	13.2	1.4	N
B 6/4BL	0.29	1740	23	2000	none	0	2	0.80	12	112	790	16.0	1.3	N
B 6/5BL	0.29	1740	23	2000	none	0	2	0.80	15	140	980	19.7	1.3	N
BR 3	0.21	127	23	2000	5 nm PEG (3M)	1	2	0.50	2	19	570	101	2.7	Y

Table 4-2 (continued)

Exp.	ϕ	K (mD)	T (°C)	P _{outlet} (psi)	NP type	%NP	Salt %TDS	Fg	Q (ml/min)	V _{sup} (ft/d)	Shear rate (s ⁻¹)	dP (psi)	Core μ_{app} (cP)	Foam in view cell
BR 4/1	0.21	175	23	2000	5 nm PEG (3M)	1	2	0.50	1	9	250	n/a	0.72*	N
BR 4/2	0.21	175	23	2000	5 nm PEG (3M)	1	2	0.50	1.5	14	370	n/a	2.82*	Y
IL 1/1	0.18	7	23	1500	5 nm PEG (3M)	1	2	0.50	0.3	3	380	124	4.6	Y
IL 1/2	0.18	7	23	1500	5 nm PEG (3M)	1	2	0.50	0.5	5	640	178	3.5	Y
IL 1/3	0.18	7	23	1500	5 nm PEG (3M)	1	2	0.50	0.7	7	890	228	3.3	Y
IL 1/4	0.18	7	23	1500	5 nm PEG (3M)	1	2	0.50	0.9	8	1140	255	2.8	Y
IL 1/5	0.18	7	23	1500	5 nm PEG (3M)	1	2	0.50	1.5	14	1900	357	2.4	Y
IL 1/1BL	0.18	7	23	1500	none	0	2	0.50	0.3	3	380	86	1.6	N
IL 1/2BL	0.18	7	23	1500	none	0	2	0.50	0.5	5	640	123	1.5	N
IL 1/4BL	0.18	7	23	1500	none	0	2	0.50	0.9	8	1140	210	1.5	N
BS 1/1	0.29	3230	50	2000	EOR-5xs	1	2	0.57	3.5	32	170	7.5	4.5	N
BS 1/2	0.29	3230	50	2000	EOR-5xs	1	2	0.57	7.0	65	340	30.4	9.3	Y
BS 1/3	0.29	3230	50	2000	EOR-5xs	1	2	0.57	10.4	97	500	50	10.2	Y
BS 1/4	0.29	3230	50	2000	EOR-5xs	1	2	0.57	13.9	130	670	70.1	10.8	Y
BS 1/5	0.29	3230	50	2000	EOR-5xs	1	2	0.57	17.4	162	840	88.9	11.0	Y
BS 1/6	0.29	3230	50	2000	EOR-5xs	1	2	0.75	3	28	150	2.2	1.5	N
BS 1/7	0.29	3230	50	2000	EOR-5xs	1	2	0.75	6	56	290	5	1.8	N
BS 1/8	0.29	3230	50	2000	EOR-5xs	1	2	0.75	9	84	430	9.6	2.2	Y
BS 1/9	0.29	3230	50	2000	EOR-5xs	1	2	0.75	12	112	580	17.1	3.1	Y
BS 1/10	0.29	3230	50	2000	EOR-5xs	1	2	0.75	15	140	720	26.8	3.9	Y

Table 4-2 (continued)

Exp.	ϕ	K (mD)	T (°C)	P _{outlet} (psi)	NP type	%NP	Salt %TDS	Fg	Q (ml/min)	V _{sup} (ft/d)	Shear rate (s ⁻¹)	dP (psi)	Core μ_{app} (cP)	Foam in view cell
BS 1/11	0.29	3230	80	2000	EOR-5xs	1	2	0.75	5	47	240	2.8	1.4	N
BS 1/12	0.29	3230	80	2000	EOR-5xs	1	2	0.75	10	93	480	7.6	1.7	N
BS 1/13	0.29	3230	80	2000	EOR-5xs	1	2	0.75	15	140	720	11.2	1.5	N
BS 1/14	0.29	3230	80	2000	EOR-5xs	1	2	0.75	20	186	960	14.8	1.5	N
BS 1/15	0.29	3230	80	2000	EOR-5xs	1	2	0.75	25	233	1200	20.3	1.7	N
BS 1/16	0.29	3230	80	2000	EOR-5xs	1	2	0.75	40	373	1920	28.4	1.6	N
BS 1/1BL	0.29	3230	50	2000	none	0	2	0.57	3.5	32	170	2.8	1.6	N
BS 1/2BL	0.29	3230	50	2000	none	0	2	0.57	7.0	65	340	6.7	2.2	N
BS 1/3BL	0.29	3230	50	2000	none	0	2	0.57	10.4	97	500	13.1	2.7	N
BS 1/4BL	0.29	3230	50	2000	none	0	2	0.57	13.9	130	670	16.6	2.6	N
BS 1/5BL	0.29	3230	50	2000	none	0	2	0.57	17.4	162	840	21.1	2.6	N
BS 1/6BL	0.29	3230	50	2000	none	0	2	0.75	3	28	150	1.5	1.3	N
BS 1/7BL	0.29	3230	50	2000	none	0	2	0.75	6	56	290	4.2	1.5	N
BS 1/8BL	0.29	3230	50	2000	none	0	2	0.75	9	84	430	6.3	1.6	N
BS 1/9BL	0.29	3230	50	2000	none	0	2	0.75	12	112	580	10.1	1.7	N
BS 1/10BL	0.29	3230	50	2000	none	0	2	0.75	15	140	720	11.9	1.7	N
BS 1/11BL	0.29	3230	80	2000	none	0	2	0.75	5	47	240	2.6	1.3	N
BS 1/12BL	0.29	3230	80	2000	none	0	2	0.75	10	93	480	7.8	1.6	N
BS 1/13BL	0.29	3230	80	2000	none	0	2	0.75	15	140	720	10.5	1.6	N
BS 1/14BL	0.29	3230	80	2000	none	0	2	0.75	20	186	960	15	1.6	N
BS 1/15BL	0.29	3230	80	2000	none	0	2	0.75	25	233	1200	20.9	1.8	N
BS 2/1	0.29	2250	80	2200	EOR-5xs	1	2	0.50	10	93	580	5	0.8	N
BS 2/2	0.29	2250	80	2200	EOR-5xs	1	2	0.50	15	140	860	8	0.8	N
BS 2/3	0.29	2250	80	2200	EOR-5xs	1	2	0.50	20	186	1150	14	1.1	N
BS 2/4	0.29	2250	80	2200	EOR-5xs	1	2	0.50	25	233	1440	17.5	1.1	N
BS 2/5	0.29	2250	80	2200	EOR-5xs	5	2	0.50	25	233	1440	15	0.9	N

Table 4-2 (continued)

Exp.	ϕ	K (mD)	T (°C)	P _{outlet} (psi)	NP type	%NP	Salt %TDS	Fg	Q (ml/min)	V _{sup} (ft/d)	Shear rate (s ⁻¹)	dP (psi)	Core μ_{app} (cP)	Foam in view cell
BS 2/6	0.29	2250	80	2200	EOR-5xs	5	2	0.50	40	373	2290	28	1.1	N
BS 2/7	0.29	2250	80	2200	EOR-5xs	1	4	0.50	10	93	580	6	0.9	N
BS 2/8	0.29	2250	80	2200	EOR-5xs	1	4	0.50	15	140	860	10	1.0	Y
BS 2/9	0.29	2250	80	2200	EOR-5xs	1	4	0.50	20	186	1150	31	2.4	Y
BS 2/10	0.29	2250	80	2200	EOR-5xs	1	4	0.50	25	233	1440	45	2.7	Y
BS 2/11**	0.29	2250	80	2200	EOR-5xs	1	4	0.50	5	47	290	11	3.4	Y
BS 2/12**	0.29	2250	80	2200	EOR-5xs	1	4	0.50	10	93	580	65	9.9	Y
BS 2/13**	0.29	2250	80	2200	EOR-5xs	1	4	0.50	15	140	860	80	8.1	Y
BS 2/14**	0.29	2250	80	2200	EOR-5xs	1	4	0.50	20	186	1150	100	7.6	Y
BS 2/15**	0.29	2250	80	2200	none	0	4	0.50	5	47	290	4.7	1.4	N
BS 2/16**	0.29	2250	80	2200	none	0	4	0.50	10	93	580	16	2.4	N
BS 2/17**	0.29	2250	80	2200	none	0	4	0.50	15	140	860	28	2.8	N
BS 2/1BL	0.29	2250	80	2200	none	0	4	0.50	5	47	290	2.3	0.7	N
BS 2/2BL	0.29	2250	80	2200	none	0	4	0.50	10	93	580	5.2	0.8	N
BS 2/3BL	0.29	2250	80	2200	none	0	4	0.50	15	140	860	7.5	0.8	N
BS 2/4BL	0.29	2250	80	2200	none	0	4	0.50	20	186	1150	9.6	0.7	N
BS 2/5BL	0.29	2250	80	2200	none	0	4	0.50	25	233	1440	12.2	0.7	N
BS 3/1	0.30	3000	80	2200	EOR-5xs	1	2	0.50	4	37	200	3.4	0.9	N
BS 3/2	0.30	3000	80	2200	EOR-5xs	1	2	0.50	8	75	390	4.9	0.8	N
BS 3/3	0.30	3000	80	2200	EOR-5xs	1	2	0.50	12	112	590	6.5	0.8	N
BS 3/4	0.30	3000	80	2200	EOR-5xs	1	2	0.50	16	149	780	8.5	0.9	N
BS 3/5	0.30	3000	80	2200	EOR-5xs	1	2	0.50	20	186	980	11.8	1.0	Y
BS 3/6	0.30	3000	80	2200	EOR-5xs	1	2	0.50	24	224	1170	15.5	1.1	Y
BS 3/7	0.30	3000	80	2200	EOR-5xs	1	3	0.50	8	75	390	3.5	0.9	N

Table 4-2 (continued)

Exp.	ϕ	K (mD)	T (°C)	P _{outlet} (psi)	NP type	%NP	Salt %TDS	Fg	Q (ml/min)	V _{sup} (ft/d)	Shear rate (s ⁻¹)	dP (psi)	Core μ_{app} (cP)	Foam in view cell
BS 3/8	0.30	3000	80	2200	EOR-5xs	1	3	0.50	12	112	590	5.4	0.9	N
BS 3/9	0.30	3000	80	2200	EOR-5xs	1	3	0.50	16	149	780	8.8	1.1	Y
BS 3/10	0.30	3000	80	2200	EOR-5xs	1	3	0.50	20	186	980	13.3	1.4	Y
BS 3/11	0.30	3000	80	2200	EOR-5xs	1	3	0.50	24	224	1170	18.0	1.5	Y
BS 3/12	0.30	3000	80	2200	EOR-5xs	1	4	0.50	30	280	1470	1.6	0.8	Y
BS 3/13	0.30	3000	80	2200	EOR-5xs	1	4	0.50	8	75	390	3.7	0.9	Y
BS 3/14	0.30	3000	80	2200	EOR-5xs	1	4	0.50	12	112	590	6.2	1.1	Y
BS 3/15	0.30	3000	80	2200	EOR-5xs	1	4	0.50	16	149	780	10.0	1.3	Y
BS 3/16	0.30	3000	80	2200	EOR-5xs	1	4	0.50	20	186	980	14.0	1.4	Y
BS 3/17	0.30	3000	80	2200	EOR-5xs	1	4	0.50	24	224	1170	18.0	1.5	Y
BS 3/1BL	0.30	3000	80	2200	none	0	2	0.50	4	37	200	1.6	0.8	N
BS 3/2BL	0.30	3000	80	2200	none	0	2	0.50	8	75	390	3.5	0.9	N
BS 3/3BL	0.30	3000	80	2200	none	0	2	0.50	12	112	590	5.2	0.9	N
BS 3/4BL	0.30	3000	80	2200	none	0	2	0.50	16	149	780	7.2	0.9	N
BS 3/5BL	0.30	3000	80	2200	none	0	2	0.50	20	186	980	8.8	0.9	N
BS 3/6BL	0.30	3000	80	2200	none	0	2	0.50	24	224	1170	10.2	0.9	N
BS 4/1	0.31	3360	57	2200	EOR-5xs	0.1	7.2	0.75	5	47	230	3	1.4	Y
BS 4/2	0.31	3360	57	2200	EOR-5xs	0.1	7.2	0.75	10	93	460	6.6	1.5	Y
BS 4/3	0.31	3360	57	2200	EOR-5xs	0.1	7.2	0.75	15	140	680	11.2	1.7	Y
BS 4/4	0.31	3360	57	2200	EOR-5xs	0.1	7.2	0.75	18	168	820	13.6	1.7	Y
BS 4/5	0.31	3360	57	2200	EOR-5xs	0.1	7.2	0.75	22	205	1000	17.3	1.9	Y
BS 4/6	0.31	3360	57	2200	EOR-5xs	0.5	7.2	0.75	5	47	230	7	3.2	Y
BS 4/7	0.31	3360	57	2200	EOR-5xs	0.5	7.2	0.75	10	93	460	38.2	8.7	Y
BS 4/8	0.31	3360	57	2200	EOR-5xs	0.5	7.2	0.75	15	140	680	76.5	11.6	Y
BS 4/10	0.31	3360	57	2200	EOR-5xs	0.5	7.2	0.75	22	205	1000	102	10.3	Y

Table 4-2 (continued)

Exp.	ϕ	K (mD)	T (°C)	P _{outlet} (psi)	NP type	%NP	Salt %TDS	Fg	Q (ml/min)	V _{sup} (ft/d)	Shear rate (s ⁻¹)	dP (psi)	Core μ_{app} (cP)	Foam in view cell
BS 4/11	0.31	2940	57	2200	EOR-5xs	1	7.2	0.75	5	47	230	9	3.61	Y
BS 4/12	0.31	2940	57	2200	EOR-5xs	1	7.2	0.75	10	93	460	63.2	12.6	Y
BS 4/13	0.31	2940	57	2200	EOR-5xs	1	7.2	0.75	15	140	680	113	15.0	Y
BS 4/15	0.31	2940	57	2200	EOR-5xs	1	7.2	0.75	22	205	1000	161	14.6	Y
BS 4/1BL	0.31	3360	57	2200	none	0	7.2	0.75	5	47	230	1.6	0.8	N
BS 4/2BL	0.31	3360	57	2200	none	0	7.2	0.75	10	93	460	3.1	0.8	N
BS 4/3BL	0.31	3360	57	2200	none	0	7.2	0.75	15	140	680	4.5	0.8	N
BS 4/4BL	0.31	3360	57	2200	none	0	7.2	0.75	18	168	820	5.6	0.8	N
BS 4/5BL	0.31	3360	57	2200	none	0	7.2	0.75	22	205	1000	6.9	0.8	N
BRS 1/1	0.21	220	80	2200	EOR-5xs	1	4	0.5	2	19	400	15	1.1	N
BRS 1/2	0.21	220	80	2200	EOR-5xs	1	4	0.5	3	28	600	37	1.8	Y
BRS 1/3	0.21	220	80	2200	EOR-5xs	1	4	0.5	4	37	800	55	2.0	Y
BRS 1/4	0.21	220	80	2200	EOR-5xs	1	4	0.5	6	56	1190	105	2.6	Y
BRS 1/5	0.21	220	80	2200	EOR-5xs	1	4	0.5	8	75	1590	160	2.9	Y
BRS 1/1BL	0.21	220	80	2200	none	0	4	0.5	2	19	400	15	1.1	N
BRS 1/2BL	0.21	220	80	2200	none	0	4	0.5	3	28	600	27	1.3	N
BRS 1/3BL	0.21	220	80	2200	none	0	4	0.5	4	37	800	35	1.3	N
BRS 1/4BL	0.21	220	80	2200	none	0	4	0.5	6	56	1190	60	1.5	N
BRS 1/5BL	0.21	220	80	2200	none	0	4	0.5	8	75	1590	76	1.4	N
BRS 2/1	0.21	170	57	2200	EOR-5xs	0.5	7.2	0.75	1	9	250	18.2	2.17	N
BRS 2/2	0.21	170	57	2200	EOR-5xs	0.5	7.2	0.75	2	19	490	53.8	3.05	Y
BRS 2/3	0.21	170	57	2200	EOR-5xs	0.5	7.2	0.75	3	28	740	109	4.22	Y
BRS 2/4	0.21	170	57	2200	EOR-5xs	0.5	7.2	0.75	4	37	980	171	5.01	Y
BRS 2/5	0.21	170	57	2200	EOR-5xs	0.5	7.2	0.75	6	56	1470	298	5.74	Y

Table 4-2 (continued)

Exp.	ϕ	K (mD)	T (°C)	P _{outlet} (psi)	NP type	%NP	Salt %TDS	Fg	Q (ml/min)	V _{sup} (ft/d)	Shear rate (s ⁻¹)	dP (psi)	Core μ_{app} (cP)	Foam in view cell
BRS 2/6	0.21	170	57	2200	EOR-5xs	0.5	7.2	0.75	8	75	1960	442	6.35	Y
BRS 2/1BL	0.21	170	57	2200	none	0	7.2	0.75	1	9	250	3.9	0.55	N
BRS 2/2BL	0.21	170	57	2200	none	0	7.2	0.75	2	19	490	11	0.78	N
BRS 2/3BL	0.21	170	57	2200	none	0	7.2	0.75	3	28	740	13.4	0.63	N
BRS 2/4BL	0.21	170	57	2200	none	0	7.2	0.75	4	37	980	18.5	0.65	N
BRS 2/5BL	0.21	170	57	2200	none	0	7.2	0.75	6	56	1470	35.7	0.83	N

4.1.2 Foam Generation Experiments with Liquid CO₂

Co-injection experiments were first carried out at ambient temperature (23 °C) and 2000 psi to test the ability of nanoparticles to stabilize CO₂ droplets. At this condition, CO₂ was in a liquid state, having the density of 0.877 g/ml (see Figure 3-5). For the simplicity, the term foam was used to describe liquid-CO₂/water emulsion observed in the following experiments.

4.1.2.1 Experiments in very high permeability Boise sandstone cores (~2000 mD)

The first experiment (B4) was carried out in a 6-inch unfractured Boise sandstone core at 2000 psi and 23 °C. Following the procedure stated in Chapter 3, the baseline apparent viscosity was first established by injecting DI water and CO₂ at a volumetric phase ratio of 1:1. The dispersion of 1 wt% 5 nm 3M PEG-coated nanoparticles was then prepared using DI water and co-injected into the core with CO₂ at the same volumetric phase ratio. Pressure drops were measured across the core in both experiments and later converted into apparent viscosities. For comparison, the plots of apparent viscosity versus pore volume injected for the baseline and foam experiments were shown in Figure 4-1 and Figure 4-2, respectively. It can be observed that the baseline apparent viscosity was relatively insensitive to the injection rates and was approximately 1.7 cP in average.

Nanoparticle-stabilized CO₂ foam was successfully generated in the Boise sandstone core as suggested by the increase in an apparent viscosity and the view cell observation (Table 4-3). The highest apparent viscosity was 2.6 cP or MRF of around 1.6 at the injection rate of 12 ml/min. At each injection rate, the apparent viscosity always approached a certain value and became stable as the foam generation and transport reached the steady state. The steady pressure drop implies that the nanoparticle-stabilized CO₂ foam did not damage the rock matrix (such damage would be cumulative during co-injection and

thus cause steadily increasing pressure drop). This suggests the feasibility of a long-range foam transport.

Although the increase in apparent viscosity from baseline was small at the injection rate below 6 ml/min, the viscosity trend and the appearance of fluids/foam was significant at the injection rate of 8 ml/min and above. This suggested that the critical shear rate of foam generation occurred between the injection rate of 6 and 8 ml/min, which could be calculated as between 380 and 500 s⁻¹. This threshold value was consistent with the critical shear rate of 460 s⁻¹ reported by Hariz (2012) with the same rock type and experiment conditions. Figure 4-3 compared the core MRF of this coreflood (B4) with Hariz's results (open symbols mean no foam in view cell; filled symbols mean foam present in view cell; photographs of view cell in Figure 4-2).

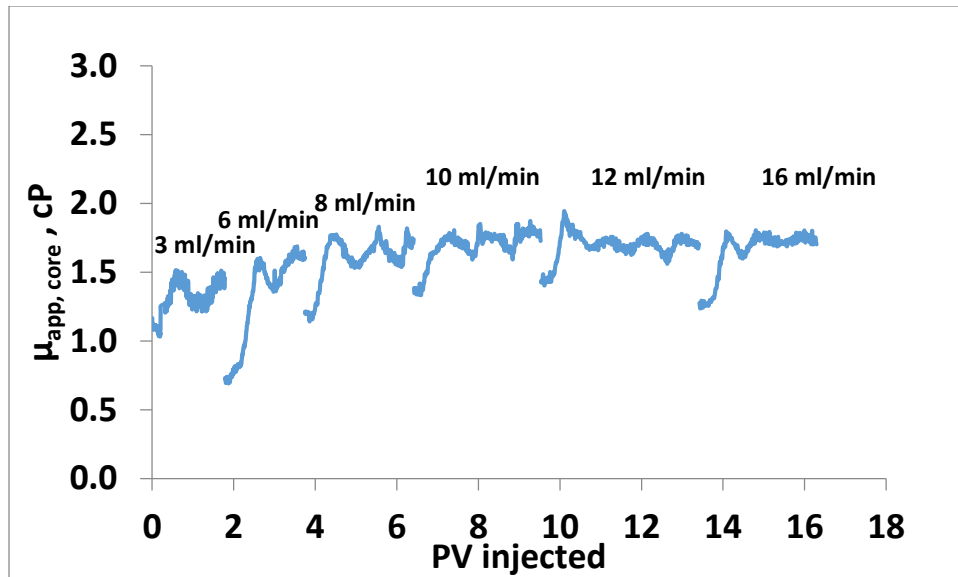


Figure 4-1 Apparent viscosity measured across core B4 in the baseline experiment (DI water + CO₂) plotted against pore volumes injected. The experiment was performed at 2000 psia and 23 °C, using volumetric phase ratio of 1:1.

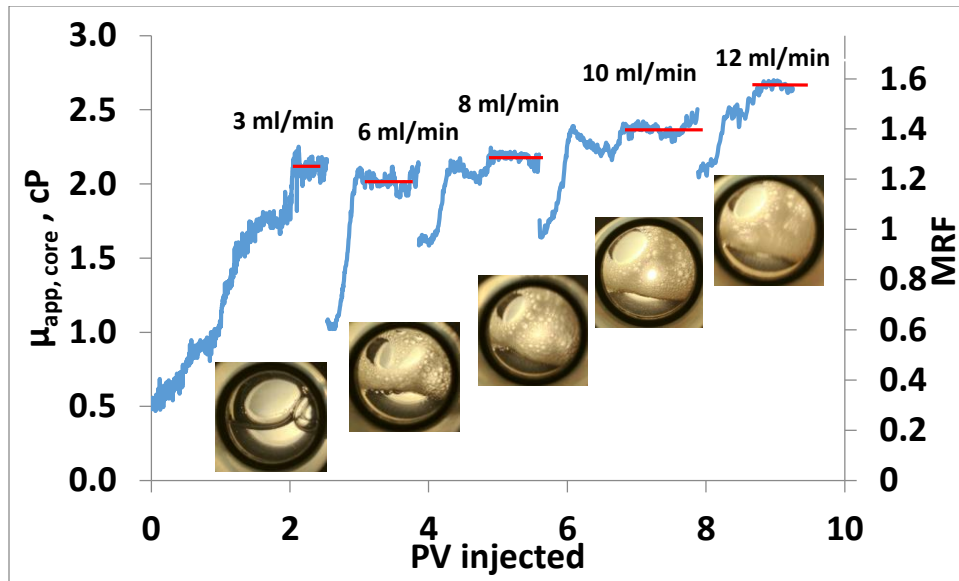


Figure 4-2 Apparent viscosity measured across core B4 in foam experiment (1wt% 3M PEG-coated nanoparticle in DI water + CO₂) plotted against pore volumes injected. The experiment was performed at 2000 psia and 23 °C, using volumetric phase ratio of 1:1 (foam quality of 0.5). Core MRF were calculated based on baseline apparent viscosity of 1.69 cP.

Two additional corefloods (B5 and B6) in 12-inch Boise sandstone cores were conducted to see the feasibility of foam generation at higher qualities, 0.67 and 0.80. Instead of using DI water, 5 nm 3M PEG-coated nanoparticles was dispersed in 2 wt% NaCl brine to obtain 1 wt% nanoparticle dispersion. The increase in aqueous phase salinity should promote foam stabilization by increasing the nanoparticle affinity to be at the interface between the aqueous phase and CO₂ (Worthen et al., 2012; Worthen et al., 2013a). According to the MRF plot in Figure 4-4, an increase in the core MRF started at around 400 s⁻¹ in both cases which could be considered to be the critical shear rate for foam generation. However, the trends of increasing MRF were more gradual in the cases at the higher foam qualities. The shear rate required to generate foam tended to increase with increasing foam quality.

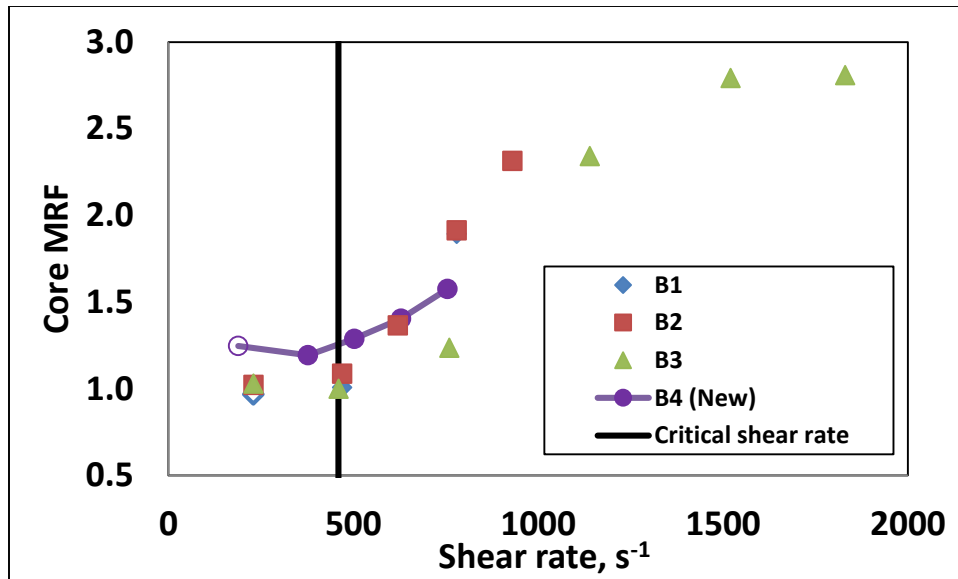


Figure 4-3 Core MRF versus core shear rate measured in core B4 (purple dots, this work), plotted in comparison with the experiment data from Hariz (2012). Open symbols indicate no foam visible in view cell; filled symbols indicate visible foam. All experiments performed at 2000 psia and 23 °C, using 1 wt% 3M PEG-coated nanoparticle in DI water and foam quality of 0.5.

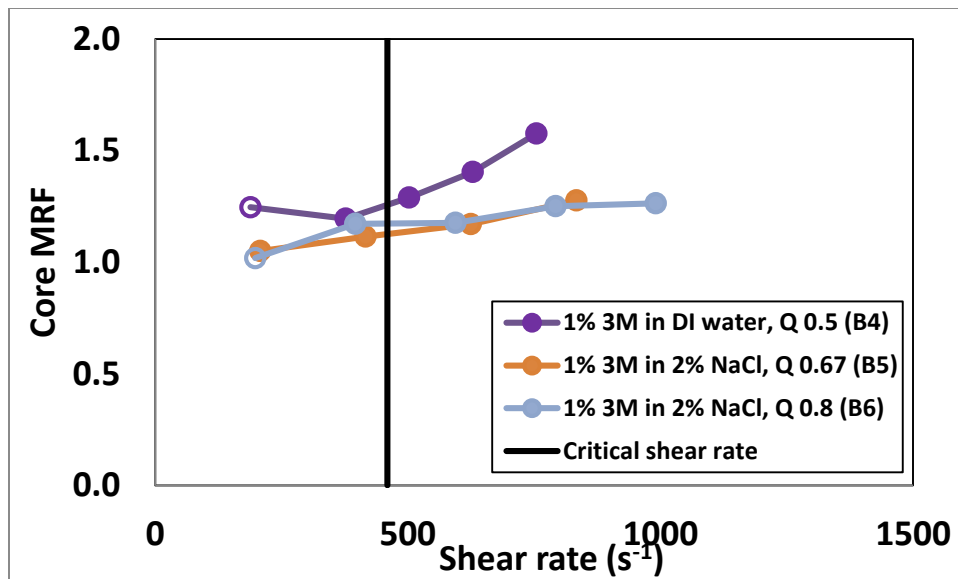
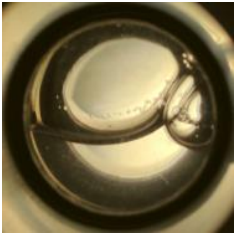
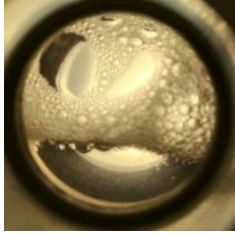

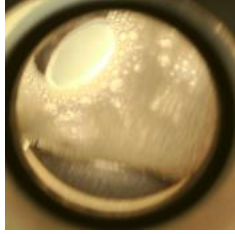

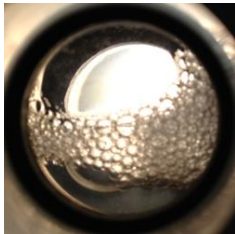
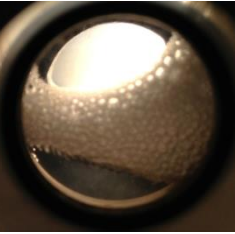
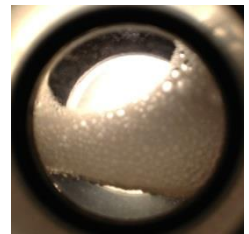
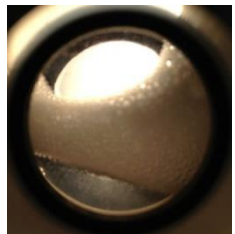
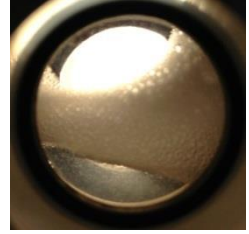




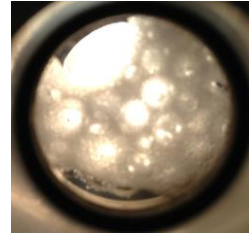


Figure 4-4 plot of core MRF vs. core shear rate, showing influence of foam quality Q and salinity on foam generation. Open symbols indicate no foam visible in view cell; filled symbols indicate visible foam. All experiments performed at 2000 psia and 23 °C, using 1 wt% 3M PEG-coated nanoparticle dispersion. Salinity and foam quality were varied.

Table 4-3 Summary of view cells observation of foam experiment in Boise sandstone core B4, B5 and B6.

Flow rate →	3 ml/min	6 ml/min	9 ml/min	12 ml/min	15 ml/min
Core ↓	$\sim 200 \text{ s}^{-1}$	$\sim 400 \text{ s}^{-1}$	$\sim 600 \text{ s}^{-1}$	$\sim 800 \text{ s}^{-1}$	$\sim 1000 \text{ s}^{-1}$
Core B4 $f_g = 0.5$ 1 wt% 5 nm 3M in DI water					
Core B5 $f_g = 0.67$ 1 wt% 5 nm 3M in 2 wt% NaCl					
Core B6 $f_g = 0.8$ 1 wt% 5 nm 3M in 2 wt% NaCl					

The view cell observations (Table 4-3) were also consistent with the MRF trends as the fine texture foam was observed at the shear rate above 200 s^{-1} . However, the bubble size distribution was large in the case with foam quality of 0.8 (inspected with unaided eyes). The large CO_2 bubbles, possibly formed by the coalescence of unstable foam, were evident among the finer opaque foam. This may suggest that the dryer foam with a quality of 0.8 was less stable as the lamellae were thinner and easier to break. As a result, this dryer foam has lower apparent viscosity and seems to require larger shear rate to refine its texture.

The internal pressure tap measurements in experiments B5 and B6 provided an insightful information of foam generation in three separate sections of the core. With the internal pressure taps, pressure drops were measured individually in three 4-inch sections; upstream, middle, and downstream sections. The sectional pressure drops of experiment B5 were converted to apparent viscosities and plotted in Figure 4-5 and Figure 4-6 for baseline and foam experiments, respectively.

As shown in Figure 4-5, apparent viscosities of the baseline experiment were approximately 1.3 cP for all three sections at every injection rate. However, this was not the case for the foam generation experiment. Shown in Figure 4-6 at 6 ml/min, the apparent viscosity remained at a baseline level in the upstream section but increased in the middle and downstream sections. It is possible that the low shear rate at 6 ml/min was barely sufficient to move nanoparticles to the interface in the upstream section, resulting in low nanoparticle surface coverage and high rate of coalescence. As a result, only small amount of lamellae survived the destruction, showing minimal increase in an apparent viscosity over the baseline in the upstream section. As this small number of surviving lamellae continued to travel along the middle section, they possibly accumulated more particle coverage that was high enough to resist lamellae destruction. The lamellae population would then become larger in the middle section as the lamellae multiplied themselves in

numbers through the lamellae division mechanism. This large population of lamellae led to the larger apparent viscosity in the middle section than in the upstream section. The same idea may also apply to the downstream section and to explain why its apparent viscosity was highest among the three sections.

When the injection rate was increased to 9 ml/min, the apparent viscosity in all sections increased to the same level, in contrast to the apparent viscosity gradient observed at 6 ml/min. At 9 ml/min, the shear rate was sufficient to move enough nanoparticles to the interface, so that foam generation was considered to start in the upstream section. However, there were no further increase in apparent viscosity as foam continued to travel through the middle and downstream sections. At this flow rate and foam quality, lamellae population might have reached its maximum density early in the upstream section so the foam apparent viscosity did not increase further in the later sections. This explanation would be verified if the foam evolution could be investigated at higher injection rate, i.e. 12 ml/min. However, it was not possible as the pressure tap at the end of upstream section (which is also the beginning of middle section) was blocked, causing erroneous pressure measurement the upstream section and middle section.

Figure 4-7 showed the sectional pressure drop data converted as the apparent viscosity for experiment B6 where foam quality was increased to 0.8. At this higher foam quality, the difference in apparent viscosity between sections of the core was even more pronounced. The foam generated in core B6 at 6 ml/min clearly started in the downstream section where the apparent viscosity increased and stabilized at about 2.0 cP throughout the experiment. On the contrary, the apparent viscosities in both upstream and middle sections remained close to the baseline value at 6 ml/min and increased with the increasing injection rates (and shear rates).

It should be noted that none of these results was corrected for capillary end effect that induced higher water saturation at the downstream section of the core. CO₂ relative permeability decreased as water saturation increased, resulting in higher pressure drop (and so apparent viscosity) in the downstream section. Especially in core B6 where the CO₂ volume fraction was larger, the contrast in water saturation between upstream and downstream section was more significant. Partially, the capillary end effect may have contributed to this significant difference in apparent viscosities between the upstream and downstream sections.

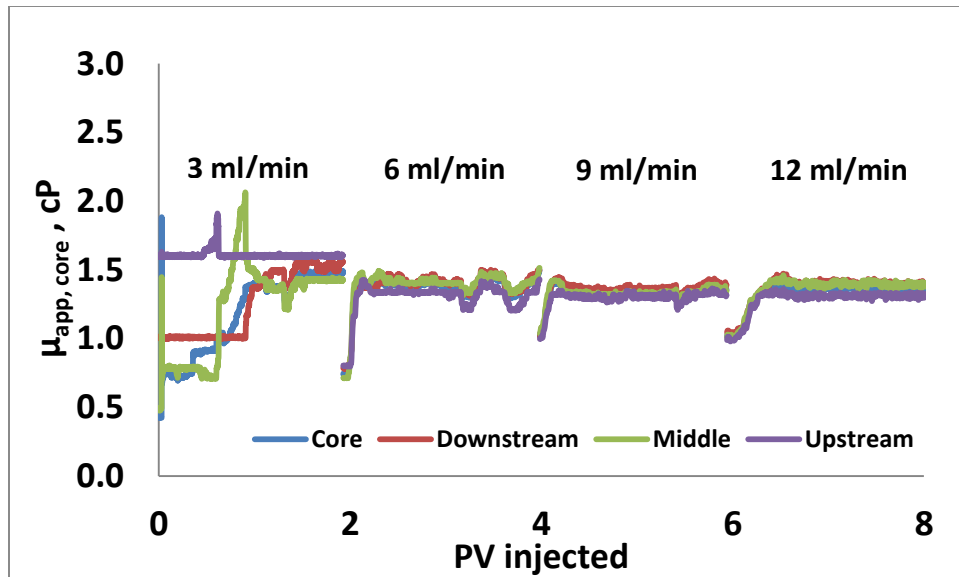


Figure 4-5 Apparent viscosity measured across the Boise core B5 and 3 intermediate sections (through pressure taps) in the baseline experiment (2 wt% NaCl brine + CO₂). The experiment was performed at 2000 psia and 23 °C, using volumetric phase ratio of 2:1.

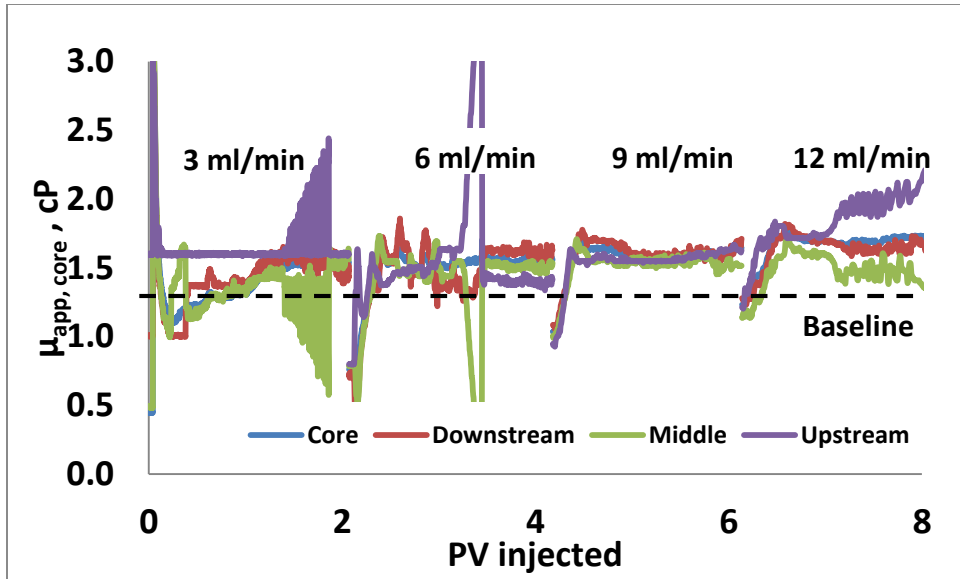


Figure 4-6 Apparent viscosity measured across the Boise core B5 and 3 intermediate sections (through pressure taps) in foam experiment (1wt% 3M PEG-coated nanoparticle in 2 wt% NaCl brine + CO₂). The experiment was performed at 2000 psia and 23 °C, using volumetric phase ratio of 2:1. (foam quality of 0.67)

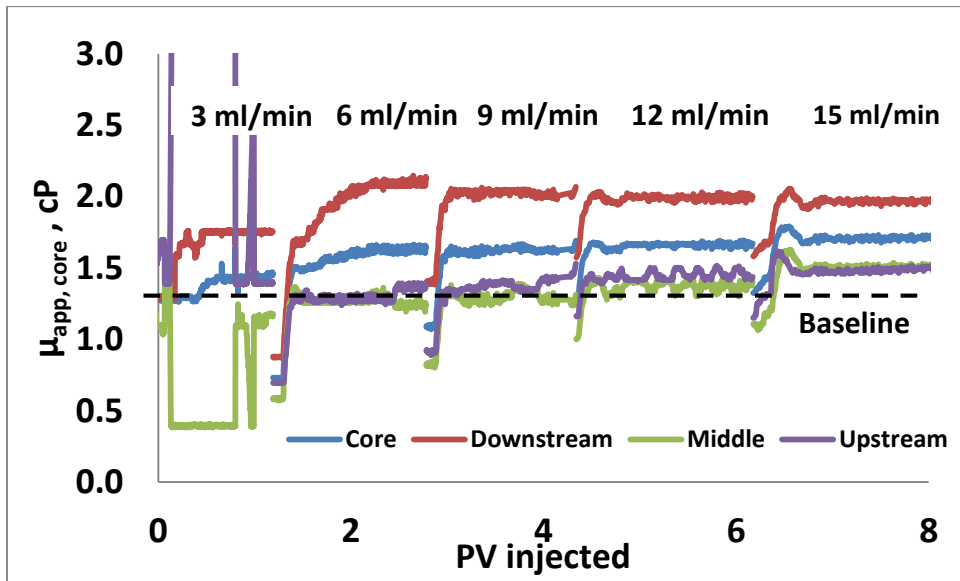


Figure 4-7 Apparent viscosity measured across the Boise core B6 and 3 intermediate sections (through pressure taps) in foam experiment (1wt% 3M PEG-coated nanoparticle in 2 wt% NaCl brine + CO₂). The experiment was performed at 2000 psia and 23 °C, using volumetric phase ratio of 4:1. (foam quality of 0.8)

4.1.2.2 Experiments in fractured Boise sandstone cores

The generation of nanoparticle-stabilized CO₂ in fractured sandstone discussed in this section was also studied earlier by Hariz (2012). As described in his thesis, coreflood experiments were conducted in two 6-inch Boise sandstone cores in which a fracture was generated at the center of the core cross-section, lengthwise, with different fracture aperture sizes, 104 and 65 microns, respectively. The matrix permeability of both cores were approximately 1,650 mD. Based on the fracture and matrix permeabilities, the amount of fluid flow through the each fracture, F_f , was estimated by Hariz using a parallel permeability model. Table 4-4 provided the properties of the two fractured sandstone cores.

Table 4-4 Properties of fractured Boise sandstone core F1 and F2 (Hariz, 2012).

Experiment	L_{core} (in.)	\bar{k} (mD)	H (μm)	$Net P_{conf}$ (psia)	F_f (%)
F1	6	6425	105	1400	76.7
F2	6	2830	66	950	42.1

The 5 nm PEG-coated (3M) silica particles were dispersed in DI water (1 wt% concentration) and co-injected into the fractured cores at 2000 psi and 23 °C. According to the overall pressure drop measured from both corefloods, the increase in pressure drop occurred at only the highest injection rate despite the foam observed earlier in the view cell at lower injection rates. Since co-injection through Boise sandstone matrix (unfractured core) is known to generate foam, we propose a method to interpret these coreflood results by decoupling the foam generation in the fracture and in matrix.

In order to subtract the effect of foam generation contributed by the matrix portion of the core, MRF data from unfractured corefloods (Figure 4-3) was used. The approximate method to calculate the matrix and fracture contributions for foam flow was described previously in 3.4.10 (assuming no crossflow between fracture and matrix). The apparent foam viscosity vs. the effective shear rate in the fracture for the two experimented cores

were plotted in Figure 4-8, together with the overall apparent viscosity of the entire core (i.e. treating the core as a single equivalent continuum, rather than attempting the flow decoupling calculation proposed in section 3.4.10).

As depicted in Figure 4-8, the concept of threshold shear rate for foam generation applies not only for porous media but also for fractures. The fracture in both cores, F1 and F2, demonstrated a threshold shear rate behavior but with different threshold values. A sharp increase in an apparent viscosity was observed at an effective shear rate in the fracture of around 4000 s^{-1} for core F1 (105 microns), and 6000 s^{-1} for core F2 (66 microns). Above the critical shear rate, the apparent viscosity increased drastically from the baseline value (2 cP) to 5.65 cP in core F1 and 3.14 cP in core F2. The time of high apparent viscosity increase also corresponded to the fine texture of the foam observed in the view cell for core F1. However, the view cell picture of core F2 also showed the fine-texture foam below the fracture critical shear rate. The decoupling calculation suggested that the critical shear rate in the matrix was met before that in the fracture, since only around 42% of the injected fluid was going through the fracture (Table 4-6).

An interesting aspect of the flow allocation calculation between fracture and matrix is that, once foam generation happens in the fracture, more of the injected fluid can be diverted (allocated) to the matrix despite the fact that foam is also generated in the matrix. This phenomenon was demonstrated in Table 4-5 with the calculated results for core F1. At the injection rate of 14 ml/min and lower, the shear rates in both fracture and matrix were below the threshold, thus no foam was generated. The calculation given in Table 4-5 indicated that 75% of the injected fluid was allocated to the fracture. On the other hand, at 20 ml/min, foam was generated in both matrix and fracture with 59% of the injected fluid allocated to the fracture. This effect can be enhanced by varying the foam quality, concentration of nanoparticles, salinity, etc.

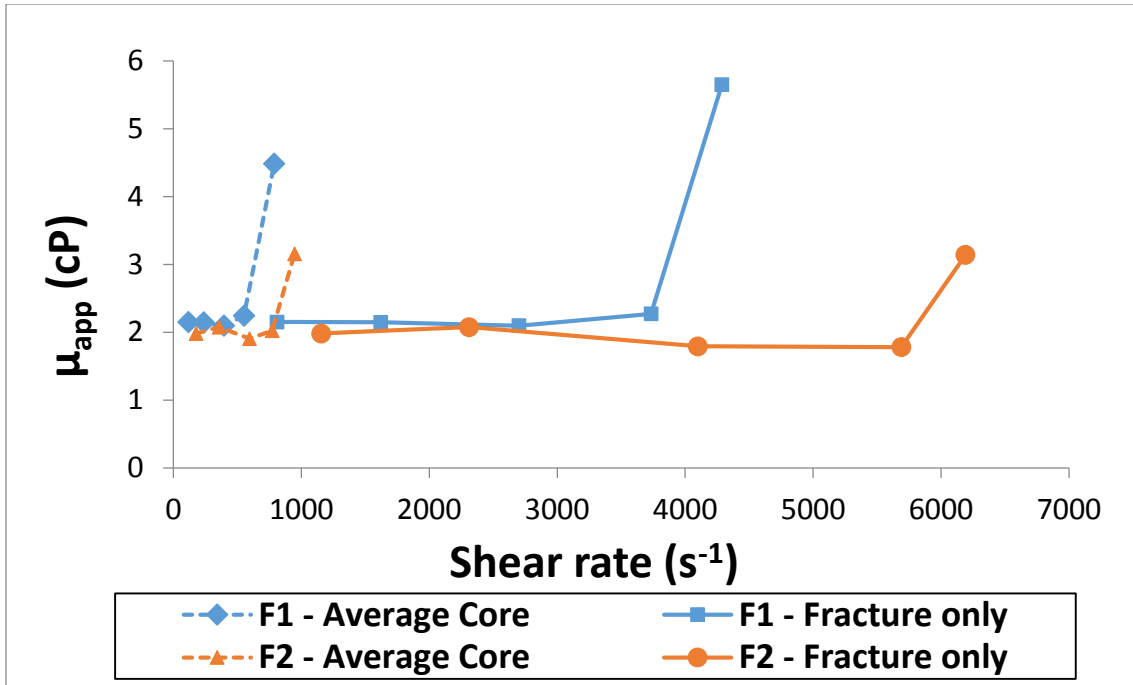


Figure 4-8 Core apparent viscosity vs. fracture shear rate from the two foam experiments in fractured Boise sandstone coreflood under the same experiment condition. Fracture apertures for cores F1 and F2 were 104 microns and 65 microns, respectively. Dash lines are core-average value (combined matrix and fracture flow). The solid lines show the estimated shear rate and viscosity in the fracture

Table 4-5 Decoupling flow in matrix from flow in fracture of core F1. The number in bold indicate the condition where the critical shear rate (either in matrix or fracture) was exceeded.

Q (cc/min)	F_f	Core μ_{app} (cP)		Shear rate (s ⁻¹)	
		Matrix	Fracture	Matrix	Fracture
3	74.5	2.15	2.15	60	810
6	74.5	2.15	2.15	120	1600
10	74.5	2.10	2.10	200	2700
14	73.5	2.16	2.27	290	3700
20	59.1	2.80	5.65	640	4300

Table 4-6 Decoupling flow in matrix from flow in fracture of core F2. The number in bold indicate the condition where the critical shear rate (either in matrix or fracture) was exceeded.

Q (cc/min)	F_f	Core μ_{app} (cP)		Shear rate (s^{-1})	
		Matrix	Fracture	Matrix	Fracture
3	42	1.99	1.99	130	1200
6	42	2.09	2.09	270	2300
10	45	2.02	1.80	430	4100
13	48	2.26	1.79	530	5700
16	42	3.16	3.18	640	6100

4.1.2.3 Experiments in fractured and unfractured Berea sandstone cores (~200 mD)

In coreflood experiments with unfractured Berea sandstone core, the state of stabilized pressure drop could be obtained only when the flow rate was low and no foam was generated in the core. A significant decrease in permeability both after baseline (no nanoparticles) and foam (nanoparticles in the aqueous phase) experiments suggested that formation damage occurred, possibly from the interaction between 2 wt% NaCl brine and clay particles in acidic condition. The acidity was due to the dissolution of CO₂ into the aqueous phase.

The first coreflood experiment, Berea 3, was conducted in a 12-inch core with the initial permeability of 127 mD. By co-injecting 2 wt% NaCl brine and CO₂ at a fixed volumetric phase ratio of 1:1, the baseline apparent viscosity (without nanoparticles) was estimated to be ~1.2 cP at 2 ml/min injection rate. However, the permeability after the baseline experiment decrease to 80 mD. When the dispersion of 1 wt% 5 nm 3M PEG-coated particle was co-injected with CO₂ at the same phase ratio and injection rate, the critical shear rate for foam generation was estimated to be between 600 – 700 s^{-1} (considering the change in matrix permeability from formation damage).

As shown in Figure 4-9, the core apparent viscosity (blue line) increased to as high as 2.7 cP. This also corresponded to the fine texture of the foam observed in the view cell. The intermediate pressure tap data indicated that the generation of viscous foam possibly started early in the upstream section. Foam was then propagated through the core section by section. This was indicated by the 0.25-PV delay from the point of first foam generation in the upstream section as indicated by a sharp increase in pressure (at 1.0 PV) and the point where foam first reached the downstream section (at 1.25 PV). Without the presence of foam, this kind of delay were not observed since the high mobility CO₂ rapidly channeled through the core. In the baseline experiments, the pressure drops in all three sections typically responded at the same time, almost instantly after CO₂ was introduced into the core.

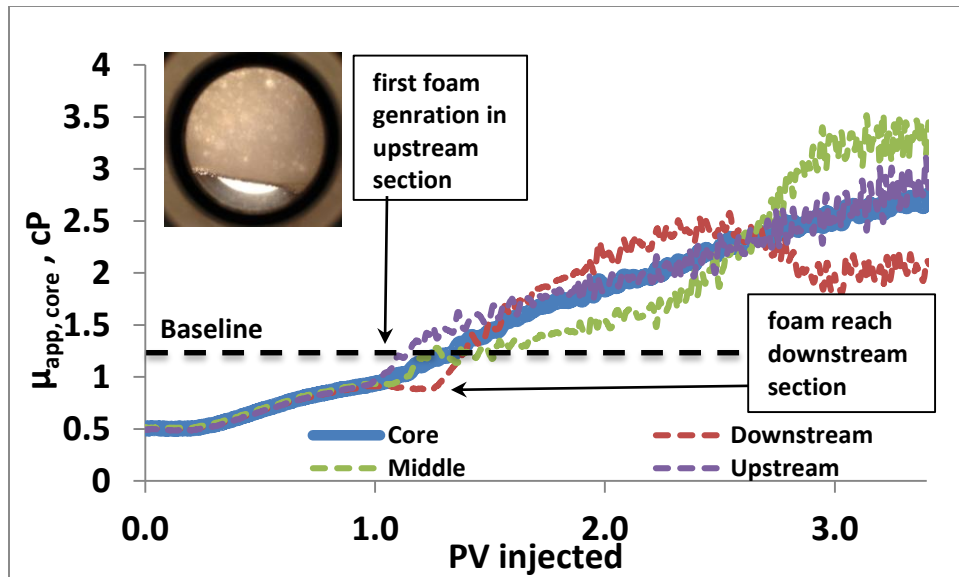


Figure 4-9 Apparent viscosity measured across core Berea 3 and its intermediate sections (through pressure taps) in foam experiment (1wt% 3M PEG-coated nanoparticle in 2 wt% NaCl brine + CO₂). The experiment was performed at 2000 psia and 23 °C, using volumetric phase ratio of 1:1.

Although the first coreflood proved the ability of Berea sandstone in generating nanoparticle stabilized foam, the critical shear rate could not be determined as a clear foam/no-foam transition could not be seen. In an attempt to locate this transition, the Berea 4 (175 mD) coreflood was conducted using the same operating conditions and nanoparticle dispersion, but with lower injection rates starting from 1 ml/min. Again, it was even more difficult to infer the core MRF from the pressure drop because the matrix permeability also decreased. After the foam experiment, the permeability of the core was 81 mD, less than half of the original permeability. Nevertheless, the apparent viscosity measurements from the capillary tube downstream of the core obviously showed a critical shear rate for foam generation, Figure 4-10.

For the Berea 4 experiment, the co-injection of 1 wt% 5 nm 3M PEG-coated in 2 wt% NaCl dispersion and CO₂ at the estimated core shear rate of 240 s⁻¹ yielded the same apparent viscosity as the baseline experiment without nanoparticles. When the shear rate was increased to 370 s⁻¹, an increase in the apparent viscosity was observed, and the presence of foam was confirmed by the view cell observation. The peak apparent viscosity was as high as 3.5 cP, almost 5 times the value observed in the baseline experiment (~ 0.7 cP). Thus, 370 s⁻¹ could be approximated as the threshold shear rate for the unfractured Berea core at 2000 psia and 23 °C.

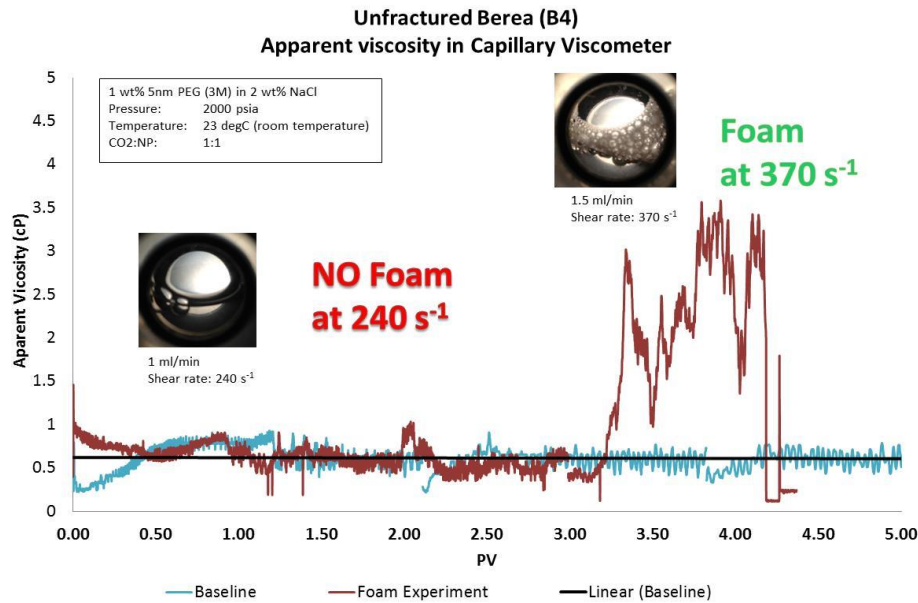


Figure 4-10 Apparent viscosity measured in the capillary tube downstream of an unfractured Berea sandstone. 1 wt% PEG-coated silica in 2 wt% NaCl brine and CO₂ were co-injected using phase ratio of 1:1 at 2000 psia and 23 °C. The foam generation threshold falls between shear rates of 244 s⁻¹ and 366 s⁻¹.

Similar to the previous fractured Boise sandstone experiments, the co-injection of nanoparticle dispersion and CO₂ was conducted in the 5.5-inch fractured Berea sandstone core. The Berea matrix permeability was an order of magnitude lower than that of the Boise sandstone (127-175 md vs. 1800 md), while the fracture aperture was larger (165 microns vs. < 110 microns). Therefore, almost all of the injected fluid flowed through the fracture. As it was difficult to obtain the foam apparent viscosity in the Berea sandstone matrix, a simplifying assumption that all fluid went into the fracture was made to calculate the fracture apparent viscosity. The results from the fractured Berea coreflood were shown in Figure 4-11, with the view cell pictures at the corresponding shear rates. The foam flow in the fracture of the Berea core showed qualitatively similar behavior to those in the Boise cores, indicating the existence of a critical shear rates. The apparent viscosity was about 3.5 cP below the critical shear rate and slowly increased as the fracture shear rate increased.

When the fracture shear rate became larger than 3400 s^{-1} , the apparent viscosity increased substantially (The slope was five times larger than that below the critical shear rate).

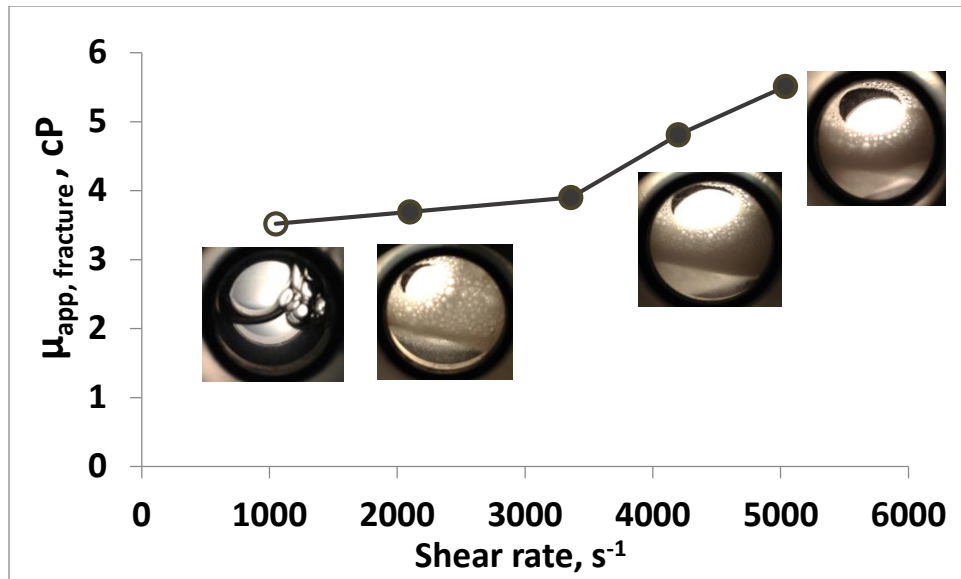


Figure 4-11 Apparent viscosity vs. fracture shear rate obtained from a fractured Berea sandstone coreflood. Fracture gap size was 165 microns. 1 wt% PEG-coated silica in 2 wt% NaCl brine and CO_2 were co-injected using phase ratio of 1:1 at 2000 psia and $23 \text{ }^\circ\text{C}$. Critical shear rate was estimated to be 3400 s^{-1} . Open symbols indicate no foam visible in view cell; filled symbols indicate visible foam.

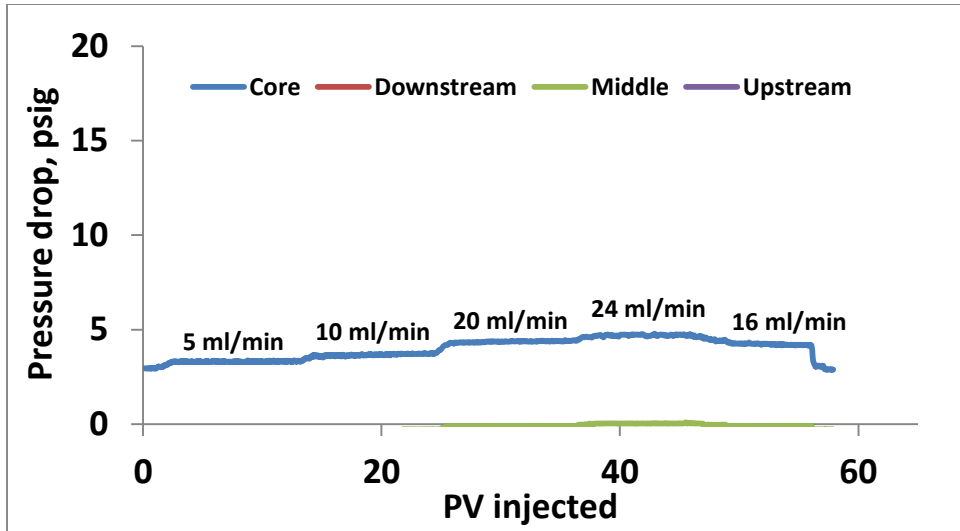


Figure 4-12 Apparent viscosity measured across fractured Berea core (B2F) and its intermediate sections (through pressure taps) in the baseline experiment (2 wt% NaCl brine + CO₂). The experiment was performed at 2000 psia and 23 °C, using volumetric phase ratio of 1:1. Pressure drops in the upstream, middle and downstream sections were smaller than measuring range, thus cannot be observed.

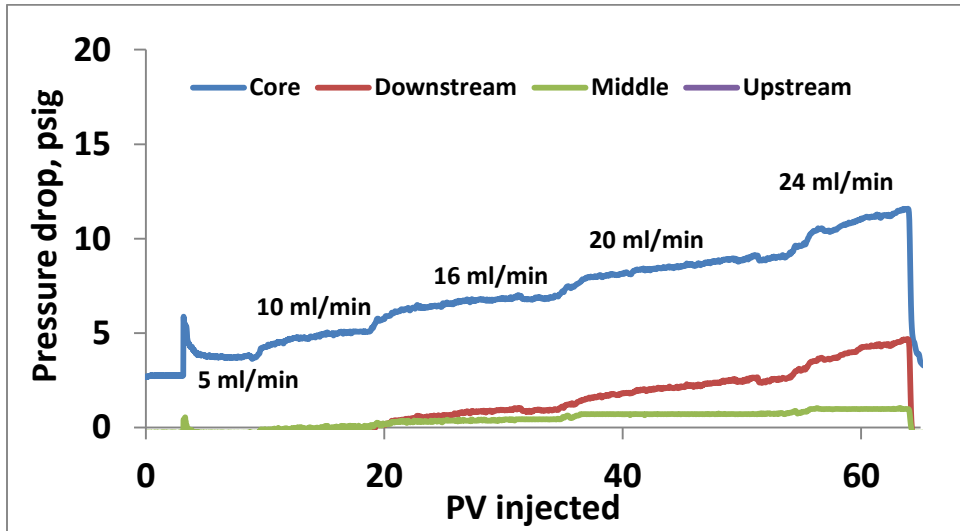


Figure 4-13 Apparent viscosity measured across fractured Berea core (B2F) and its intermediate sections (through pressure taps) in foam experiment (1wt% 3M PEG-coated nanoparticle in 2 wt% NaCl brine + CO₂). The experiment was performed at 2000 psia and 23 °C, using volumetric phase ratio of 1:1.

Moreover, the intermediate pressure taps were also employed in this fractured Berea coreflood to identify the location where the foam was first generated. Since the fractured core was limited to 5.5 inches long, the three sections were unequally divided as 1-inch upstream section, 4-inch middle section, and 0.5-inch downstream section. In our attempt that the pressure taps only measure the pressure drop inside the fracture, at each pressure tap outlet, a hole was drilled from the core surface all the way through to the fracture. However, the sectional pressure drops in the baseline experiment were too small, thus could not be picked up by the transducers used in the experiment. Therefore, only the total pressure drop across the core could be seen in Figure 4-12 (blue line). It was also the same for the foam experiment below the critical shear rate (Figure 4-13). In contrast, when the shear rate was higher than the threshold value (>16 ml/min), the pressure drops in the middle and downstream could be seen. In any case, the pressure drop of upstream section remained absent. This suggested that the foam generation started in the middle section, then continued to refine its texture when flowing through the downstream section. Although it was difficult to compare the foam apparent viscosity between sections as the permeability measurement by section was not possible, the foam in the downstream section most likely provided the highest apparent viscosity. In spite of its shortest length (0.5 inch), the pressure drop in the downstream section was the highest among the three (at least two times of that of the 4-inch middle section).

4.1.2.4 Experiments in Indiana limestones (7 mD)

The co-injection experiment was also carried out in an Indiana limestone with a matrix permeability of 5 mD. The dispersion of 1 wt% 5 nm 3M PEG coated particle in DI water was co-injected into the core with CO₂ at a fixed phase ratio of 1:1 and ambient temperature of 23 °C. The outlet pressure was controlled at 1500 psia, to make sure that

the injection pressure would not exceed the system limit. Figure 4-14 showed the core apparent viscosities at different injection rates across the experiment. The baseline apparent viscosity without nanoparticle was measured to be 1.5 cP.

Stable foam was generated in the Indiana limestone matrix from the first injection rate of 0.3 ml/min as indicated by the view cell observation and the large increment in an apparent viscosity. The apparent viscosity was also highest at this injection rate (~ 4.5 cP). A transition between foam/no-foam was not observed at all injection rates in this experiment. Due to the limitation of the experiment setup, it was unable to find the shear rate threshold by reducing the injection rate rate below 0.3 ml/min without compromising the reliability of the data.

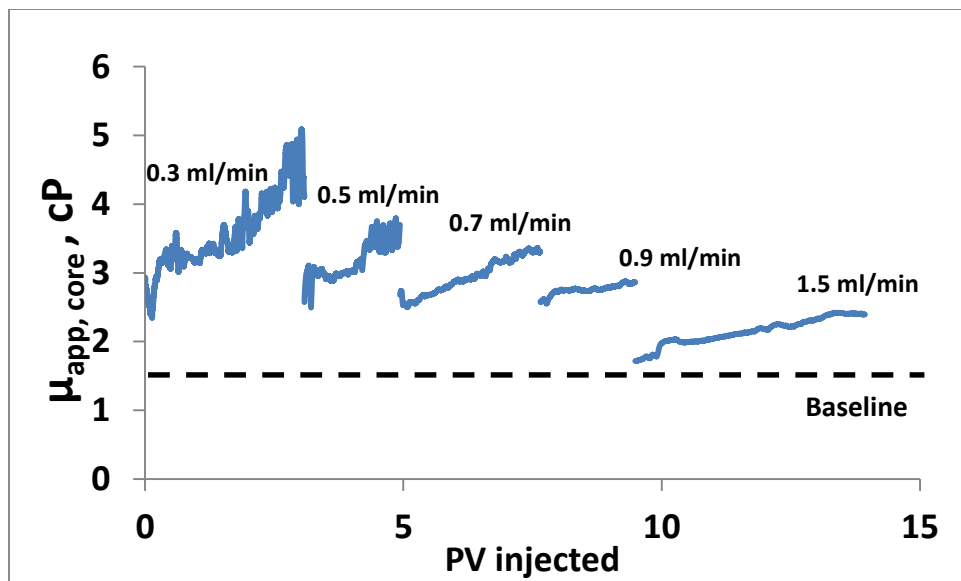


Figure 4-14 Apparent viscosity measured across Indiana limestone core (IL1) in foam experiment (1 wt% 3M PEG-coated nanoparticle in 2 wt% NaCl brine + CO₂). The experiment was performed at 1500 psia and 23 °C, using volumetric phase ratio of 1:1 (foam quality of 0.5).

For the Indiana limestone coreflood, Figure 4-15 further illustrated the relationship between core MRF and shear rate. Unlike other types of matrix experimented in this thesis, this limestone coreflood showed a decreasing trend of MRF with an increase in shear rate. After foam experiment, steady injection of brine showed that the matrix permeability changed only slightly during the foam flow. This suggested that the foam may have reached its finest texture possible and became shear thinning, same as those usually seen in the surfactant-stabilized foam. The threshold shear rate for foam generation might have been far below 380 s^{-1} , which was the first data point of this experiment.

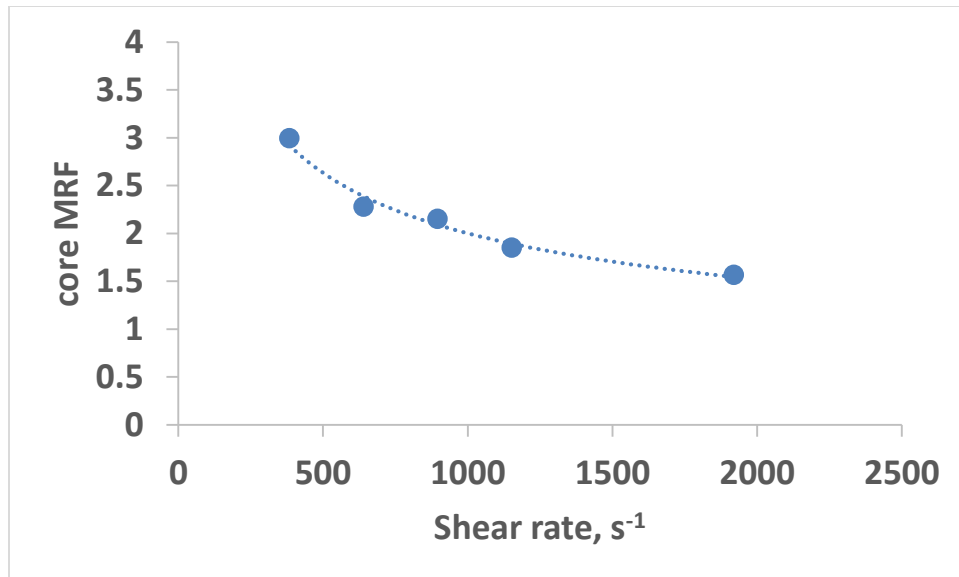


Figure 4-15 Core apparent viscosity versus core shear rate measured in Indiana limestone core. The experiment was performed at 1500 psia and 23 °C, using 1wt% 3M PEG-coated nanoparticle in DI water and foam quality of 0.5.

In an attempt to obtain a better resolution on the nature of this shear thinning behavior, the second foam experiment was carried out in the same Indiana limestone core but it was unsuccessful. The main challenge encountered was that the acidic injected fluid dissolved the limestone matrix and increased the core permeability. In this second experiment, it appeared that the injected fluid might have created worm holes through the core because the pressure drop was so small it could not be detected by the pressure transducers. The measured matrix permeability increased to 75 mD after this experiment (10 times larger than the original value). No further experiment was performed in the limestone matrix, and the focus was placed on the sandstone matrix study.

4.1.3 Foam Generation Experiments with Supercritical CO₂

The ability of silica nanoparticle to stabilize CO₂-water foam was also tested at elevated temperature in order to prove its feasibility for wider oilfield applications. In general, a geothermal gradient is about 25 °C per km of depth (Fridleifsson et al., 2008); therefore, the reservoir temperature can be as high as 70 °C at 6000 ft. At this high temperature, CO₂ transforms from liquid state to supercritical state, resulting in a drastic change in CO₂ physical properties. This significant change in the phase behavior of CO₂ could affect the foam stabilization process and was the subject of study in this section.

4.1.3.1 Experiments in very high permeability Boise sandstone cores (~3000 mD)

At 50 °C and 2000 psi, an aqueous dispersion of 1 wt% EOR-5xs silica nanoparticle in 2 wt% NaCl was co-injected with CO₂ into a 12-inch Boise sandstone core. Stable foam was successfully generated at this condition as exhibited in Figure 4-16 (the filled circles indicated the experiment with which stable foam was observed in the view cell). The view cell observation pictures were given in Table 4-7. The critical shear rate for foam generation was 330 s⁻¹ for the foam quality of 0.57 and 440 s⁻¹ for the foam quality of 0.75.

For the foam quality of 0.57, the core apparent viscosity rapidly increased to 9 cP and continued increasing to as high as 11 cP with increasing shear rate. However, the increasing leveled off at the maximum core MRF of 4.4, with the baseline apparent viscosity of ~2 cP.

When the foam quality was increased to 0.75, the more viscous foam was expected as the foam quality was closer to the optimum value, as suggested by Aroonsri et al. (2013). However, in this experiment, not only the threshold shear rate was higher than that of the 0.57 foam quality experiment, the largest core MRF was only 2.7, only about half of the maximum MRF obtained with 0.57 foam quality at the same shear rate range. This suggested that the optimum foam quality was not universal but changed with other parameters.

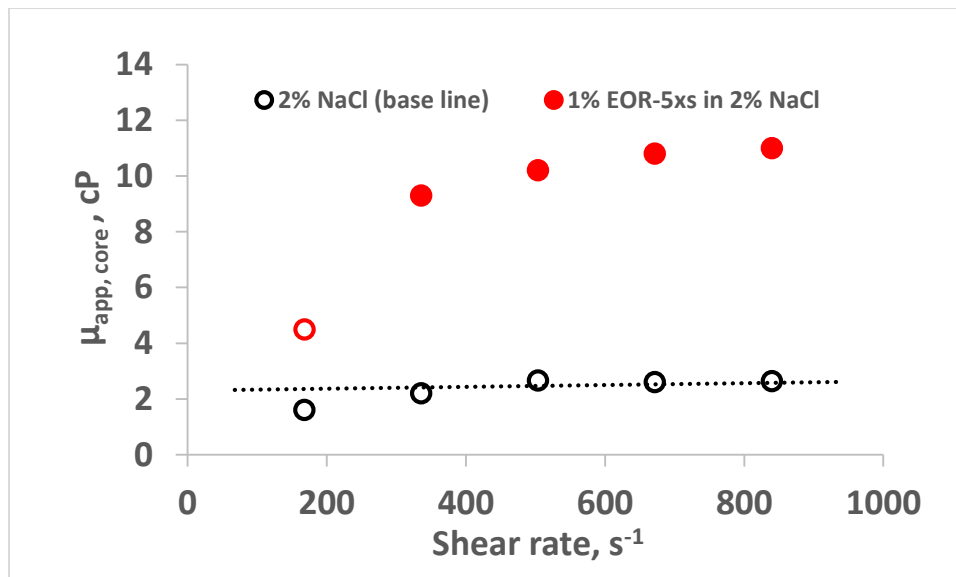


Figure 4-16 Apparent viscosity measured across Boise sandstone core vs. shear rate in foam experiment at 50 °C and 2000 psia. The experiment was performed using 1 wt% EOR-5xs nanoparticle in 2 wt% NaCl brine at foam quality of 0.57. Open symbols indicate no foam visible in view cell; filled symbols indicate visible foam. Baseline apparent viscosity was also plotted in black as a reference.

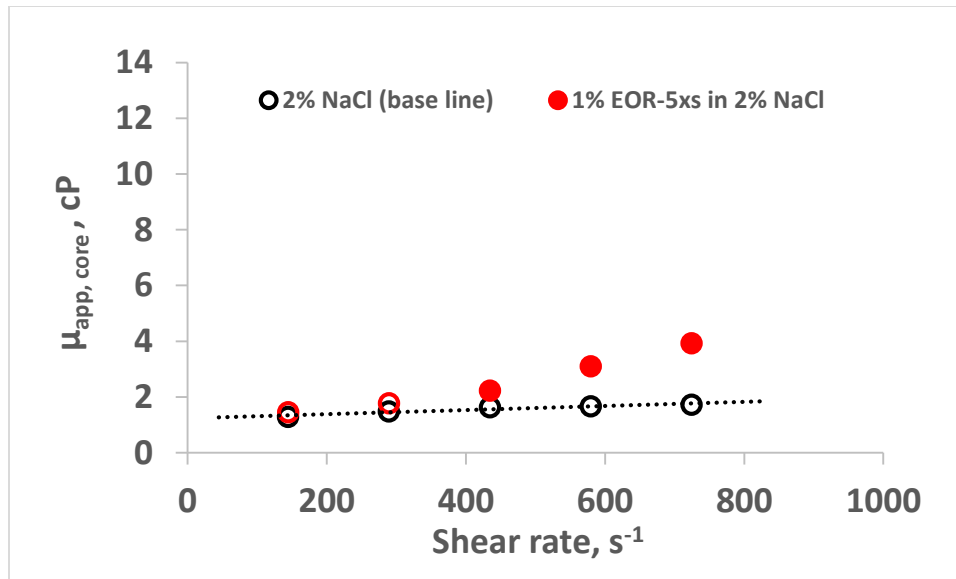


Figure 4-17 Apparent viscosity measured across Boise sandstone core vs. shear rate in foam experiment at 50 °C and 2000 psia. The experiment was performed using 1wt% EOR-5xs nanoparticle in 2 wt% NaCl brine at foam quality of 0.75. Open symbols indicate no foam visible in view cell; filled symbols indicate visible foam. Baseline apparent viscosity was also plotted in black as a reference.

The effects of temperature were then studied by running coreflood experiments at a higher temperature of 80 °C, where the density of supercritical CO₂ was only half of that at the ambient temperature (23 °C). When 1 wt% EOR-5xs silica nanoparticle in 2 wt% NaCl was injected together with CO₂ at the foam quality of 0.7, both pressure data (Figure 4-18) and view cell observations (Table 4-7) revealed that no foam was generated at any point. As the temperature increased, it was possible that the critical shear rate for this system may be higher than 1200 s⁻¹. The increasing critical shear rate with increasing temperature was also reported by Espinosa et al. (2010). As demonstrated by his beadpack experiment at 1350 psi, critical shear rate for foam generation increased from about 3000 s⁻¹ to 4000 s⁻¹ when the temperature increased from 75 to 90 °C. According to a study by Bachu and Bennion (2008), the interfacial tension (IFT) between water and CO₂ at 80 °C

was approximately 25% greater than that at 50°C. This increase in IFT means a 25% increase in adsorption energy required to move the particles to the interface. Another reason for the increased threshold shear rate could be the over-optimum CO₂ volume fraction as seen in the previous experiment at 50 °C. A large difference between the density of the nanoparticle dispersion and CO₂ could also accelerate the destabilization of foam due to gravity, even though such an effect was more for the bulk foams.

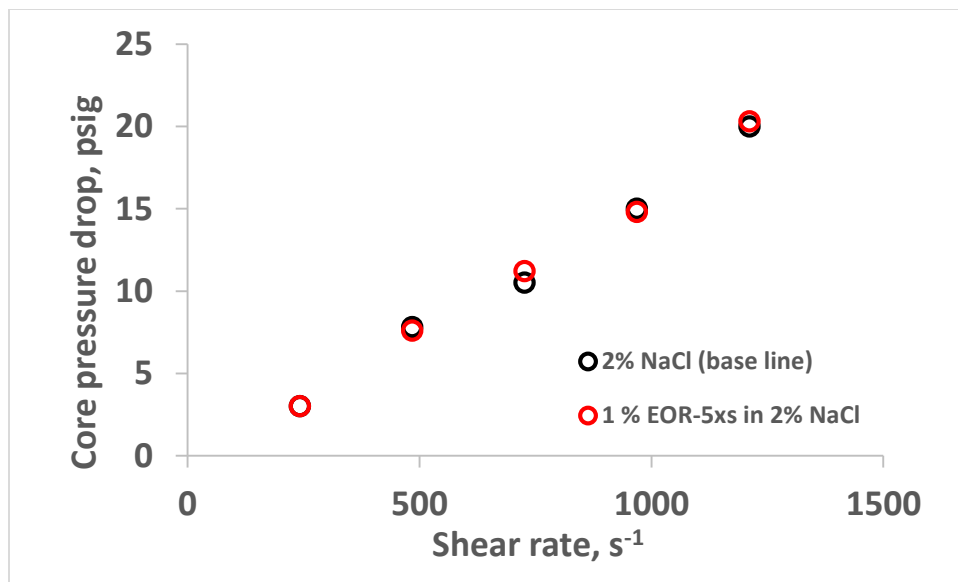












Figure 4-18 Pressure drop measured across Boise sandstone core vs. shear rate in foam experiment at 80 °C and 2000 psia. The experiment was performed using 1 wt% EOR-5xs nanoparticle in 2 wt% NaCl brine at foam quality of 0.75. Open symbols indicate no foam visible in view cell; filled symbols indicate visible foam. Baseline apparent viscosity was also plotted in black as a reference.

Table 4-7 Summary of view cell observation during supercritical CO₂ foam experiment in Boise sandstone core at foam quality of 0.57 and 0.75. These experiments were carried out at 2000 psi and 50 °C, using 1 wt% EOR-5xs nanoparticle dispersion in 2 wt% NaCl brine. The black belts observed at the low shear rates were the reflection from CO₂-water interface.

Flow rate →	3.5 ml/min	7.0 ml/min	10.4 ml/min	13.9 ml/min	17.4 ml/min
Core ↓	170 s ⁻¹	340 s ⁻¹	500 s ⁻¹	670 s ⁻¹	840 s ⁻¹
Boise core f _g = 0.57					
Flow rate →	3 ml/min	6 ml/min	9 ml/min	12 ml/min	15 ml/min
Core ↓	150 s ⁻¹	290 s ⁻¹	440 s ⁻¹	580 s ⁻¹	720 s ⁻¹
Boise core f _g = 0.75					

Further foam generation experiments were carried out in a Boise sandstone core at 80 °C. In an effort to lower the critical shear rate for foam generation, the injected CO₂ volume fraction was reduced to 0.5 and, at the same time, the system pressure was increased to 2200 psi. In addition, the aqueous phase salinity and nanoparticle concentration were also varied to see their possible effects on foam generation potential. Results from all the trials were plotted together on Figure 4-19 for comparison. A filled circle indicated the experiment with which foam was observed in the view cell, while an open circle represented a “no foam” experiment. The baseline experiment, with which only 2 wt% NaCl brine and CO₂ was injected, was shown as black open circles and dotted line. Table 4-8 and Table 4-9 summarized the view cell pictures of these experiments.

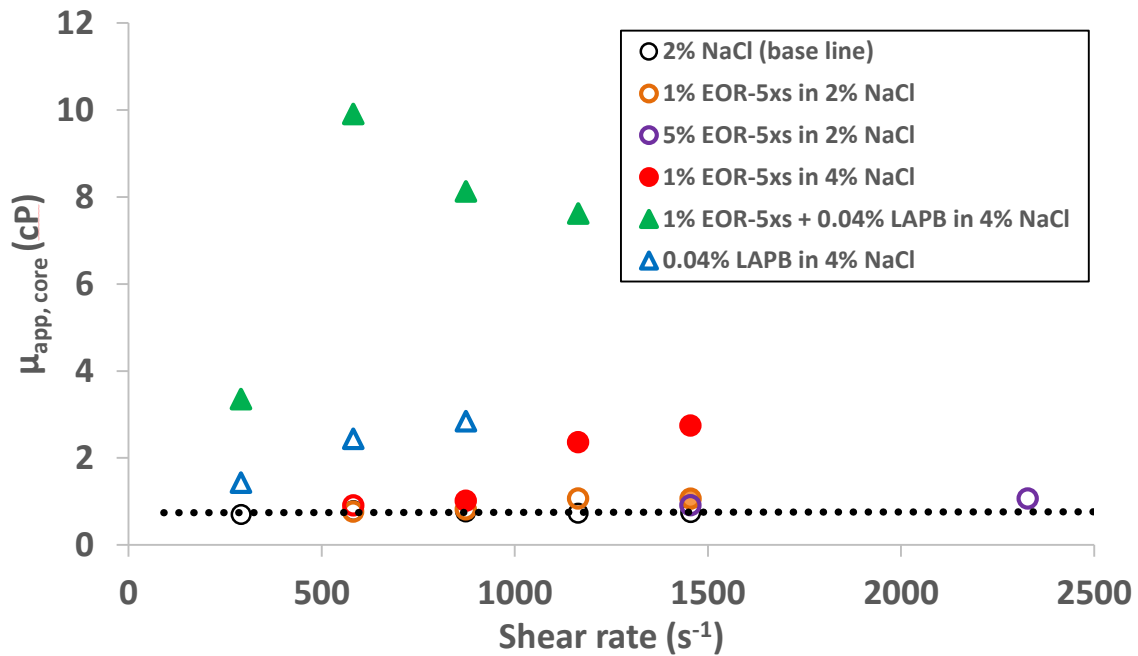


Figure 4-19 Core apparent viscosity measured across Boise sandstone core vs. shear rate in foam experiment at 80 °C and 2200 psia. The experiment was performed using 5 different mixes of the aqueous phase at foam quality of 0.5. Open symbols indicate no foam visible in view cell; filled symbols indicate visible foam. Baseline apparent viscosity was also plotted in black as a reference.

Table 4-8 Summary of view cell observation during supercritical CO₂ foam experiment in Boise sandstone core at foam quality of 0.5. These experiments were carried out at 2200 psi and 80 °C, using several type of aqueous phase recipe.


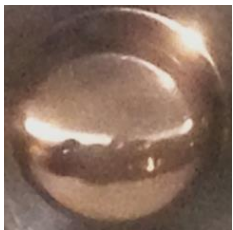

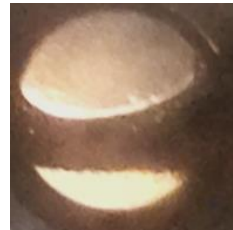



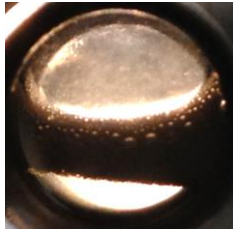









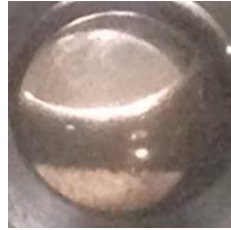
Flow rate →	10 ml/min	15 ml/min	20 ml/min	25 ml/min	40 ml/min
Core ↓	580 s ⁻¹	870 s ⁻¹	1160 s ⁻¹	1460 s ⁻¹	2330 s ⁻¹
1 wt% EOR-5xs in 2 wt% NaCl					
5 wt% EOR-5xs in 2 wt% NaCl					
1 wt% EOR-5xs in 4 wt% NaCl					

Table 4-9 Summary of view cell observation during supercritical CO₂ foam experiment in Boise sandstone core at foam quality of 0.5. These experiments were carried out at 2200 psi and 80 °C, using 0.04 wt% LAPB in 4 wt% NaCl with and without nanoparticle.

Flow rate →	5 ml/min	10 ml/min	15 ml/min	20 ml/min
Core ↓	290 s ⁻¹	580 s ⁻¹	870 s ⁻¹	1160 s ⁻¹
0.04 wt% LAPB in 4 wt% NaCl				
1 wt% EOR-5xs + 0.04 wt% LAPB in 4 wt% NaCl				

The first experiment, shown with the orange open circles, used 1 wt% EOR-5xs dispersed in 2 wt% NaCl brine which was the same recipe used in the previous experiment in a Boise sandstone core at 80 °C and 2000 psi. The results demonstrated that reducing CO₂ volume fraction to 0.5 and increasing the pressure to 2200 psi was not enough to generate the foam at 80 °C (the core apparent viscosity barely deviated from the baseline experiment). However, it should be noted that the 200 psi pressure increment did not significantly alter CO₂ properties.

In an attempt to achieve a better foam stabilization by increasing nanoparticle coverage on the bubbles, the second experiment was conducted using 5 wt% EOR-5xs dispersed in 2 wt% NaCl brine. The more nanoparticles adsorbed onto the surface should provide a more rigid barrier and, therefore, reduce the rate of bubble coalescence. This attempt however was not successful. The core apparent viscosity measured in this experiment continued to stay close to the baseline value despite the high shear rate (2300 s⁻¹). From this result, it can be inferred that the problem was not the amount of particles put in as dispersion, but rather the particles were not brought to the interface between CO₂ and aqueous phase.

In the third experiment, the salinity of the aqueous dispersion was increased to 4 wt% NaCl. The added sodium chloride was expected to reduce the electrostatic repulsion between nanoparticles, thus, driving more particles to the interface (Binks et al., 2007; Worthen et al., 2013a) (also, note that the change in interfacial tension between CO₂ and aqueous phase with increasing salt concentration was negligible (Bachu and Bennion, 2008)). As anticipated, the salinity increase reduced the critical shear rate for foam generation and allowed CO₂ foam to be generated at 80 °C. Represented by the red dots, the results indicated a threshold shear rate for foam generation at 870 s⁻¹. The highest apparent viscosity observed was 2.7 cP at 1450 s⁻¹ or a core MRF of 3. This suggested that

the salinity was a key parameter determining threshold shear rate. Foam generated at higher salinity was also found to have a greater apparent viscosity (Aroonsri et al., 2013). The effect of salinity on foam generation was discussed further in the discussion section.

The last two experiments in this series, shown as triangles, adopted the synergy between nanoparticles and surfactants, as reported by Worthen et al. (2013b). The presence of surfactant in the system reduced the interfacial tension between water and CO₂, and accordingly lowered the energy required to move nanoparticles to the interface. In other words, the critical shear rate for foam generation should be reduced, increasing the possibility to generate stable CO₂ foam in a high temperature environment at lower shear rate.

Since surfactants stabilize the foam by itself, a control experiment was conducted to see if the surfactant alone at a low concentration would generate a stable foam. A solution of 0.04 wt% lauramidopropyl betaine (LAPB) in 4 wt% NaCl brine was injected together with CO₂ into the core, using the same volumetric phase ratio, temperature, and pressure as the previous baseline experiment (0.5, 80°C, and 2200 psi, respectively). As represented by blue open triangles, a clear evidence of viscosification in the core was seen, yet, no foam was observed in the view cell at any point of the experiment. It was suspected that foam lamellae were created inside the core matrix, resulted in increasing apparent viscosity. However, those lamellae might not be stable once they exited the core due to the low concentration of surfactant and the ability of the surfactant molecules to move freely to and from the interface. The bulk foam might coalesce and break while travelling to the view cell.

Next, the 1 wt% EOR-5xs dispersion mixed with 0.04 wt% LAPB and 4 wt% NaCl was prepared and used in the last experiment, denoted by filled green triangles. Stable foam was observed in the view cell, starting from the lowest shear rate point at 290 s⁻¹. The

corresponding apparent viscosity at 290 s^{-1} was 3.4 cP, higher than the highest point observed earlier using only nanoparticles. When the core shear rate was increased to 580 s^{-1} , the apparent viscosity then jumped to 9.9 cP. This high apparent viscosity corresponded to an MRF of 11 and about 4 times greater than the viscosity of the control experiment with surfactant alone. This finding obviously demonstrated the synergy between nanoparticles and surfactants. As surfactants assisted nanoparticles to adsorb onto the interface between CO_2 and water, adsorbed particles formed a rigid shield that prevent the foam bubbles from coalescing. In contrast to the control experiment without nanoparticles, a stable fine-texture bulk foam was observed in the view cell (Table 4-9).

Many earlier results demonstrated that salinity was one of the key factors that strongly influenced both critical shear rate and foam apparent viscosity. The next set of experiments was carried out to quantify the sensitivity of foam generation to salinity. The dispersions of 1 wt% EOR-5xs nanoparticles were prepared in brine with three different NaCl concentrations (2 wt%, 3 wt%, and 4 wt%). At 2200 psi and $80 \text{ }^\circ\text{C}$, these dispersions were then co-injected with CO_2 at the volumetric phase ratio of 1:1. Shown in Figure 4-20, the critical shear rate for foam generation decrease almost linearly with the increase in salinity. The critical shear rates, based on the change in apparent viscosity, were estimated to be 1180 s^{-1} , 790 s^{-1} , and 390 s^{-1} for the aqueous phase salinity of 2 wt%, 3 wt%, and 4 wt%, respectively. Again, this result confirmed the effectiveness of salt in easing the adsorption of nanoparticles onto the interface. Comparing the cases of 2 wt% and 3 wt% salinity, the trend of increasing apparent viscosity with shear rate increase was more obvious at higher salt concentration. However, when looking at the cases of 3 wt% and 4 wt% salinity, the two increasing trends appeared to converge and finally meet at the shear rate of 1180 s^{-1} . There seemed to be a limit on the influence of salinity.

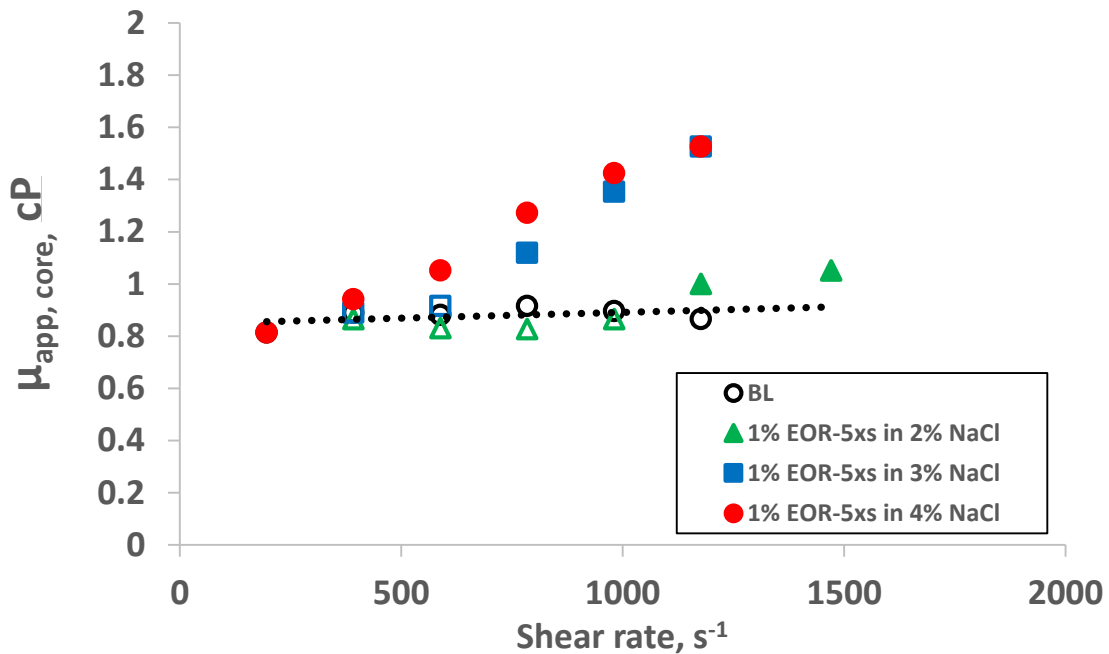


Figure 4-20 Core apparent viscosity measured across Boise sandstone core vs. shear rate in foam experiment at 80 °C and 2200 psia. The experiment was performed using the dispersion of 1wt% EOR-5xs nanoparticle in 1 wt%, 2 wt% and 4 wt% NaCl brine with foam quality of 0.5. Baseline apparent viscosity was also plotted in black as a reference. Open symbols indicate no foam visible in view cell; filled symbols indicate visible foam.

The final set of experiments in a Boise sandstone core (~3500 mD) explored the feasibility of foam generation in the extreme saline condition using 7.2 wt% TDS brine, consisting mostly NaCl and 0.3 wt% Ca^{2+} divalent cations. The high salt concentration and the presence of divalent ions should positively influence the foam generation process by driving nanoparticles to the interface. However, if the salinity is too high, nanoparticles may become unstable, and aggregate and drop out of the brine. Three different concentrations of EOR-5xs nanoparticle dispersion were tested in this series of experiments, ranging from 0.1wt% to 1wt%, in an attempt to quantify its effect on foam apparent viscosity. Using CO_2 volumetric phase ratio of 3:1 (foam quality of 0.75), the co-injection experiments were carried out at 57 °C and 2200 psia.

Figure 4-21 summarized the apparent viscosity results of all three foam generation experiments and compared them against the baseline apparent viscosity (black open circle with dotted line). In all three experiments, foam was successfully generated at the shear rate of 200 s^{-1} and above, even with the nanoparticle concentration as low as 0.1 wt%. However, the exact critical shear rate could not be determined as the foam/no foam transition was not observed. View cell observations were summarized in Table 4-10.

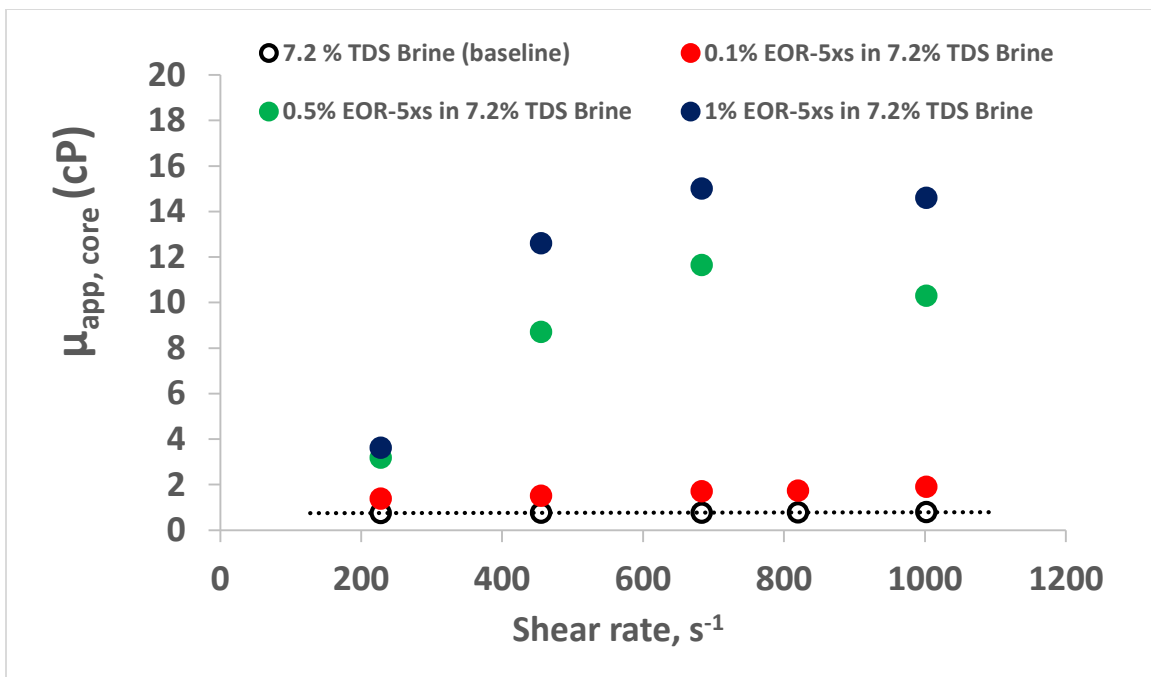


Figure 4-21 Core apparent viscosity measured across Boise sandstone core vs. shear rate in foam experiment at $57 \text{ }^\circ\text{C}$ and 2200 psia. The experiment was performed using the dispersion of EOR-5xs nanoparticle at 0.1, 0.5 and 1wt% in 7.2 wt% TDS brine with foam quality of 0.75. Baseline apparent viscosity was also plotted in black as a reference. Open symbols indicate no foam visible in view cell; filled symbols indicate visible foam.

As the shear rate increased, the foam became more viscous in all three cases. However, at the same shear rate, the dispersion of higher nanoparticle concentration appeared to generate a more viscous foam than the lower concentration ones. For 0.1 wt% concentration of nanoparticle, the largest apparent viscosity observed was only around 1.9 cP or MRF of 2.5 (the baseline apparent viscosity without nanoparticles was 0.76 cP). When the nanoparticle concentration was increased to 0.5 wt% and 1 wt%, the apparent viscosity jumped to 11.6 cP and 15 cP, respectively (MRF of 15 and 20, respectively). The increased nanoparticle concentration must have increased the amount of nanoparticles on the interface, providing a more rigid shield at the bubble surface.

In addition, the intermediate pressure tap data recorded from these experiments also provided insight on foam generation and transport in the core. Although our core sample was only 12 inches, the matrix permeability was not exactly uniform throughout the length of the core. In this 3500-mD Boise sandstone core, the permeability by section were 2930, 3330, and 4550 mD for upstream, middle, and downstream sections, respectively. The change in permeability along the core appeared to affect the foam generation and transport in the core. The measurement from the three cases with different nanoparticle concentrations showed similar trends. Thus, the results from the experiment with 1 wt% nanoparticle concentration was selected as an example, shown in Figure 4-22. The other two data sets at lower nanoparticle concentration were provided in the appendix.

At all injection rates, it was clearly shown that foam generation started in the upstream section of the core where the foam apparent viscosity was lowest. As foam continued to propagate into the middle section, foam apparent viscosity became at least 3 times larger than that of the upstream section. Although the foam apparent viscosity continued to increase in the middle section, the trend did not persist in the downstream section. On the other hand, the foam apparent viscosity decreased as foam propagated from

the lower permeability middle section to the higher permeability downstream section. This suggested the influence of matrix permeability on foam generation and that foam endlessly evolves in the matrix through coalescing-regenerating process. Shown by many earlier experiments, the foam viscosity depended on shear rate as well as matrix type. Thus, the foam in the downstream section might be less viscous than that in the middle section with lower permeability but higher shear rate, given that the flow rate was constant at all locations.

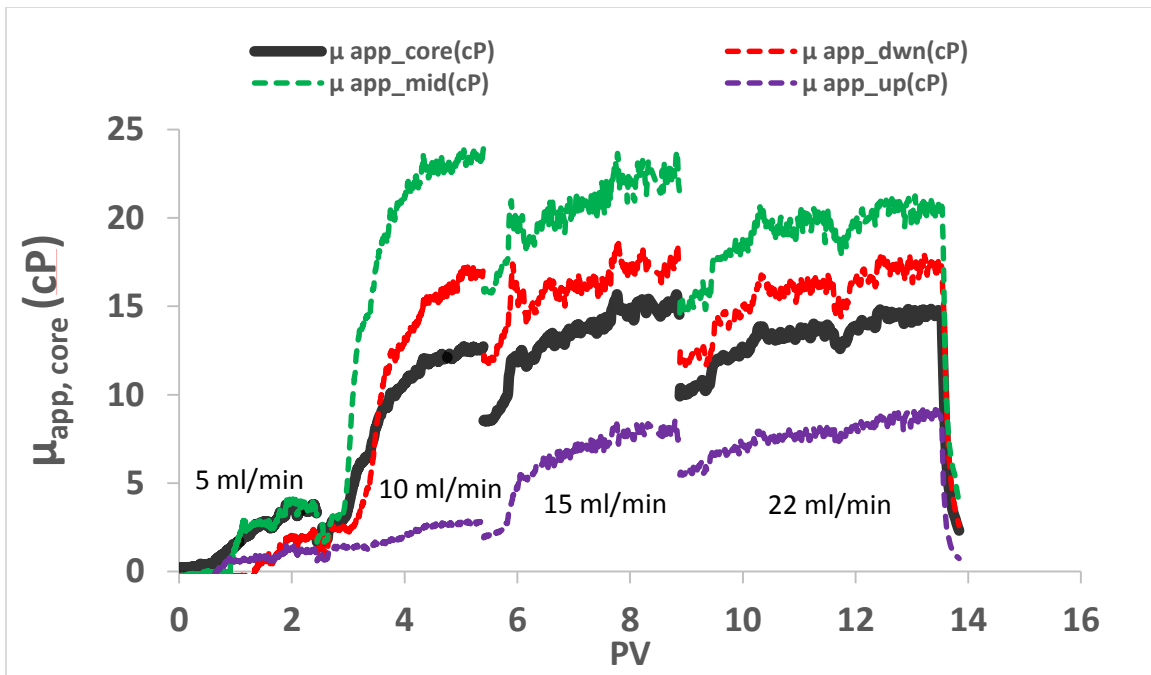
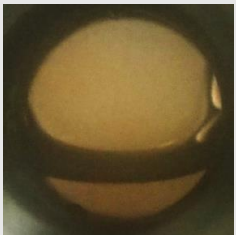

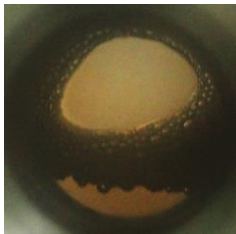












Figure 4-22 Apparent viscosity measured across Boise sandstone core and its intermediate sections in foam experiment (1 wt% EOR-5xs nanoparticle in 7.2 wt% TDS brine + CO₂). The experiment was performed at 2200 psia and 57 °C, using volumetric phase ratio of 3:1 (foam quality of 0.75). Shear thinning observed in the middle section.

The pressure tap data in this experiment not only indicated where the foam generation started but also suggested that nanoparticle-stabilized foam, similar to surfactant-stabilized foam, was shear thinning at high shear rates. As shown in the middle section of the core (green dash line), the foam apparent viscosity was highest at the injection rate of 10 ml/min (460 s^{-1}) then became smaller as the injection rate was increased to 15 ml/min and 22 ml/min. However, the shear thinning behavior was observed neither in the upstream section nor the downstream section of this core. Given the current shear rate, the lamellae density in this two sections might not yet have reached their limits, most likely dictated by pore geometry (permeability).

Table 4-10 Summary of view cell observation of foam generation experiment at various particle concentration.

Shear rate → NP conc ↓	230 s ⁻¹ 5 ml/min	460 s ⁻¹ 10 ml/min	680 s ⁻¹ 15 ml/min	820 s ⁻¹ 18 ml/min	1000 s ⁻¹ 22 ml/min
Baseline					
0.1% EOR-5xs					
0.5% EOR-5xs					
1% EOR-5xs					

4.1.3.2 Experiments in high permeability Berea sandstone cores (~200 mD)

Foam generation experiments with supercritical CO₂ were also conducted in the Berea sandstone cores to study the influence of matrix type on foam generation. The permeability of the first Berea sandstone core was 250 mD, an order of magnitude lower than that of the Boise sandstone. Shown as the red circles in Figure 4-23, the dispersion of 1 wt% EOR-5xs nanoparticle in 4 wt% NaCl was co-injected with CO₂ (at a fixed volumetric phase ratio of 1:1) into a 12-inch Berea sandstone core at 80 °C and 2200 psi. The apparent viscosity of the baseline experiment without nanoparticle was also plotted as black open circles (and dotted line).

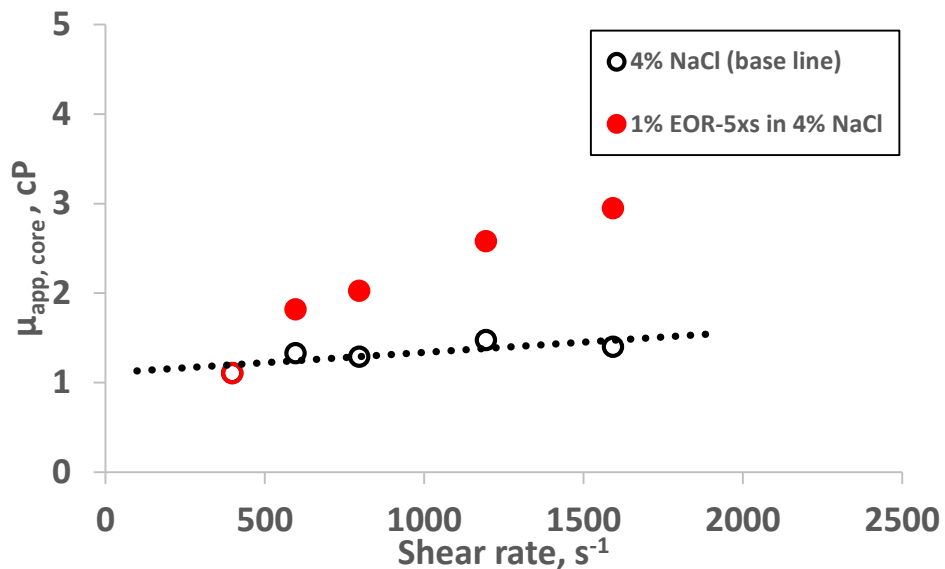


Figure 4-23 Core apparent viscosity measured across Berea sandstone core vs. shear rate in foam experiment at 80 °C and 2200 psia. The experiment was performed using 1 wt% EOR-5xs nanoparticle in 4 wt% NaCl brine at foam quality of 0.5. Open symbols indicate no foam visible in view cell; filled symbols indicate visible foam. Baseline apparent viscosity was also plotted in black as a reference.

With the dispersion of 1 wt% EOR-5xs in 4 wt% NaCl brine, a stable foam was successfully generated in the Berea sandstone core at 80 °C. The critical shear rate for foam generation was 600 s⁻¹ with a significant increase in apparent viscosity and the presence of foam in the view cell (Table 4-11). The apparent viscosity continued to increase up to 2.9 cP at 1600 s⁻¹, the largest shear rate investigated. Comparing the critical shear rate at the same temperature and pressure, the Berea sandstone value of 600 s⁻¹ was lower than the 870 s⁻¹ of Boise sandstone. This result again suggested that the matrix permeability was one of the key parameters dictating the threshold shear rate.

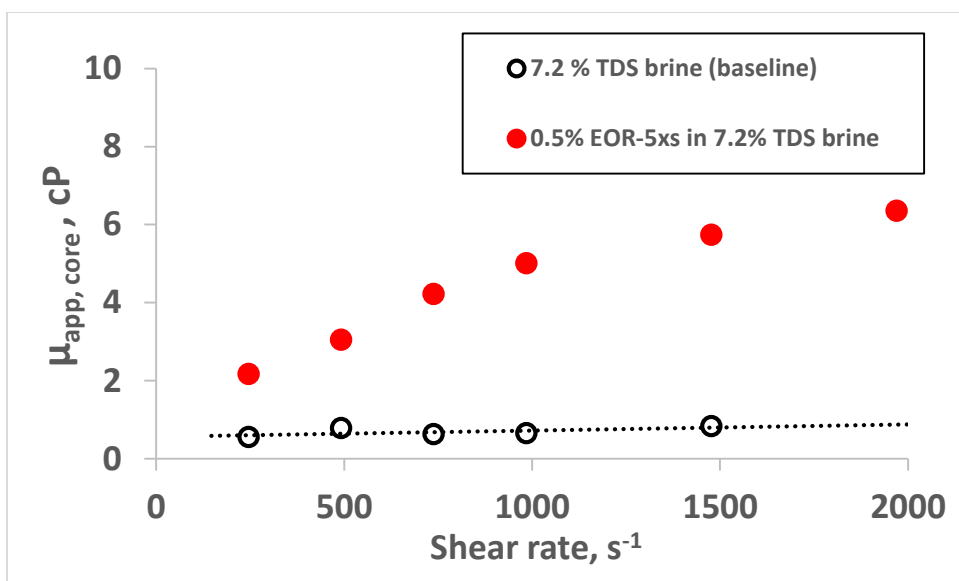
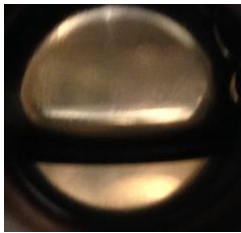

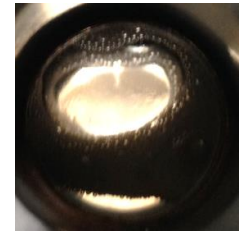

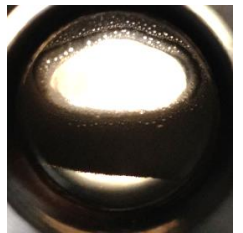
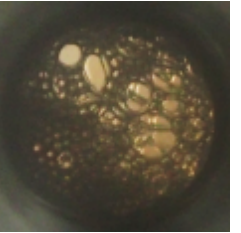
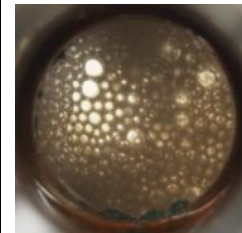
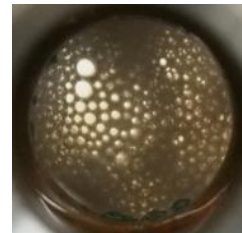
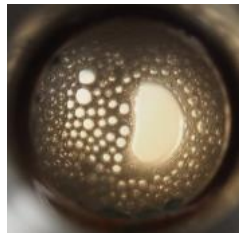
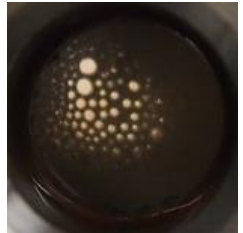


Figure 4-24 Core apparent viscosity measured across Berea sandstone core vs. shear rate in foam experiment at 57 °C and 2200 psia. The experiment was performed using 1wt% EOR-5xs nanoparticle in 7.2 wt% TDS brine at foam quality of 0.75. Open symbols indicate no foam visible in view cell; filled symbols indicate visible foam. Baseline apparent viscosity was also plotted in black as a reference.

Foam generation in a high salinity condition was also experimented in the second 200-mD Berea sandstone core at 80 °C and 2200 psia. A dispersion of 0.5 wt% EOR-5xs nanoparticle in 7.2 wt% TDS brine (6.4 wt% NaCl + 0.8 wt% CaCl₂) and CO₂ were co-injected into the core at a volumetric phase ratio of 3:1. The apparent viscosity of generated foam (red filled circles) and the baseline apparent viscosity (black open circles) were shown together in Figure 4-24. As indicated by both the view cell observation and an increase in apparent viscosity, foam was successfully generated, starting from the lowest shear rate of 230 s⁻¹. The foam apparent viscosity then continued to increase with increasing shear rates as the foam texture improved. However, the increasing trend started to level off as the shear rate went above 1000 s⁻¹. The largest apparent viscosity observed was 6.4 cP at the shear rate 1820 s⁻¹. This apparent viscosity was approximately twice the value observed in the previous experiment in Berea sandstone core with lower salinity at the same temperature and pressure, shown in Figure 4-23. This suggested a strong positive influence of increasing salt concentration, since the later experiment had almost twice the amount of salt, but only half of the nanoparticle concentration and higher foam quality compared to the previous experiment.

Table 4-11 Summary of view cell observation during supercritical CO₂ foam experiment in Berea sandstone core at 2200 psi, however at different temperature and salinity. The view cell was being filled from the side in the top row, instead was filled from the top in the second row.

Flow rate →	2 ml/min	3 ml/min	4 ml/min	6 ml/min	8 ml/min
Core ↓	400 s ⁻¹	600 s ⁻¹	800 s ⁻¹	1200 s ⁻¹	1600 s ⁻¹
f _g = 0.5 @ 80 °C 1 wt% EOR-5xs in 4 wt% NaCl					
Flow rate →	1 ml/min	3 ml/min	4 ml/min	6 ml/min	8 ml/min
Core ↓	250 s ⁻¹	740 s ⁻¹	990 s ⁻¹	1480 s ⁻¹	1970 s ⁻¹
f _g = 0.75 @ 57 °C 1 wt% EOR-5xs in 7.2 wt% TDS brine					

4.1.4 Discussion on the Influences of the Key Parameters in Foam Generation

4.1.4.1 Critical shear rate for foam generation and the effect of shear rate.

All experiments, both in fractured and unfractured cores, exhibited the critical shear rate for foam generation. Below this threshold, apparently viscosity of the CO₂/nanoparticle dispersion mixture tended to stay on the same level with that of a baseline experiment without nanoparticle. However, when the critical shear rate was overcome, the apparent viscosity rapidly increased with the increase in shear rate as foam continued to refine its texture. Figure 4-3 and Table 4-3 provided a good example of this behavior in sandstone matrix while Figure 4-8 and Figure 4-11 did the same for the fractured system. The critical shear rate did not appear to be a single definite value for all type of cores but rather varied with the core permeability and the presence of the fractures. Moreover, the factors that influenced foam viscosity and stability, such as salinity, foam quality, pressure, and temperature also affected the threshold shear rate. The effects of these parameters were discussed next.

In some of the experiments at high shear rates, nanoparticle-stabilized foam exhibited a shear thinning behavior after reaching the peak apparent viscosity (Figure 4-19, Figure 4-22), similar to surfactant-stabilized foam. However, the shear thinning behavior of foam in the Indiana limestone core occurred at a relatively lower shear rate, due to its low matrix permeability (Figure 4-15).

4.1.4.2 Effect of foam quality (CO₂ volume fraction)

Foam quality, i.e. the volume fraction of CO₂ in foam, appeared to have a strong influence on the foam apparent viscosity. There seemed to be a sweet spot of foam quality that yielded the highest apparent viscosity in a particular system. Reported by Aroonsri et

al. (2013), from the 22.5-Darcy beadpack experiments, a clear optimum foam quality of 0.75 yielded the highest apparent viscosity in most cases regardless of the experiment conditions. Although a considerable fraction of CO₂ volume is required to create sufficient lamellae to yield a significant apparent viscosity, too much CO₂ fraction may thin out the lamellae causing them to be less stable. The thin lamellae are easier to coalesce according to the oscillating-structural force theory since they may only have a monolayer coverage of nanoparticle (the last stage before the lamellae break). It is also known that foam is sometimes unable to form at a very high quality, due to insufficient aqueous phase to support foam generation. As the lamellae population becomes smaller at high quality, foam may change from discontinuous-gas foam (all pathways for gas flow are blocked by lamellae (Rossen, 1995)), to continuous-gas foam. As can be seen in Table 4-3, the open CO₂ pathway in the continuous-gas foam greatly increased the gas phase mobility and caused the large CO₂ bubbles as observed in the view cell.

The optimum foam quality shifted to a lower value when the permeability was shifted from a high value (beadpack) to a lower one (consolidated rock cores). At 23 °C, the foam generated in the Boise sandstone core at the quality of 0.67 and 0.8 yielded lower apparent viscosity than that of foam at the quality of 0.5 (Figure 4-4). Moreover, at 50 °C, the apparent viscosity was smaller and the threshold shear rate increased when the foam quality was increased from 0.57 to 0.75 (Figure 4-16 vs. Figure 4-17).

Further studies were also performed to determine the optimum foam quality in a Boise (3000 mD) and a Berea (260 mD) sandstone core. Results are shown in the following Figure 4-25, Figure 4-26 and Figure 4-27. Unlike the beadpack experiments, the results from these coreflood experiments at a constant injection rate did not show a clear optimum foam quality. Instead, the relationship between apparent viscosity and foam quality in all

the sandstone experimented tended to be flat. The apparent viscosity was less sensitive to foam quality below the value of 0.5. Above this value, the foam apparent viscosity began to drop. Again, the decline in apparent viscosity at larger CO₂ fractions can be explained by the transition from discontinuous-gas to continuous-gas foam with the transition point at the foam quality of 0.5. Therefore, this transition was considered as the optimum foam quality because it was the largest foam quality that yielded highest apparent viscosity. The temperature did not seem to affect the optimum foam quality as the trends were similar at 23, 50, and 80 °C. The changing CO₂ properties did not appear to affect the optimum foam quality.

The resulted optimum foam quality of 0.5 at 80 °C (close to a typical reservoir condition) posed a challenge in the field implementation of nanoparticle-stabilized CO₂ foam. The high-quality foam (>0.9) is more ideal in the oilfield application as it requires less amount of water and delivers a larger amount of CO₂ into the reservoir. However, the high-quality foam comes with a compromise in the apparent viscosity which is the most-important requirement for mobility control purpose. A good balance between these two needs is crucial for a successful implementation of mobility control using nanoparticle stabilized CO₂ foam.

As the permeability decreased by an order of magnitude at a time; 22.5-D beadpack, 3000-mD Boise sandstone core, and 280-mD Berea sandstone core, one would expect a continual decline in the optimum foam quality. However, the experiments in Boise and Berea sandstone cores gave close values of the optimum foam quality. A certain permeability cutoff, where the influence permeability on optimum foam quality became negligible, might exist.

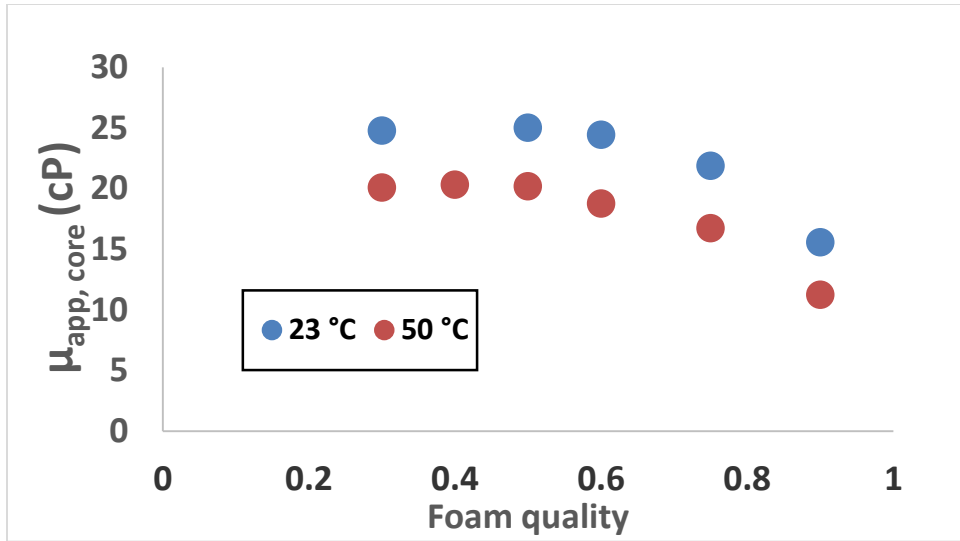


Figure 4-25 Core apparent viscosity measured across Boise sandstone core vs. foam quality, showing an optimum point around the quality of 0.5. The experiment was performed at 2000 psia using 1 wt% EOR-5xs nanoparticle in 2 wt% NaCl brine. Temperature were at 23 °C (blue) and 50 °C (red). The total injection rate was 10 ml/min (490 s^{-1} in term of shear rate).

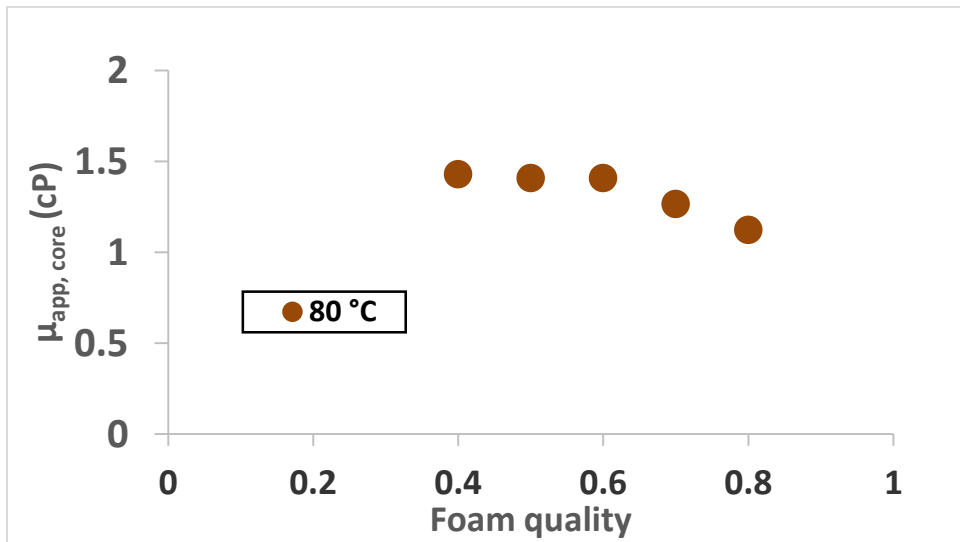


Figure 4-26 Core apparent viscosity measured across Boise sandstone core vs. foam quality, showing an optimum point around the quality of 0.5. The experiment was performed at 80 °C and 2200 psia using 1 wt% EOR-5xs nanoparticle in 4 wt% NaCl brine. The total injection rate was 10 ml/min (490 s^{-1} in term of shear rate).

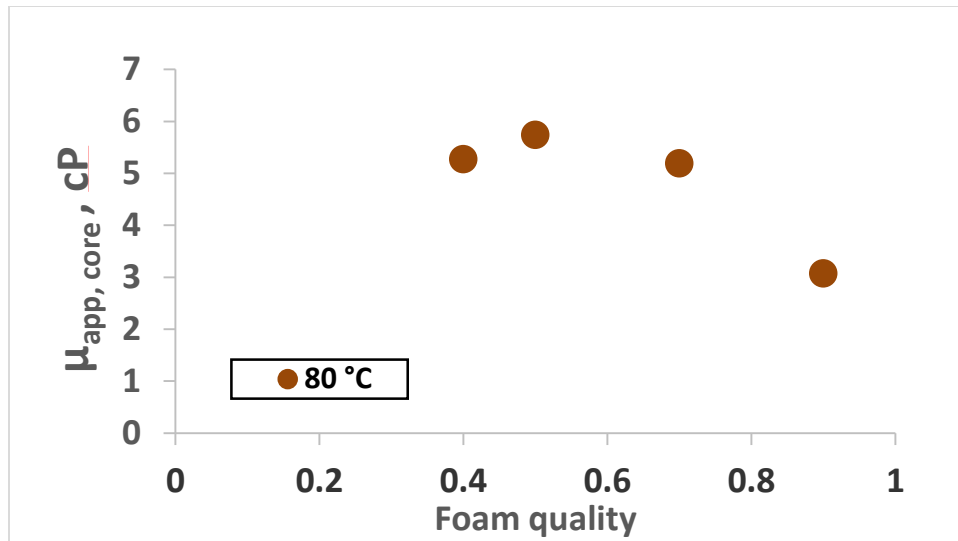


Figure 4-27 Core apparent viscosity measured across Berea sandstone core vs. foam quality, showing an optimum point around the quality of 0.5. The experiment was performed at 80 °C and 2200 psia using 1 wt% EOR-5xs nanoparticle in 4 wt% NaCl brine. The total injection rate was 6 ml/min (1190 s^{-1} in term of shear rate).

4.1.4.3 Effect of salinity (salt concentration)

The presence of salt in the aqueous phase provides a positive influence in foam generation. Increasing aqueous phase salinity reduces the electrostatic repulsion between nanoparticles, thus increasing the affinity of nanoparticles to be at the interface (Binks et al., 2007; Worthen et al., 2013a). This phenomenon eases the adsorption of nanoparticles on to bubble interfaces and leads to a larger nanoparticle coverage which better protect lamellae. Shown in Figure 4-20, at 80 °C, increasing salinity not only reduced the critical shear rate for foam generation, but also increased the apparent viscosity of the generated foam. However, it appeared there was a limit where increasing salinity no longer increased the apparent viscosity as the apparent viscosity trend of the experiment at 3 wt% and 4 wt% NaCl converged at high shear rates (Figure 4-20). The more extreme example on the

positive effect of salt was demonstrated in Figure 4-19 that foam was only generated with 4 wt% salinity; no foam at all was generated with 2 wt% salinity.

Although the added salt in the aqueous phase is beneficial for foam generation, too much salt can destabilized nanoparticles, forcing them to aggregate and drop out of the aqueous phase. The problem can be alleviated with steric stabilization by coating the particles with hydrocarbon chains, e.g. PEG. With the EOR-5xs nanoparticles, the highest salinity tested in this thesis was 7.2 wt% TDS (with 0.3 wt% of calcium divalent cations). Despite the possible aggregation of unstable nanoparticles, foam was successfully generated in this highly saline environment. The apparent viscosity yielded was as high as 15 cP (Figure 4-21).

4.1.4.4 Effect of temperature

Shown earlier in the results section, foam generation was more difficult at high temperature. This could be due to the lower CO₂ density and higher CO₂-water interfacial tension (IFT) (Bachu and Bennion, 2008). The higher IFT raised the adsorption energy required to move nanoparticles to the interface while the lower density of CO₂ promoted foam destabilization due to buoyancy. The drainage velocity of the thin liquid film also increased as the water viscosity decreased with increasing temperature, accelerating phase separation. According to the experiment in a Boise sandstone core, the same condition that created foam at 60 °C no longer created foam at 80 °C (Figure 4-17 vs. Figure 4-18). Also, the critical shear rate for foam generation increased with increasing temperature. Espinosa et al. (2010) reported a larger critical shear rate for foam generation in a beadpack at higher operating temperature. However, of all the sandstone experiments shown in this thesis, one cannot compare any of the liquid CO₂ cases directly with the supercritical CO₂ cases because different nanoparticles were used.

4.1.4.5 Effect of matrix permeability

The critical shear rate for foam generation changed with rock types even though the other experimental conditions were kept the same. The threshold shear rate tended to decrease when the matrix permeability became lower. As seen in liquid CO₂ foam experiments, the threshold shear rates were 470 s⁻¹ and about 300 s⁻¹ in the high permeability Boise (1700 mD) and the lower permeability Berea (200 mD) sandstone cores, respectively. Although the critical shear rate of the 5 mD Indiana limestone could not explicitly be determined, it appeared to follow the same trend with permeability as the strongest foam observed in this rock was generated at the lowest shear rate used (380 s⁻¹). The argument that threshold shear rate is smaller for the less permeable matrix still holds true for foam experiments with supercritical CO₂. At 80 °C, the critical shear rate for foam generation was 870 s⁻¹ in a Boise sandstone core (3000 mD) (Figure 4-20) while it was 600 s⁻¹ in a less permeable Berea sandstone core (250 mD) (Figure 4-23), at identical pressure, salinity, nanoparticle coating, and particle concentration. This trend was consistent with the critical shear rate of 3000 s⁻¹ in 22.5-D beadpack at 75 °C, reported by Espinosa et al. (2010). This suggested that the smaller pore throats facilitated the creation of bubbles and thereby reduced the shear rate needed to generate foam.

In addition to the critical shear rate, the apparent viscosity of generated foam also depended on the matrix permeability. Comparing the experiment in Boise and Berea sandstone cores at 2200 psia and 57 °C (Figure 4-21 vs. Figure 4-24), at the shear rate of 1000 s⁻¹, foam apparent viscosity measured in Boise sandstone core was about twice of that measured in the Berea core despite the identical concentration of nanoparticle and salt. However, the other data set at 80 °C (using 1 wt% nanoparticle concentration and 4 wt% salinity) did not show a clear trend. At the shear rate about 1200 s⁻¹, foam apparent viscosity

determined in both types of sandstone cores were in the range of 1.5 – 2.5 cP (Figure 4-19, Figure 4-20 and Figure 4-23).

4.1.4.6 Effect of nanoparticle concentration

Increasing nanoparticle concentration clearly enhances foam apparent viscosity, possibly by means of improving lamellae stability. As depicted in Figure 4-21, the foam generated with 1 wt% EOR-5xs nanoparticle dispersion created the MRF as high as almost 20 times, while the one generated with the diluted 0.1 wt% EOR-5xs dispersion hardly achieved the MRF of 2. This was a not surprise as the higher nanoparticle concentration in the dispersion resulted in a larger nanoparticle coverage on the bubble surface that created a more rigid shield and prevented lamellae coalescence. According to the oscillating-structural force theories, disjoining pressure, i.e. the force preventing bubble coalescence, increase with the increasing nanoparticle surface coverage (Israelachvili, 1992; Kralchevsky and Denkov, 1995). However, the higher nanoparticle concentration in the aqueous phase does not always lead to a better foam stability and apparent viscosity unless the ample amount of nanoparticles available in the aqueous phase is mobilized to the interface. Figure 4-19 provided a good example that foam was not generated despite the high nanoparticle concentration of 5 wt%. The increase in nanoparticle concentration did not lower the threshold shear rate for foam generation.

4.1.4.7 Matrix system versus fracture system

The critical shear rate for foam generation was much larger in fracture than in the matrix, under the same experiment conditions. Shown earlier in Figure 4-3 and Figure 4-8, the critical shear rate was 460 s⁻¹ in the Boise sandstone matrix, but was as high as 6000 s⁻¹ in the fracture placed in the Boise sandstone cores. The critical shear rate of 3400 s⁻¹ was

also observed in fractured Berea sandstone core at the same experiment conditions, despite its relatively lower matrix critical shear rate of 370 s^{-1} (Figure 4-10 vs. Figure 4-11). Once the foam generation started in fracture, more fluid flow were diverted away from fracture into the matrix, demonstrated by the results from flow decoupling calculation in Table 4-5. The diversion of flow exhibited the mobility control ability of nanoparticle-stabilized CO_2 foam in a fractured reservoir.

In an unfractured core, the location of first foam generation could be anywhere in the core depending on the flow rate and the matrix shear rate. As shown in Figure 4-13, the viscous foam was first generated in the downstream section of the core before growing toward the injection inlet, into the middle and upstream sections. For a fractured core, the only data set with pressure tap data showed that foam generation started in the middle section of the core. Additional data would have to be acquired to determine whether the trends observed in matrix also apply in fractures.

4.1.4.8 Effect of fracture permeability

The two fractured Boise sandstone corefloods shown earlier in section 4.1.2 had the fracture aperture sizes of 104 microns and 65 microns and the critical shear rates of 3700 s^{-1} and 5800 s^{-1} , respectively (Figure 4-8). However, the fractured Berea core, with the largest aperture size of 165 microns, exhibited the critical shear rate of $\sim 3400 \text{ s}^{-1}$ (Figure 4-12). These thresholds were all larger than those observed in matrix flow, which supported the contention that smaller constrictions facilitate bubble creation. The absence of a clear trend between threshold shear rate and fracture aperture suggested that the hydraulic aperture (inferred from the flow rate vs. pressure drop measurements using the classical flow-in-a-slit formula) did not capture the distribution of constriction sizes that control

foam generation. This was not surprising, because all the fractured samples used in this work have rough-walled, irregular geometries the entire length of the core.

4.2 PRE-GENERATED FOAM COREFLOOD EXPERIMENTS

For the experiments in the preceding section, foam was generated and then transported in the same porous medium, In this section, foam transport in a core is studied, but instead of generating foam inside the rock matrix of interest, foam was generated upstream of the core in a beadpack. Nanoparticle dispersion and CO₂ were co-injected into a tube packed with 180 microns spherical glass beads, and the generated foam leaving the beadpack was routed to the core holder located downstream. Pre-generation of foam in the beadpack was beneficial in the study of foam rheology, allowing the generation process to be separated from foam transport in rock matrix. Additionally, the ability of pre-generated nanoparticle-stabilized CO₂ foam in enhanced oil recovery was also experimented in the sandstone matrix. For simplicity, all of these experiments were performed in the Boise sandstone cores at 2000 psia and 23 °C. Experiment results were shown and discussed in the following sections.

4.2.1 Rheology Measurement of Foam Flowing in Sandstone Matrix Using the Branching Manifold.

In the following experiments, the foam was pre-generated in the beadpack then routed to the branching manifold system, described in section 3.3.2.1. This branching manifold allowed us to control the foam flow rate through a rock core, while the total flow rate through the foam generating beadpack remained constant. This setting enabled the characterization of foam rheology within the core across a range of shear rate, without changing the inlet foam texture and properties. In addition, the intermediate pressure taps were also installed across the core to provide insights on foam propagation.

In this series of experiments, the Nissan EOR-5xs nanoparticle was prepared as 1 wt% dispersion in 4 wt% NaCl brine. Nanoparticle-stabilized CO₂ foam was pre-generated in the beadpack and then injected into a 12-inch Boise sandstone core (860 md) at 20 ml/min injection rate with foam qualities of 0.5 and 0.75. As an example, Figure 4-29 demonstrated the experiment results with internal pressure taps at the foam quality of 0.75 with the corresponding baseline experiment shown in Figure 4-28. The location of the pressure taps divided the core into three sections of equal length; upstream, middle, and downstream. The upstream section was damaged with a permeability of 570 mD, lower than those in the middle and downstream sections which were 1490 mD and 1450 mD, respectively.

The black line in Figure 4-28 and Figure 4-29 indicated the pressure drop across beadpack while the blue line showed the pressure drops across the core and the branching manifold system. The purple, green, and red line represented the pressure drop in the upstream, middle, and downstream section, respectively. It can be seen that the black line was constant throughout the pre-generated foam experiment, suggesting that the foam of consistent texture was generated throughout the experiment. In the first portion of the foam experiment in Figure 4-29, all fluid leaving the beadpack was injected into the core. The pressure drop across the core was around 400 psi (blue line). Once the flow path through the 20-ft tube was opened, the total pressure drop across the core-tube parallel system decreased to approximately 145 psi, as shown in the second portion of the experiment. When the flow path through the 5-ft tube was opened, further reduction in pressure drop (to approximately 35 psi) was observed, as shown in the third portion of the experiment.

In term of MRF, the pressure drop when all foam flowed through the core was equivalent to the MRF of 6. Once the 20-ft tube was introduced into the system, a portion

of foam was diverted away from the core to the 20-ft tube. The pressure drop across the entire branching system became equivalent to the MRF of 10. The increase in the overall MRF suggested that the foam was shear-thinning and its viscosity of foam increased as the flow split between the core and the tube. However, when the 20-ft tube was substituted by the 5-ft tube, the overall MRF decreased to 4. As the majority of foam was expected to flow through the 5-ft tube, it was possible that the foam flowing through the tube was shear-thinning; therefore, the overall foam resistance was less. Very small amount of foam was believed to flow through the core as the displacement of lamellae was difficult with a small pressure gradient.

Attempts were made to allocate the foam flow between the core and the tubes and calculate the corresponding foam apparent viscosity by branch, but without success. In flow allocation calculation, as the foam viscosity was flow rate dependent, using only permeability and flow resistance in tubes was not sufficient to allocate the foam flow among core and tubes. At least one direct measurement of the flow rate, preferably through the core, was required.

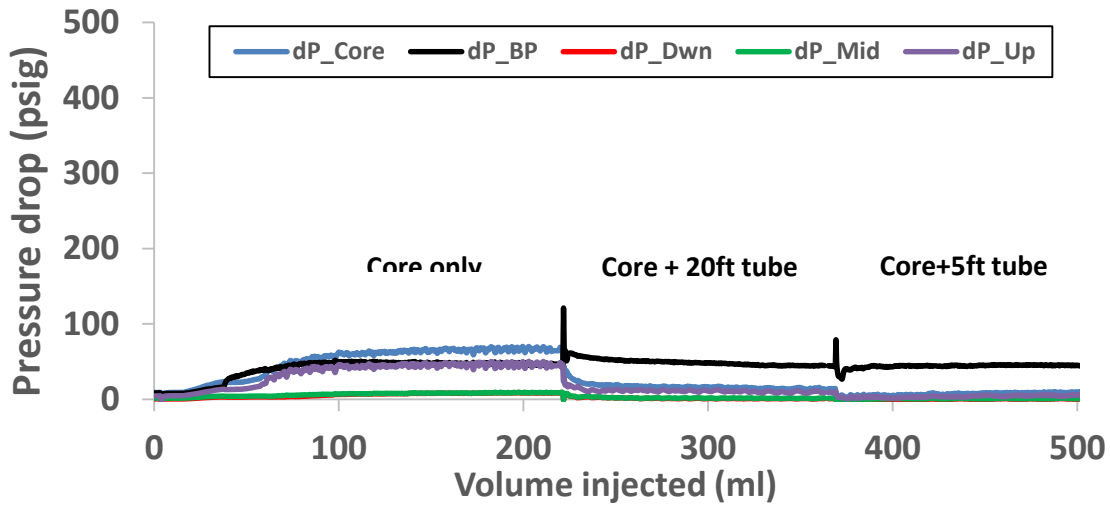


Figure 4-28 Pressure drop measured across the core and each intermediate sections of the baseline experiment in Boise sandstone (860 mD) core with the branching manifold (4 wt% NaCl brine + CO₂). The experiment was performed at 2000 psia and 23 °C, using foam quality of 0.75 (3:1). The injection rate was fixed at 20 ml/min, giving flow velocity $u = 187$ ft/day.

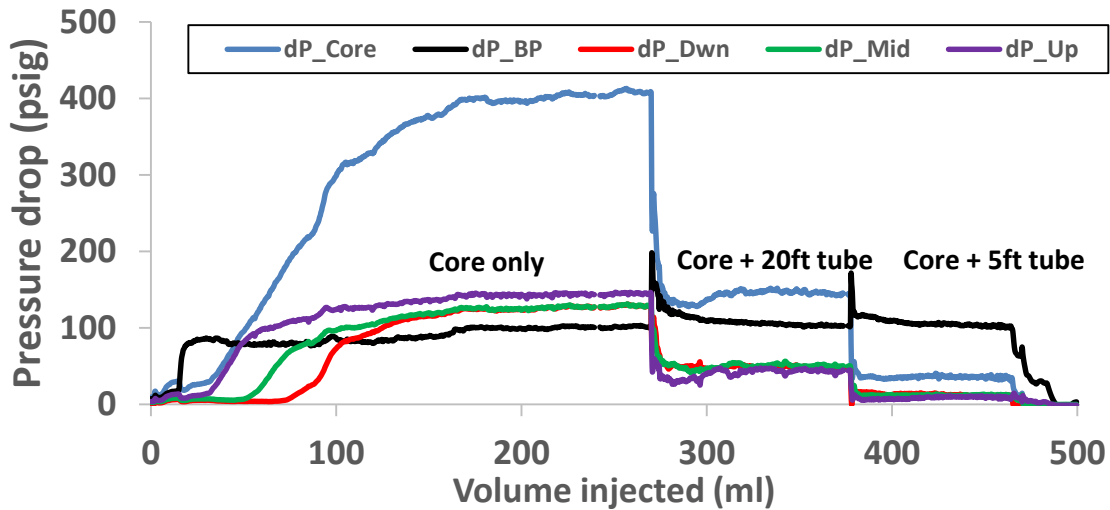


Figure 4-29 Pressure drop measured across the core and each intermediate sections of the pre-generated foam experiment in Boise sandstone core (860 mD) with the branching manifold (1 wt% EOR-5xs nanoparticle in 4 wt% NaCl + CO₂). The experiment was performed at 2000 psia and 23 °C, using foam quality of 0.75 (3:1). The injection rate was fixed at 20 ml/min, giving flow velocity $u = 187$ ft/day.

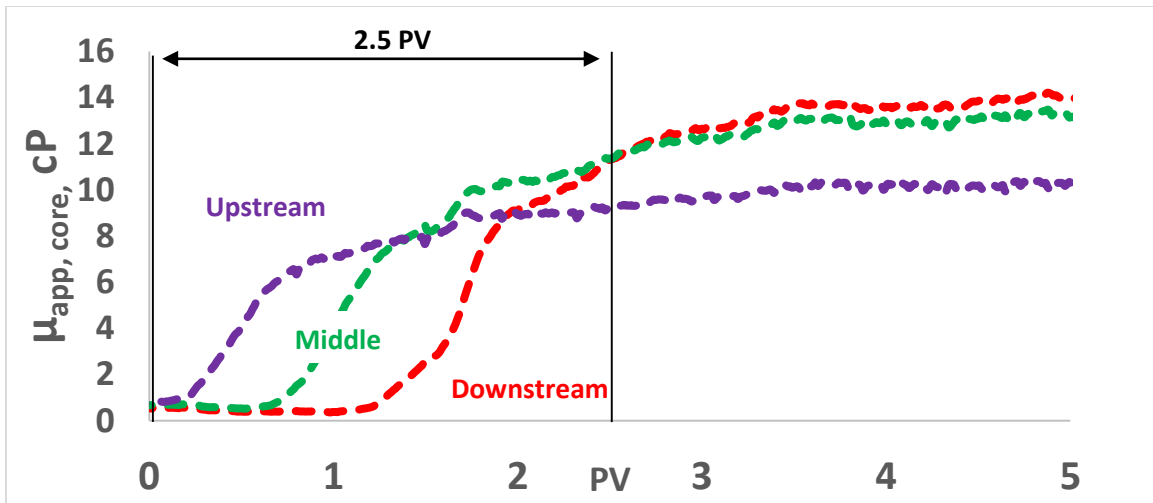


Figure 4-30 Apparent viscosity measured across each intermediate sections of the pre-generated foam experiment in Boise sandstone core (860 mD) at brine saturated condition (taken from the first portion of experiment result shown Figure 4-29, using (1 wt% EOR-5xs nanoparticle dispersion in 4 wt% NaCl brine). The experiment was performed at 2000 psia and 23 °C, using foam quality of 0.75 (3:1). The injection rate was fixed at 20 ml/min, giving flow velocity $u = 187$ ft/day.

Although we were unable to decouple the flow and fully understand the behavior of foam transport in the core-capillary tube parallel system, the internal pressure tap data provided an insight on foam transport in porous media (Figure 4-30). Unlike the injection of a single-phase incompressible fluid, it took approximately 2.5 PV for the pre-generated foam to travel through the brine-saturated core (as indicated by the sequential arrival of plateau values of apparent viscosity in all three core sections). Rossen (1995) suggested that lamellae must be breaking if foam was not propagating at the rate of injected gas and if the bubble is believed to be moving in the core. A possible explanation is that foam continually coalesced and re-generated, especially at the foam front, where the rate of lamellae destruction greatly surpassed the lamellae creation rate. This explanation would

challenge the premise that nanoparticle-stabilized bubbles are more resistant to coalescence because of the higher adsorption energy of the nanoparticles.

In order to further investigate further the hypothesis that foam continuously coalesce and regenerate, the next experiment compared the direct co-injection against the injection of pre-generated foam. The 12-inch Boise sandstone core used in this experiment had overall permeability of 440 mD, with the upstream, middle, and downstream section permeabilities of 260, 570 and 530 mD, respectively.

Figure 4-31 demonstrated the result from the foam generation through direct co-injection while Figure 4-32 showed the results from the pre-generated foam coreflood experiment at the same total flow rate of 20 ml/min and foam quality of 0.75. Presented as the black solid line in both figures was the core average apparent viscosity, showing similar steady state value of approximately 4 cP. This implied that the foam apparent viscosity in the rock core was independent of the initial foam texture. The apparent viscosity of foam was dictated by the porous media through which it propagated. Although the average core pressure responses from the two experiments were similar, the behaviors by section appeared to be different. In the co-injection experiment, the foam apparent viscosity was building up slightly as the foam was travelling through the core (Figure 4-31). However, in the pre-generated foam experiment, the pressure tap data indicated that brine was slowly displaced by relatively viscous fluid (the plateau of small apparent viscosity that precedes the arrival of a front in each core section in Figure 4-32), followed by the flow of viscous foam which reached a similar plateau value of larger apparent viscosity in all of the core sections. Again, it took more than one PV for the foam to propagate through the core. This supported the prior ‘coalescence-regeneration’ hypothesis. However, it was still unclear

why the apparent viscosity in the downstream section was slightly higher than the others; one possible explanation is the capillary end effect described in section 4.1.2.1.

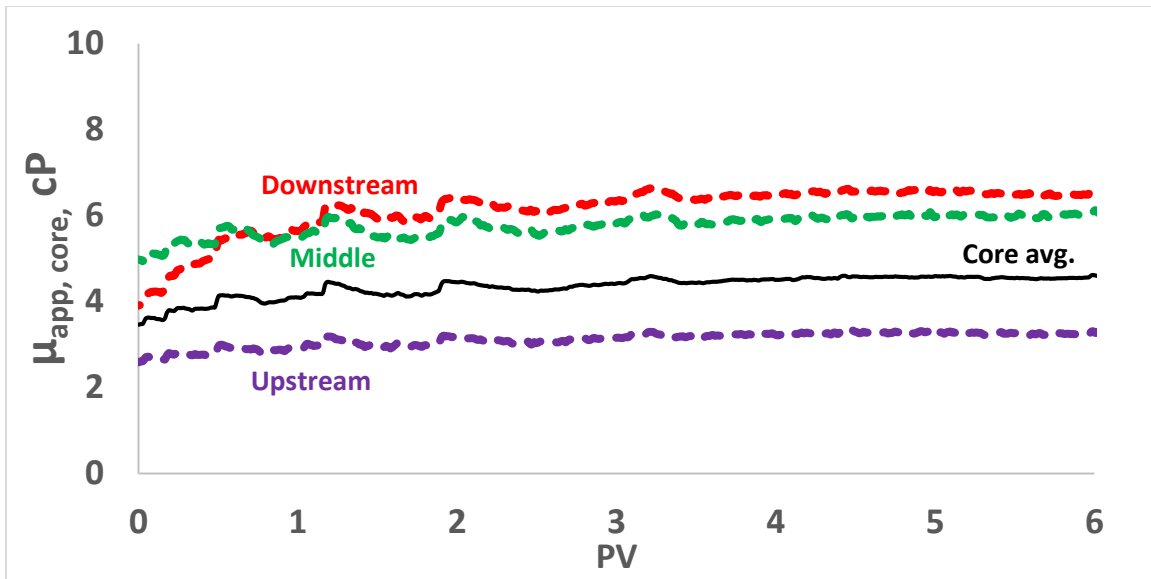


Figure 4-31 Apparent viscosity measured across the core and each intermediate sections of co-injection experiment in Boise sandstone core (440 mD) using 1wt% EOR-5xs nanoparticle dispersion in 4 wt% NaCl brine. The experiment was performed at 2000 psia and 23 °C, using foam quality of 0.75 (3:1). The injection rate was fixed at 20 ml/min, giving flow velocity $u = 187$ ft/day.

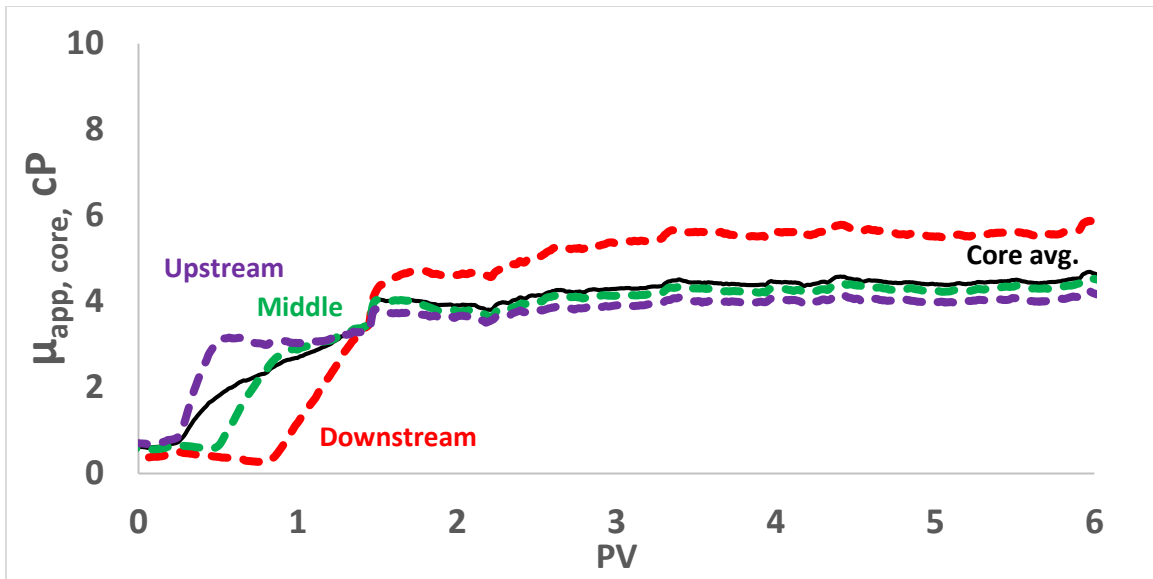


Figure 4-32 Apparent viscosity measured across the core and each intermediate sections of pre-generated foam experiment in Boise sandstone core (440 mD) using 1 wt% EOR-5xs nanoparticle dispersion in 4 wt% NaCl brine). The experiment was performed at 2000 psia and 23 °C, using foam quality of 0.75 (3:1). The injection rate was fixed at 20 ml/min, giving flow velocity $u = 187$ ft/day.

4.2.2 Oil Recovery Experiment in Sandstone Cores with Pre-generated Foam.

In this section, we attempted to determine the behavior of nanoparticle-stabilized CO₂ foam in the presence of hydrocarbon in the porous media. The foam stability, mobility, and ability to improve oil recovery were the key properties to be investigated. Understanding the foam transport behavior in hydrocarbon bearing pore networks is crucial in upscaling laboratory experiments to field pilots. An effective mobility control in CO₂ EOR can only be achieved if foam still provides flow resistance when in contact with hydrocarbon in the reservoir.

To investigate the effect of the hydrocarbon phase, decane was used to represent the oil phase. According to the PVT calculation at the experiment condition of 23 °C and 2000 psi, decane was miscible with CO₂, allowing the performance of miscible flood to be tested. This series of experiments was performed in a 12-inch Boise sandstone core (800 mD) with the residual decane saturation (S_{or}) of ~ 30%. Initially, CO₂ and 4 wt% NaCl brine were co-injected into the system to measure oil recovery and baseline apparent viscosity without nanoparticle. After the residual decane was re-established in the core (procedure described in section 3.3.2.2), the second run was performed with pre-generated foam using 1 wt% EOR-5xs nanoparticle dispersion in 4 wt% NaCl. The plots of apparent viscosity by section versus PV injected for both foam and baseline experiments were shown in Figure 4-33 and Figure 4-34, respectively. In both cases, decane was recovered, however, the amount was not measured. The results from the pre-generated foam experiment in brine-saturated core ($S_o=0$) shown in Figure 4-30 were also used for mobility comparison.

As shown in Figure 4-33, it was observed that foam still provided a notable amount of resistance despite the presence of residual oil in core. Steady state apparent viscosity

(upstream of the foam front) measured in the foam experiment ranged from 8 to 10 cP, twice the amount measured in the baseline experiment with the same residual oil condition (Figure 4-34). Still, when compared to Figure 4-30, it was obvious that the foam resistance to flow was deteriorated with the existence of residual oil since the foam apparent viscosity was as high as 14 cP in the brine-saturated core.

Comparing the movement of the flood front between Figure 4-33 and Figure 4-34, the propagation of foam was slightly slower than that of the brine-CO₂ mixture (baseline) as it took about 0.6 PV for the foam to travel the length of the core while it took only 0.4 PV for the brine-CO₂ mixture to travel the same length. However, foam in the presence of hydrocarbon propagated much faster than that in the absence. As shown in Figure 4-30, the travel time of foam in brine-saturated core was about 2.5 PV, which was more than four times of that in the core with residual oil. Additionally, the frontal velocity appeared to decrease as foam propagated along the core with residual oil. In the absence of residual oil (Figure 4-30) the delay of the responses between sections were even, but in the presence of residual oil almost immediate responses in the upstream and middle sections were observed (with some delay in the response of the downstream section) (Figure 4-33).

With the presence of residual oil, the absence of clear delay of responses between sections suggested that the inner CO₂ phase in the injected foam was able to contact and mobilize the residual oil ahead of the foam front. This forming of oil bank in front of the foam front was confirmed by the view cell observation. It was still inconclusive how the CO₂ contacted the residual oil because, in theory, the nanoparticle coverage on the interface should strengthen lamellae and prevent coalescence of CO₂ bubbles. However, the dynamic coalescence-regeneration concept of surfactant-stabilized foam in porous media, as described by Lee and Kam (2013), might also apply for nanoparticle-stabilized foam. The

coalescence of bubbles made it possible for CO₂ to become in contact with the residual oil, while the regeneration of lamellae maintained the foam ability to provide flow resistance.

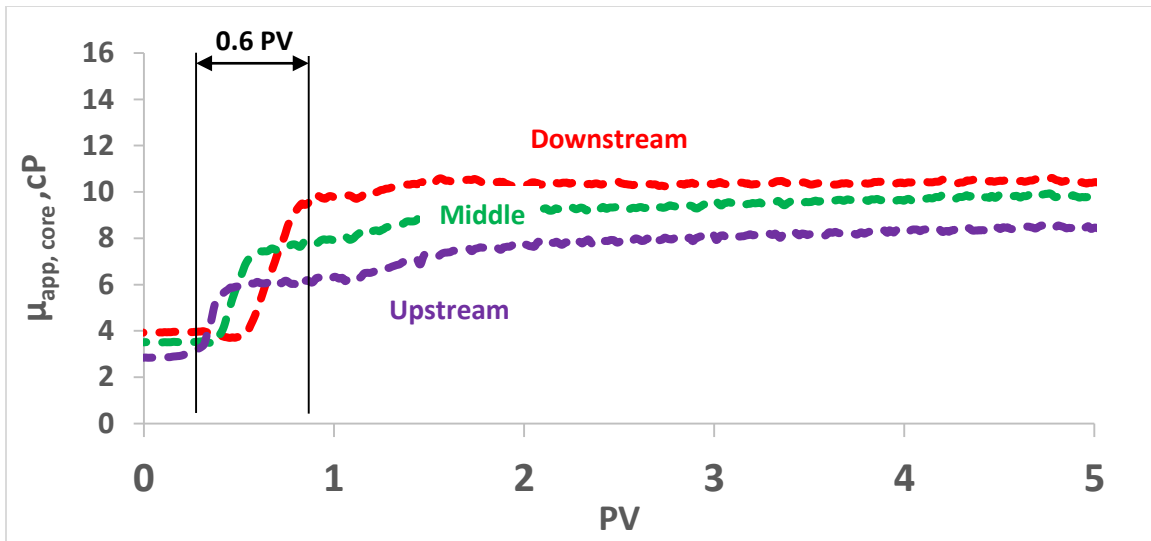


Figure 4-33 Apparent viscosity measured across each intermediate sections of the pre-generated foam experiment in Boise sandstone core at residual oil condition (1wt% EOR-5xs nanoparticle in 4 wt% NaCl + CO₂). Estimated decane saturation prior to foam injection was 30% (S_{or} to brine). The experiment was performed at 2000 psia and 23 °C, using foam quality of 0.75 (3:1). The injection rate was fixed at 20 ml/min, giving flow velocity $u = 187$ ft/day.

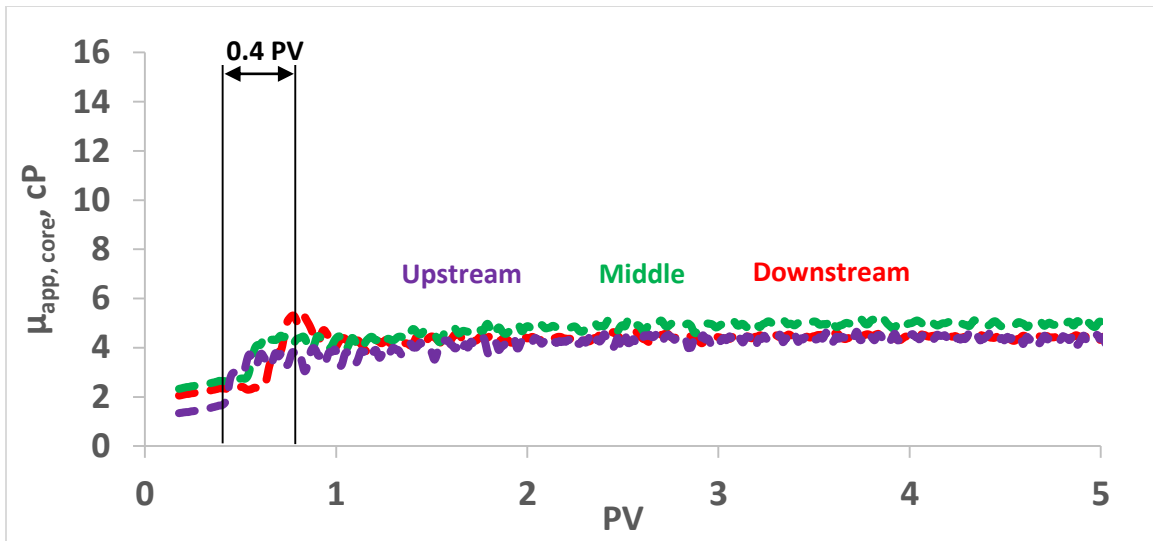


Figure 4-34 Apparent viscosity measured across each intermediate sections of the baseline experiment in Boise sandstone core at residual oil condition (4 wt% NaCl brine + CO₂). Estimated decane saturation prior to foam injection was 30% (S_{or} to brine). The experiment was performed at 2000 psia and 23 °C, using foam quality of 0.75 (3:1). The injection rate was fixed at 20 ml/min, giving flow velocity $u = 187$ ft/day.

Further investigation on the ability of foam in recovering residual oil were carried out in Boise sandstone cores, again, using decane as an oil phase. In this series of experiments, the foam, pre-generated in the beadpack using 1 wt% EOR-5xs nanoparticle dispersion in 4 wt% NaCl, was injected into the core at residual oil condition. In addition to foam injection, three others injection recipes were also investigated: brine-CO₂ flood, liquid CO₂ flood and CO₂ foam slugs. Liquid phase effluent remaining after CO₂ gas had been vented was collected using the fraction collector to determine oil cut. After each coreflood, the core was re-saturated with brine and the wet-weight was measured to estimate the residual oil saturation (using the equation in section 3.4.11). Table 4-12 summarized the key parameters and results of these experiments. The plot of apparent viscosity versus PV injected for all four experiments were also put together on Figure 4-35.

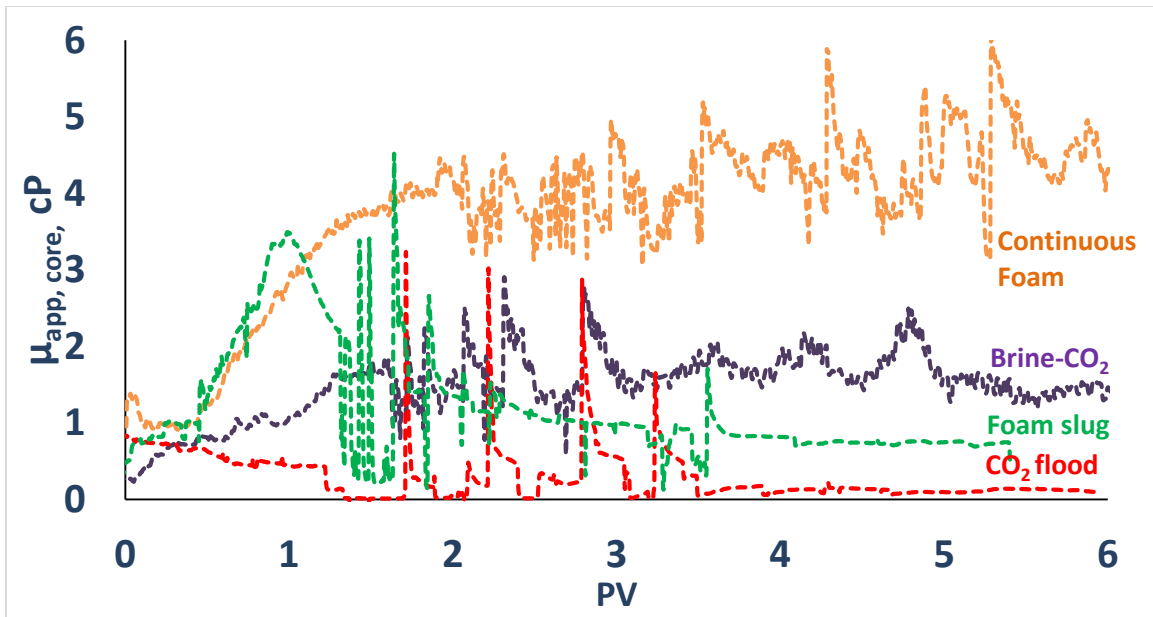


Figure 4-35 Apparent viscosity measured across the core of the pre-generated foam experiment in Boise sandstone core at residual oil condition for four types of injection fluid(s): continuous foam flood, continuous CO₂ flood, continuous Brine-CO₂ flood and foam slug injection. These experiments were performed at 2000 psia, 23 °C and fixed total injection rate of 6 ml/min, giving flow velocity $u = 56$ ft/day.

Table 4-12 Summary of coreflood results in Boise sandstone core (820 mD) at residual oil saturation. Experiment were conducted at 2000 psia and room temperature (23 °C). Use EOR-5xs nanoparticle (Nissan Chemical), constant injection rate at 6 ml/min, giving flow velocity $u = 56$ ft/day.

Injected Fluid	Aq. rate (ml/min)	CO ₂ rate (ml/min)	Particle Conc. (wt%)	Salinity (wt%)	Initial Sor	Final Sor	dP (psi)	$\mu_{app, core}$ (cP)
Liquid CO ₂	-	6	-	4	30%	6%	4	0.15
Brine/CO ₂	1.5	4.5	-	4	28%	6%	45	1.4
Cont. foam	1.5	4.5	1	4	26%	7%	140	4.5
Foam slug/CO ₂	6ml/min foam slug (0.3 PV @ Q 0.75) then 6ml/min CO ₂		1	4	30%	12%	22	0.7

As shown in Figure 4-35, nanoparticle stabilized CO₂ foam exhibited its ability in decreasing mobility of the injected CO₂, even under the influence of residual hydrocarbon phase. At steady state, the continuous flooding of pre-generated foam yielded the apparent viscosity as high as 4.5 cP, which can be inferred as the apparent viscosity behind the foam front. Comparing between different types of injection, the continuous foam flood gave the MRF of around 3 times over the brine/CO₂ flood baseline and as high as almost 30 times over the continuous liquid CO₂ injection. Unlike the apparent viscosity results shown in Figure 4-33, there were many fluctuations in these results since the effluent was being vented continuously for sample collection purpose, instead of being collected in the waste accumulator vessel. The multiphase effluent flowed through the backpressure regulators directly, resulting in fluctuations of flow and a greater swing in pressure measurement. These fluctuations in pressure drop across the core was observed to start when decane arrived at the backpressure regulators.

In term of residual oil recovery, the continuous foam flood, CO₂/brine flood and continuous CO₂ flood, all showed that residual oil saturation could be reduced from ~30% down to 6 -7% (Table 4-12). These results demonstrated that the ability of nanoparticle-stabilized CO₂ foam in enhanced oil recovery process was as good as the continuous CO₂ flood or the brine-CO₂ flood, but with the added benefit of conformance control. However, the improvement in sweep efficiency could not be observed because all of the experiments were one-dimensional flows in a rather homogeneous medium of only 12 inches long. Therefore, the potential improvement in areal and vertical sweep could not be inferred. Although the residual oil saturation theoretically can be reduced to near-zero value, as CO₂ and decane were miscible at this condition of experiment, some residual oil was found to

remain in the core. The possible explanation was that the water phase might have prevented the CO₂ phase from contacting decane in some areas.

According to view cell observations, oil banks ahead of the foam front were observed in all experiments. Figure 4-36 provided an example of view cell snapshots showing the evolution of the effluent during the continuous foam flood. Initially, the view cell was filled with brine (A) before the CO₂ was introduced into the system. Approximately 1.6 PV after the foam injection started, oil blobs began to arrive at the view cell (B) and finally turned into a continuous oil flow (C). According to the visual inspection, there appeared to be only two fluid phases residing in the view cell with a clear interface in the middle, confirming the miscibility of CO₂ and decane at this experiment condition. After 0.25 PV of continuous oil flow, nanoparticle-stabilized foam finally broke through (D) and continued to fill the view cell (E). This confirmed the stability of foam in the presence of residual oil.

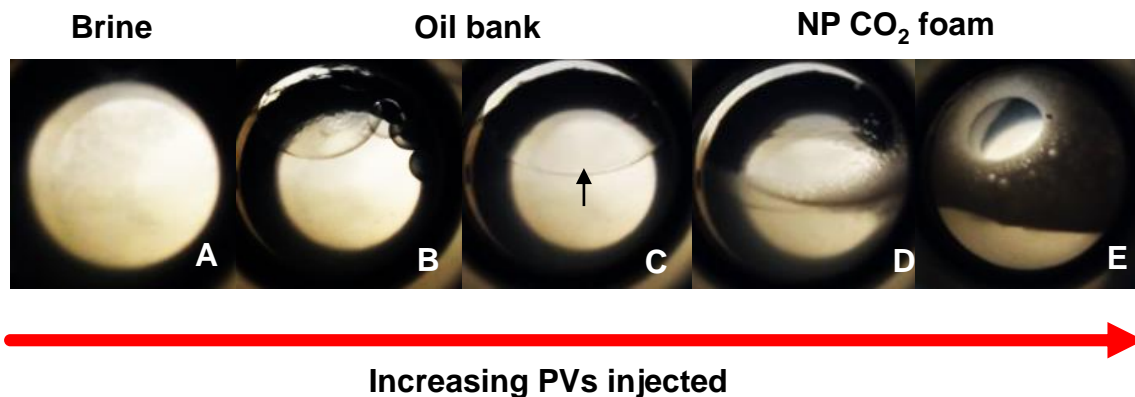


Figure 4-36 View cell snapshots from continuous foam flood experiment, showing: Initial condition filled with brine (A), oil bank arrival (B), continuous oil flow (C, black arrow indicated the interface), foam breakthrough about 0.25 PVs after oil bank arrival (D) and the continuous foam flow where steady state apparent viscosity was measured (E).

The strategy of foam slug followed by continuous CO₂ injection was also tested and the results were shown in Table 4-12. For field applications, an injection of foam slug would be a more economically feasible option as less amount of expensive nanoparticles is required. However, this injection scheme will not work if the trailing slug of CO₂ advances and breaks through the foam bank, thus disrupting its capability to improve sweep efficiency. In our foam slug experiment, 0.3 PV of pre-generated CO₂ foam was injected at 6 ml/min into the core, followed by continuous CO₂ injection at the same flow rate. Similar to the result of continuous foam injection, the core apparent viscosity increased steadily during the injection of foam slug (Figure 4-35). Once the injection mode was switched to straight liquid CO₂, the apparent viscosity continued to increase with a steeper trend, reached the peak value of 3.5 cP after a cumulative injection of 1 PV (0.3 PV foam + 0.7 PV CO₂). This trend was almost identical to the apparent viscosity trend during the continuous foam injection. As high mobility CO₂ continued to be injected and as the mobilized oil and the foam slug reached the outlet of the core, the apparent viscosity declined gradually over the next 2 PV. The steady state mobility measured during the straight CO₂ flow period was 0.7 cP, approximately 5 times larger than when only CO₂ had been injected from the start. Although there was only CO₂ flowing in both cases, at the time of measurement, the larger apparent viscosity observed in the foam slug case could be resulted by the limited gas flow path due to trapped foam. The high mobility CO₂ might have channeled through the foam slug and left behind some stable lamellae that still provided substantial flow resistance. This result suggested that foam slugs could be driven through a porous medium by a large trailing bank of CO₂.

Also, shown in Table 4-12, the injection of foam slug followed by straight CO₂ left almost twice the amount of residual oil saturation comparing to the other three injection

types. However, there was uncertainty involved with the measurement of residual oil saturation using weight difference method. As the foam slug injection was the last experiment conducted in this series, the same core already contacted at least 20 PV of CO₂. The possible geochemical reaction could have mobilized fine particles, thus reduced the core weight. This could have led to the error in estimating residual oil saturation.

Although the view cell observation for foam slug injection (Figure 4-37) showed that the oil bank was also formed, almost no stable foam arrived in the view cell afterwards. In addition to the destabilization of foam by hydrocarbon, the foam slug was rather vulnerable as lamellae became thinner with increasing volume fraction of CO₂. In the absence of stable foam production, the injection of foam slug was a success as it reduced CO₂ mobility and produced residual oil, without the presence of complicating foam/emulsion at the production site.

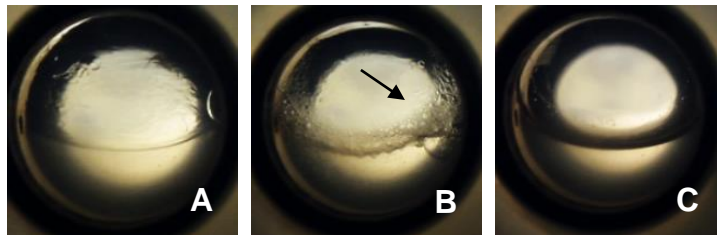


Figure 4-37 View cell snapshots from foam slug injection experiment (case #4), showing: flowing of decane-CO₂ bank in view cell (A), best visual observation of foam after oil bank. (B, black arrow indicated bulk foam at the view cell inlet) and continuous CO₂ flow period where steady state apparent viscosity was measured (C).

Another series of oil recovery experiments was also conducted in a decane-saturated core to investigate the effect of mobile oil. Again, pre-generated CO₂ foam was injected into the Boise sandstone core (3200 mD) at an injection rate of 6 ml/min. The

injection of liquid CO₂ and brine-CO₂ mixture were also tested in the same core for comparison purpose. However, the foam slug injection was not tested. **Error! Reference source not found.** Table 4-13 summarized the key parameters and results obtained from these experiments. The plots of apparent viscosity versus PV injected for all experiments were put together in Figure 4-38**Error! Reference source not found.** Despite the difference in the core permeability and initial decane saturation, steady state mobilities observed in the experiments in decane-saturated core were similar to those observed in the experiments at residual oil condition. The apparent viscosities were 1.4 cP in the brine/CO₂ baseline experiment, around 4 cP in the continuous foam flood experiment, and nearly zero in the CO₂ flood experiment. Again, fluctuations in apparent viscosity due to the multiphase flow through the BPRs were also observed in the foam and brine-CO₂ experiment but not in the single-phase miscible CO₂ flood in the decane-saturated core.

The residual oil saturation after the foam flood was 9%, similar to that of the brine-CO₂ flood. These identical residual oil saturation confirmed that the displacement efficiency of the foam flood was comparable to that of the brine-CO₂ flood baseline. However, the residual oil saturation after the CO₂ flood was significantly lower at only 3%, one-third of the foam flood value. The higher residual oil saturations observed in the foam and CO₂/brine floods were possibly consequences of phase blocking as the injected water might have prevented CO₂ from contacting decane in some locations. Unlike the prior CO₂ flood at residual oil condition where the final residual oil saturation was similar to the foam flood experiment, there was only one phase flowing during the CO₂ flood of this decane-saturated core as the water phase was immobile and the CO₂ and decane were miscible.

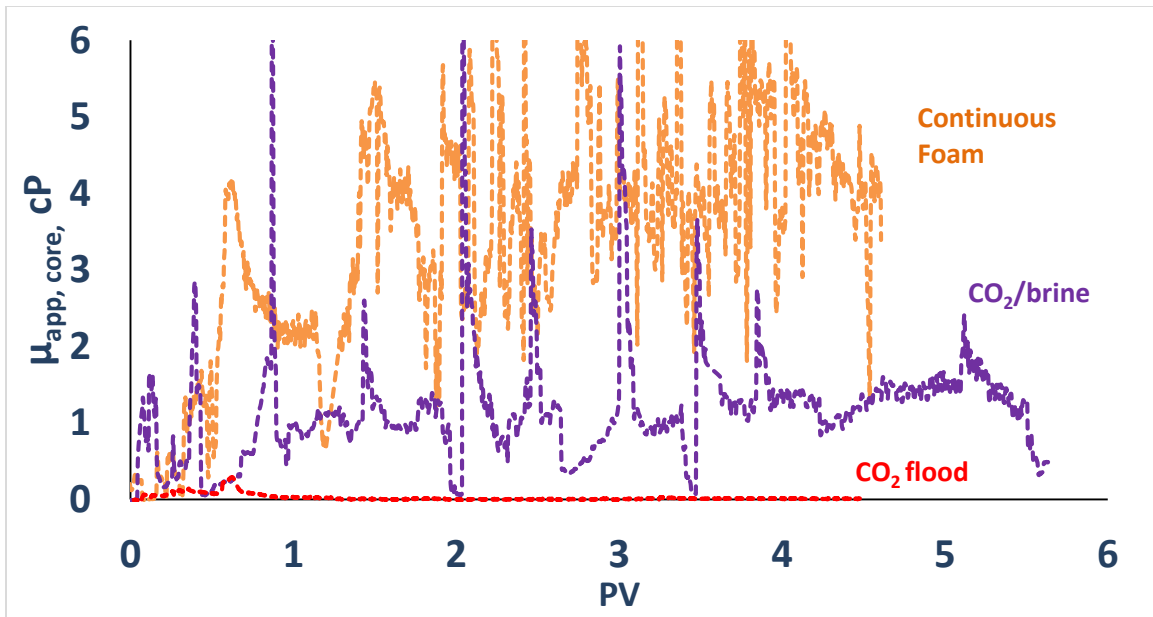


Figure 4-38 Apparent viscosity measured across the core of pre-generated foam experiment in decane-saturated Boise sandstone core. Three types of injection experimented: continuous foam flood, CO₂ flood and CO₂/brine flood. These experiment was performed at 2000 psia, 23 °C and fixed total injection rate of 6 ml/min, giving flow velocity $u = 56$ ft/day. Decane viscosity at this experiment condition was 1.02 cP (data from NIST, 2011).

Table 4-13 Summary of coreflood results in decane-saturated Boise sandstone core (3200 mD). Experiment were conducted at 2000 psia and room temperature (23 °C). Use EOR-5xs nanoparticle (Nissan Chemical) and a constant injection rate at 6 ml/min, giving flow velocity $u = 56$ ft/day.

Injected Fluid	Aq. rate (ml/min)	CO ₂ rate (ml/min)	Particle Conc. (wt%)	Salinity (wt%)	Initial Sor	Final Sor	dP (psi)	$\mu_{app, core}$ (cP)
Liquid CO ₂	-	6	-	4	69%	3.3%	~0	n/a
Brine/CO ₂	1.5	4.5	-	4	74%	9%	12	1.4
Cont. foam	1.5	4.5	1	4	73%	9%	28	4

In summary, these miscible flood experiments, both with residual and mobile oil, proved the ability of nanoparticle-stabilized CO₂ foam in reducing the residual oil saturation with the mobility control advantage. The dynamic coalescence-regeneration nature of foam transport in porous media allowed the CO₂ to contact the residual oil which formed an oil bank ahead of the foam front. The arrival of fine-texture foam after the oil bank in the continuous foam flood demonstrated the stability of foam in the presence of residual oil saturation, although the apparent viscosity was somewhat degraded compared to flows in cores with no oil phase. Despite its slightly lower oil recovery, the injection of 0.3-PV foam slug achieved the same viscosification as the continuous foam injection while using less nanoparticles. However, this series of oil recovery experiments should be repeated at high temperature, close to actual reservoir condition, where CO₂ was in the supercritical state.

Chapter 5 Conclusions and Recommendations

5.1 CONCLUSIONS

- The 5 nm surface-modified silica nanoparticles stabilized CO₂-in-water foam generated by the co-injection of CO₂ and nanoparticle dispersion into sandstone matrix at the pressure above 2000 psi, temperature up to 80 °C, and salinity as high as 7.2 wt% TDS.
- There exists a critical shear rate for foam generation in sandstone matrix. This threshold value is a function of the experiment conditions including temperature, foam quality, salinity, and matrix permeability. Nanoparticle concentration, as well as these parameters, affects foam apparent viscosity.
 - **Temperature:** the interfacial tension between CO₂ and water increases as temperature increases. This results in a larger critical shear rate.
 - **Foam quality:** increasing foam quality results in larger critical shear rate for foam generation. However, there exists an optimum foam quality that yields the highest apparent viscosity for each specific system. This optimum foam quality is sensitive to the matrix permeability but not temperature.
 - **Salinity:** increasing salinity helps drive nanoparticles to the bubble/brine interface, therefore decreases the critical shear rate for foam generation and increases the foam apparent viscosity. However, nanoparticles become unstable and aggregate at high salinity.
 - **Matrix permeability:** porous media with lower permeability tends to have a lower critical shear rate for foam generation. However, the trend in the relationship between matrix permeability and foam apparent viscosity remains unclear.

- **Nanoparticle concentration:** increasing nanoparticle concentration in aqueous phase has no effect on the critical shear rate for foam generation. However, if these particles can be driven to the interface, the larger nanoparticle surface coverage on the bubble provides greater foam apparent viscosity.
- Stable foam was generated in the fractured sandstone cores by means of co-injection of nanoparticle dispersion and CO₂ at 2000 psi and 23 °C. Flow decoupling calculation revealed the existence of critical shear rate for foam generation in the fracture system.
 - Fracture aperture size appeared to affect the critical shear rate for foam generation. However, the trend was not conclusive.
 - Flow diversion from the fracture to matrix was inferred from the flow decoupling calculation for the fractured Boise sandstone experiments once foam was generated.
- Nanoparticle-stabilized CO₂ foam was generated in the Indiana limestone matrix by the co-injection method at 1500 psi and 23 °C. No critical shear rate behavior was observed because viscous foam was generated even at the smallest experimentally accessible flow rates. Generated foam exhibited shear thinning behavior.
- Injection of the pre-generated nanoparticle-stabilized CO₂ foam into a sandstone core suggests that foam travelling through porous media undergoes ‘coalescence-regeneration’ process
 - The apparent viscosity of the foam pre-generated in a high permeability beadpack flowing into the lower permeability sandstone core was similar to

the apparent viscosity observed in the co-injection experiment. This indicated that the change in foam texture was dictated by core and not its initial texture.

- It took almost 2 PV for the pre-generated foam to travel the length of the brine-saturated sandstone core, suggesting a coalescence of foam at the foam front.
- Injection of the pre-generated nanoparticle-stabilized foam significantly reduced the residual oil saturation, with the additional advantage of mobility control.
 - The residual oil after the foam flood was comparable to those of the CO₂/brine baseline and liquid CO₂ flood; all cases were much less than residual oil saturation to water. Oil banks ahead of the foam front were observed.
 - The apparent viscosity of foam was about three times of that of the brine-CO₂ baseline and as high as thirty times of the apparent viscosity during CO₂ flood.
 - The observation supports the hypothesis of ‘coalescence-regeneration’ of nanoparticle-stabilized foam during transport in the porous media. The coalescence of foam allows the inner phase CO₂ to contact residual oil and mobilize an oil bank while the regeneration process maintains foam apparent viscosity behind the foam front.
 - Injection of 0.3 PV pre-generated foam slug with liquid CO₂ trailing achieved similar viscosification as the continuous foam injection, using only one-third of the nanoparticles. However, production of stable foam was not observed.

5.2 FUTURE WORK

5.2.1 Long-range, Low-shear Foam Transport

The work done in this thesis demonstrated the possibility of nanoparticle-stabilized CO₂ foam in the near wellbore region. However, the behavior of foam transport in the low-shear area far away from the wellbore is still needed to be investigated. Long-range foam transport can be experimented by injecting pre-generated foam into an extended length slim-tube (10 ft long or more) packed with glass beads. The slim tube usually was larger cross-sectional area than a beadpack, therefore the flow velocity and shear rate should decrease once the pre-generated foam enter the slim tube. In addition, the tube can be divided into several sections, each with its individual pressure measurement, to determine if foam degrades as it travels further from the generation point.

5.2.2 Synergy Effect between Nanoparticles and Surfactants

This thesis mainly focused on the use of surface-modified silica nanoparticle as a foaming agent in consolidated rock and only lightly touched on the synergy between nanoparticles and surfactants. However, as reported by Worthen et al. (2013b), this technology appeared to be promising as very viscous foam was generated at low shear rate when a small amount of surfactant was mixed with nanoparticles. In theory, the added surfactants reduce the interfacial tension between CO₂ and water, thus ease the adsorption of nanoparticles onto the interface. The adsorbed nanoparticles, in turn, prevent the coalescence of bubbles, resulting in a foam with superior stability than the surfactant-stabilized foam. Further investigation into this matter can be beneficial for future foam EOR process.

5.2.3 Foam Texture Analysis Using Microscope View Cell

As it is believed that the apparent viscosity of foam is strongly governed by its textures, a study of nanoparticle-stabilized foam texture will lead to a better understanding of foam rheology. However, the view cell setting in this study only allowed visual inspection which sometimes was difficult in differentiating the foam texture. An installation of microscope view cell would allow the measurement of bubble size distribution which would not only serve as a systematic means of foam classification but also provide insights for foam transport modeling.

5.2.4 Supercritical CO₂ foam in a Fractured Core

Although this thesis and the work by Hariz (2012) had examined the generation of nanoparticle-stabilized CO₂ foam in the fractured system, none of these work had been done with supercritical CO₂ at elevated temperature. As shown earlier that the critical shear rate for foam generation in the fracture was an order of magnitude higher than that in matrix at the same experiment condition, the generation of supercritical CO₂ foam in fractured can be a challenge as IFT and the critical shear rate for foam generation will increase.

5.2.5 Foam Rheology Measurement

This work attempted to measure the rheology of nanoparticle-stabilized CO₂ foam using branching manifold, yet was not successful. The main challenge in this experiment was the absence of a direct measurement of foam flow rate into the core. Knowing the flow rate through the core would allow a direct measurement of foam apparent viscosity based on a calculation from measured pressure drop.

Appendix

A. COREFLOOD EXPERIMENTS

A1. Boise sandstone coreflood BS1 (3230 mD)

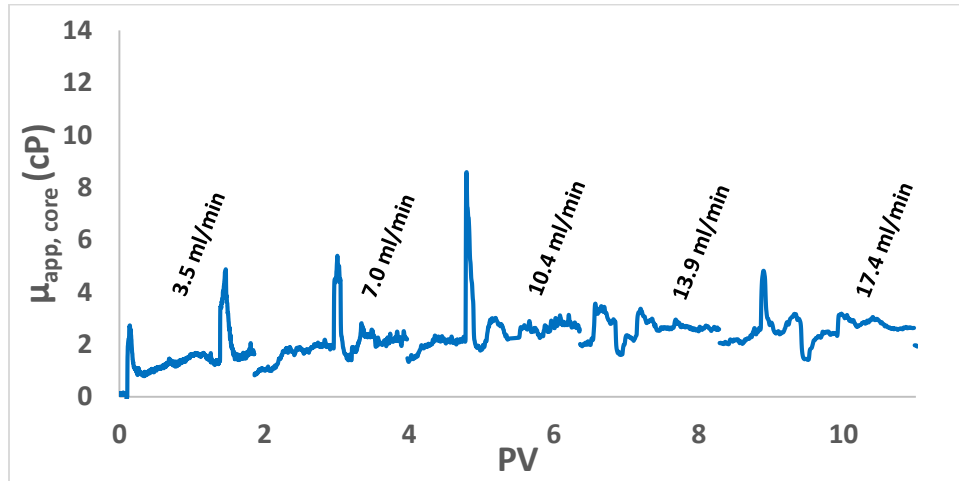


Figure A-1 Baseline apparent viscosity measured across the core BS1 versus pore volume injected. The experiment was carried out using 2 wt% NaCl brine and CO₂ at 2000 psi and 50 °C. Foam quality was fixed at 0.57.

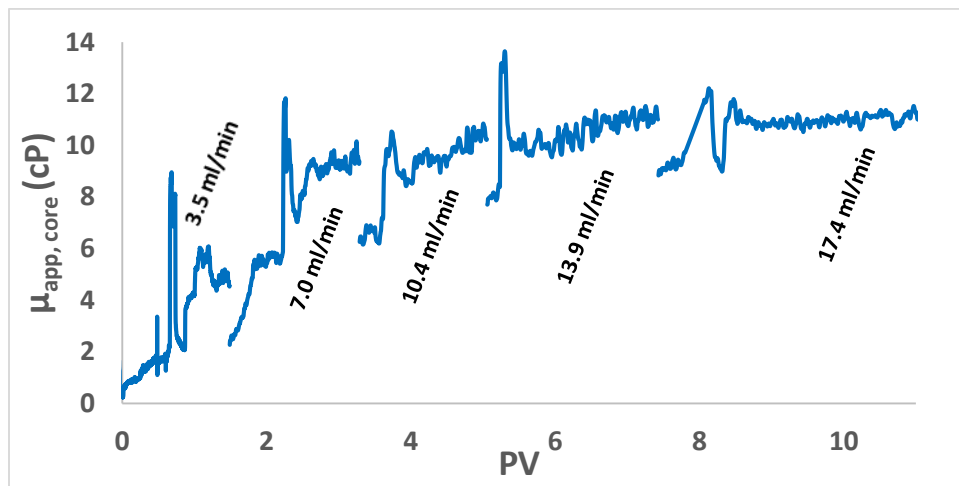


Figure A-2 Foam apparent viscosity measured across the core BS1 versus pore volume injected. The experiment was carried out using 1 wt% EOR-5xs nanoparticle dispersion in 2 wt% NaCl brine and CO₂ at 2000 psi and 50 °C. Foam quality was fixed at 0.57.

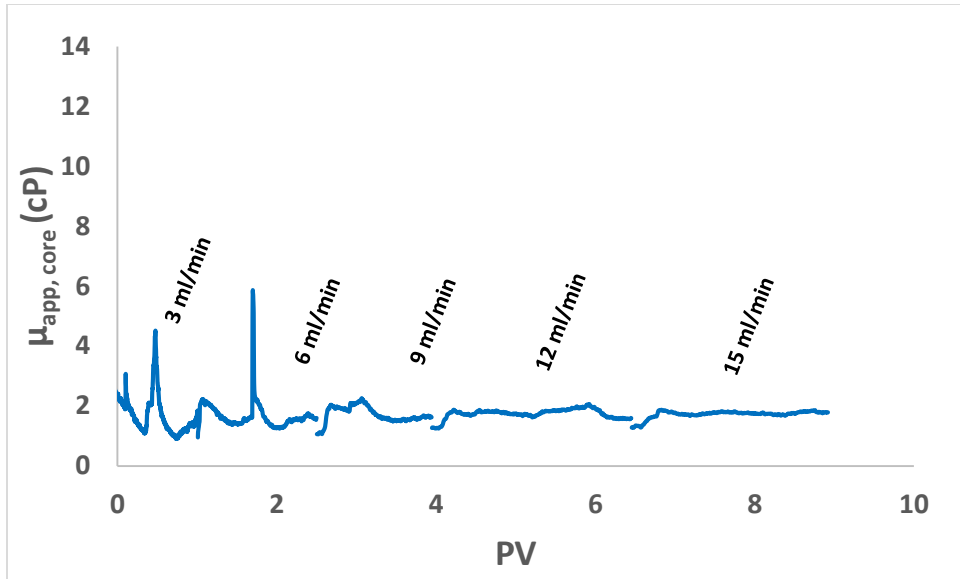


Figure A-3 Baseline apparent viscosity measured across the core BS1 versus pore volume injected. The experiment was carried out using 2 wt% NaCl brine and CO₂ at 2000 psi and 50 °C. Foam quality was fixed at 0.75.

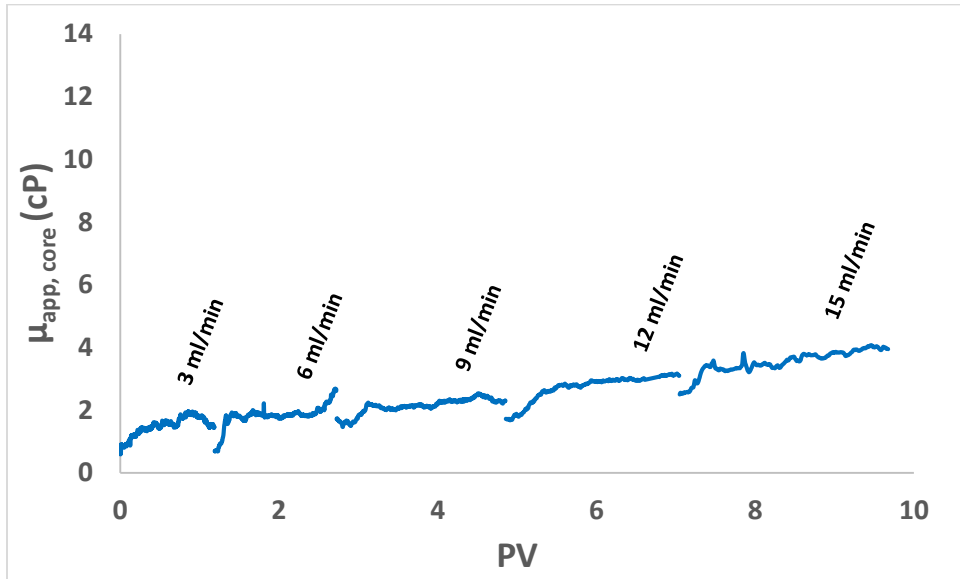


Figure A-4 Foam apparent viscosity measured across the core BS1 versus pore volume injected. The experiment was carried out using 1 wt% EOR-5xs nanoparticle dispersion in 2 wt% NaCl brine and CO₂ at 2000 psi and 50 °C. Foam quality was fixed at 0.75.

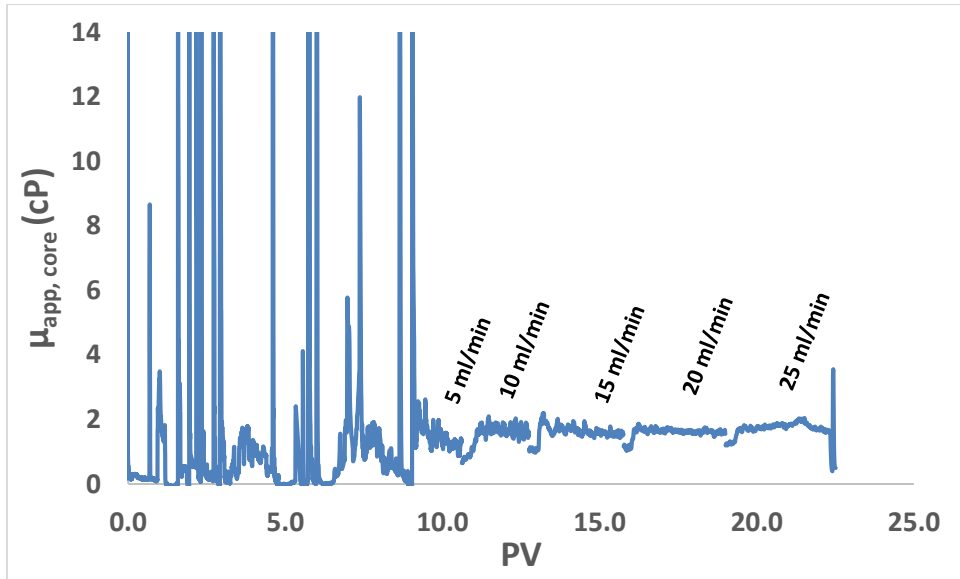


Figure A-5 Baseline apparent viscosity measured across the core BS1 versus pore volume injected. The experiment was carried out using 2 wt% NaCl brine and CO₂ at 2000 psi and 80 °C. Foam quality was fixed at 0.75.

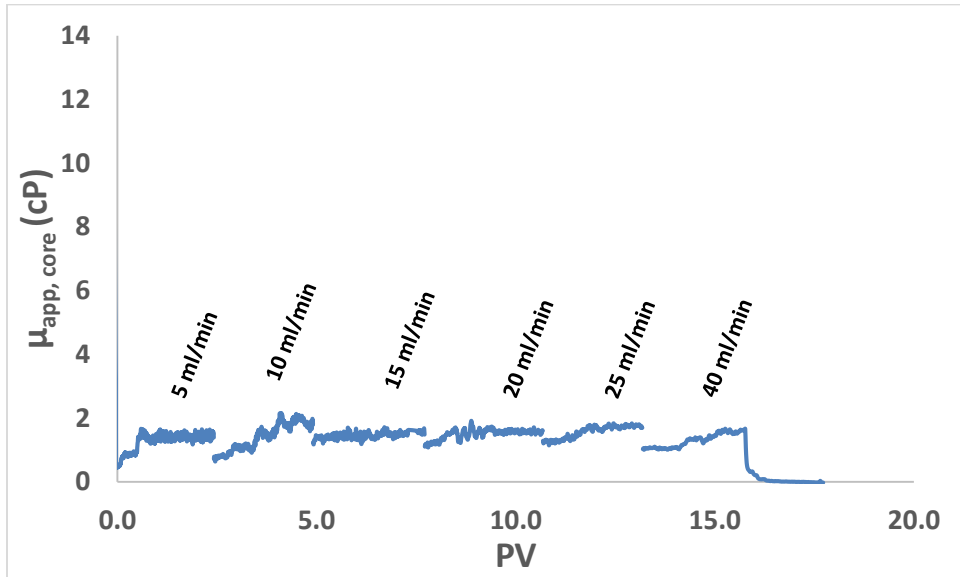


Figure A-6 Foam apparent viscosity measured across the core BS1 versus pore volume injected. The experiment was carried out using 1 wt% EOR-5xs nanoparticle dispersion in 2 wt% NaCl brine and CO₂ at 2000 psi and 80 °C. Foam quality was fixed at 0.75.

Boise sandstone coreflood BS2 (2250 mD)

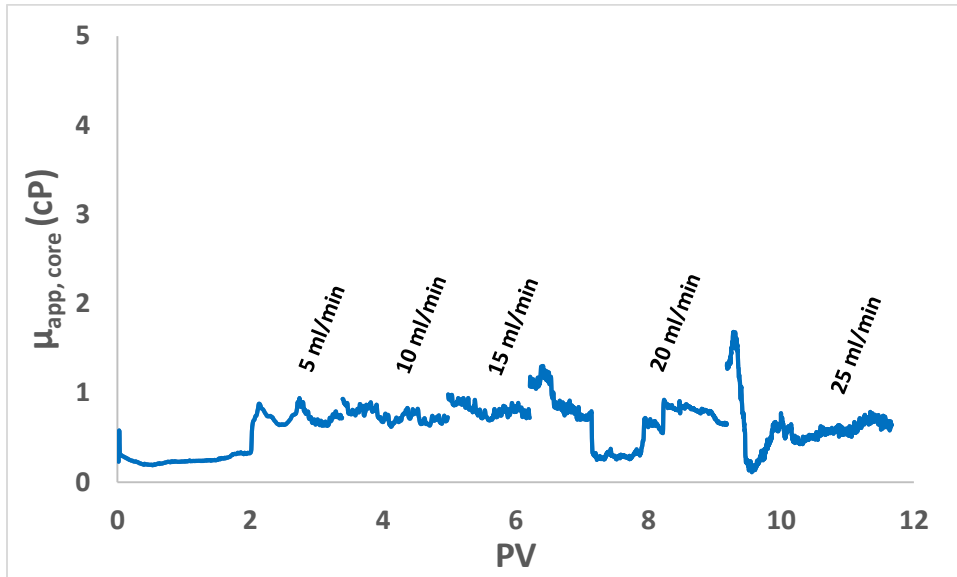


Figure A-7 Baseline apparent viscosity measured across the core BS2 versus pore volume injected. The experiment was carried out using 2 wt% NaCl brine and CO₂ at 2200 psi and 80 °C. Foam quality was fixed at 0.5.

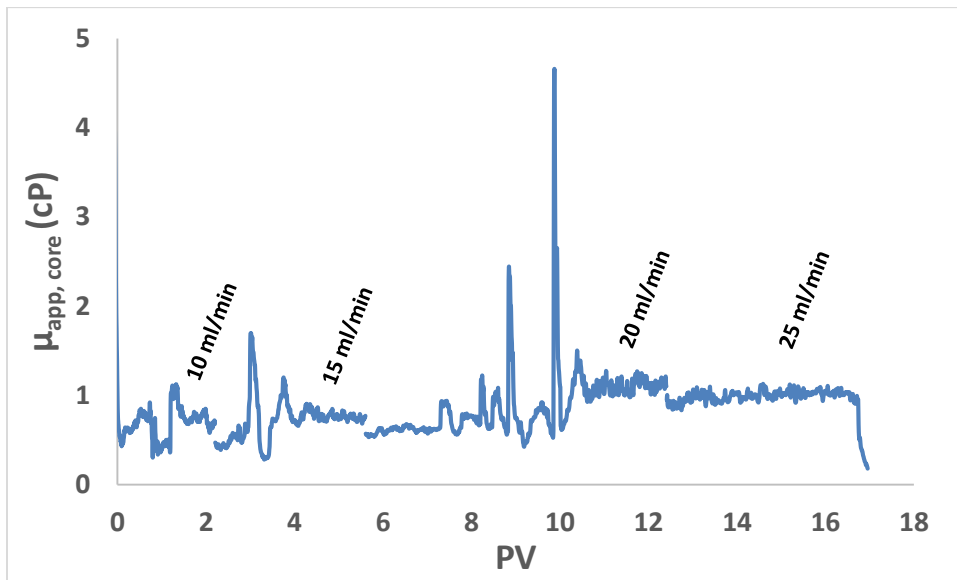


Figure A-8 Foam apparent viscosity measured across the core BS2 versus pore volume injected. The experiment was carried out using 1 wt% EOR-5xs nanoparticle dispersion in 2 wt% NaCl brine and CO₂ at 2200 psi and 80 °C. Foam quality was fixed at 0.5.

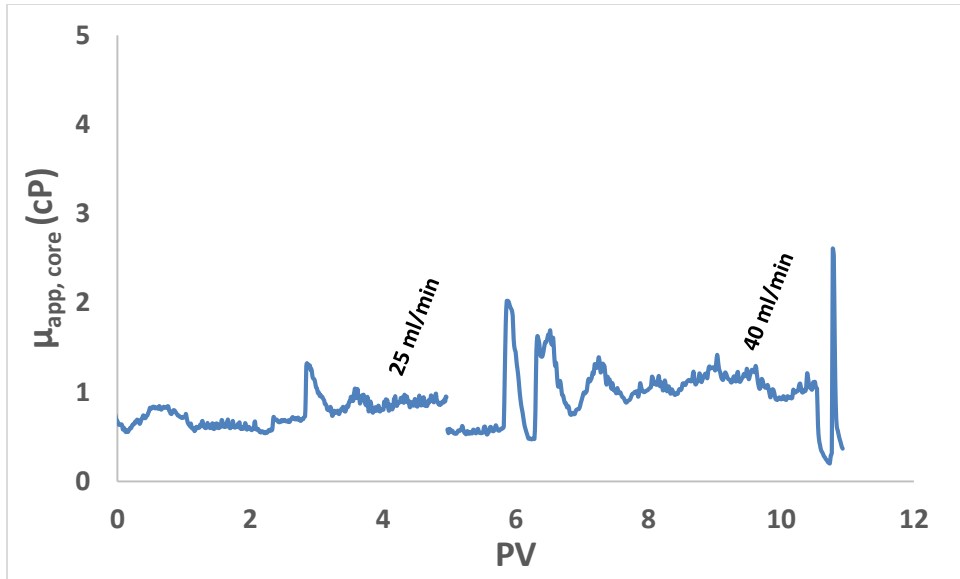


Figure A-9 Foam apparent viscosity measured across the core BS2 versus pore volume injected. The experiment was carried out using 5 wt% EOR-5xs nanoparticle dispersion in 2 wt% NaCl brine and CO₂ at 2200 psi and 80 °C. Foam quality was fixed at 0.5.

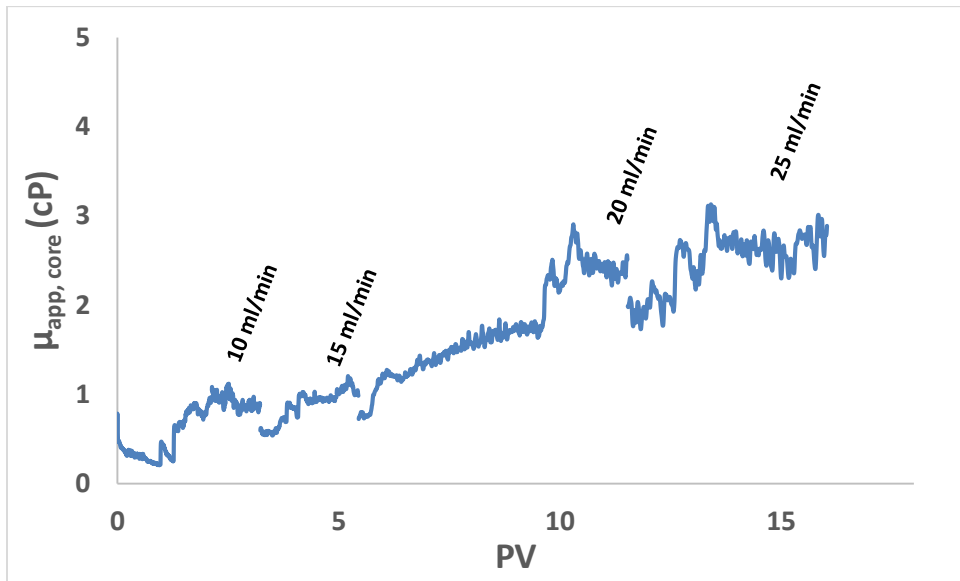


Figure A-10 Foam apparent viscosity measured across the core BS2 versus pore volume injected. The experiment was carried out using 1 wt% EOR-5xs nanoparticle dispersion in 4 wt% NaCl brine and CO₂ at 2200 psi and 80 °C. Foam quality was fixed at 0.5.

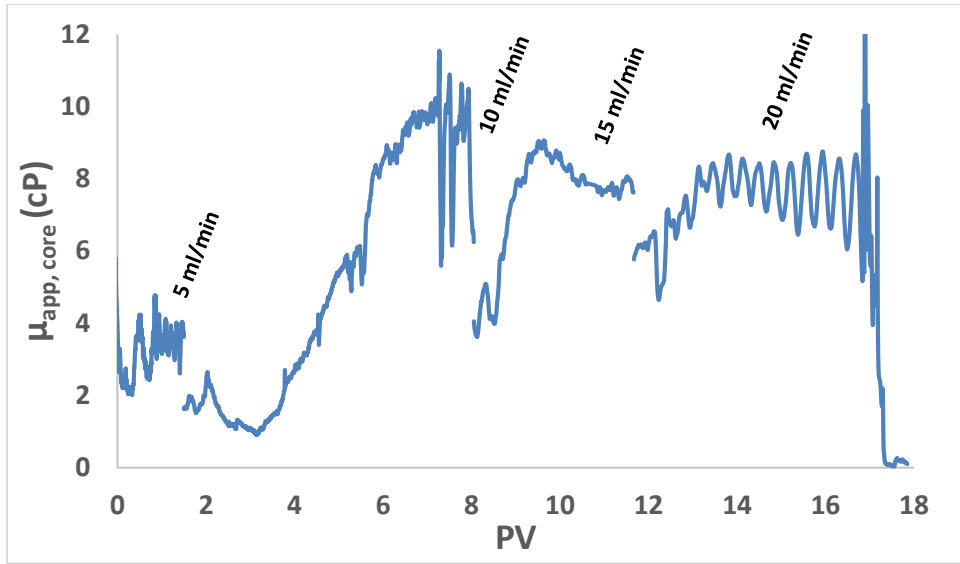


Figure A-11 Foam apparent viscosity measured across the core BS2 versus pore volume injected. The experiment was carried out using 1 wt% EOR-5xs nanoparticle dispersion + 0.04% LAPB surfactant in 4 wt% NaCl brine and CO₂ at 2200 psi and 80 °C. Foam quality was fixed at 0.5.

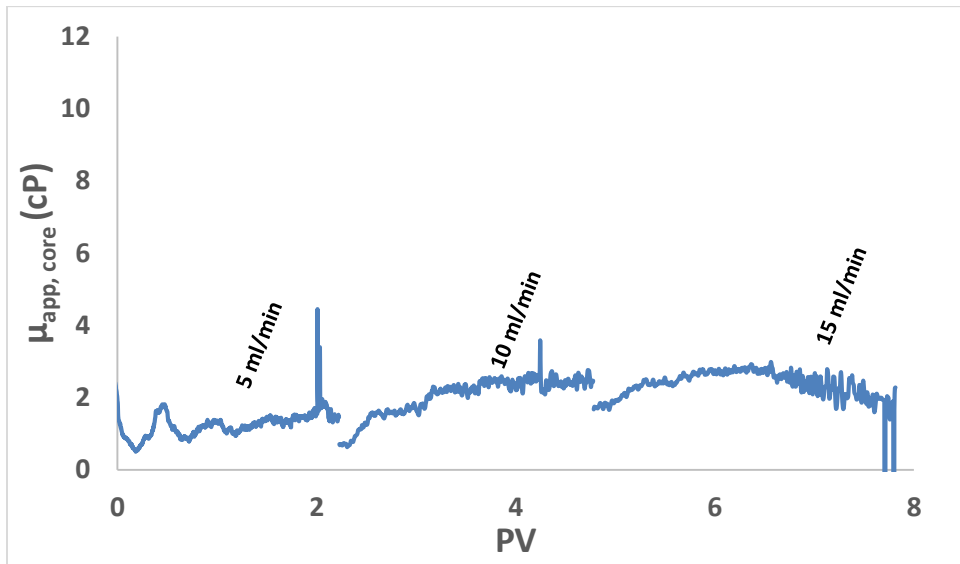


Figure A-12 Foam apparent viscosity measured across the core BS2 versus pore volume injected. The experiment was carried out using 0.04% LAPB surfactant solution in 4 wt% NaCl brine and CO₂ at 2200 psi and 80 °C. Foam quality was fixed at 0.5. Experiment was ceased after 8 PV due to the plugging of view cell inlet line.

Boise sandstone coreflood BS3 (3000 mD)

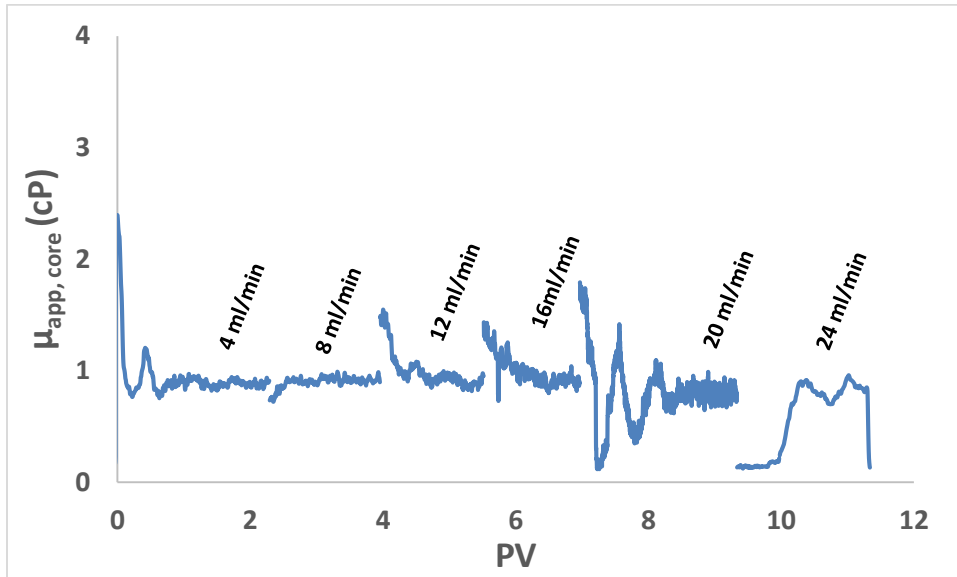


Figure A-13 Baseline apparent viscosity measured across the core BS3 versus pore volume injected. The experiment was carried out using 2 wt% NaCl brine and CO₂ at 2200 psi and 80 °C. Foam quality was fixed at 0.5.

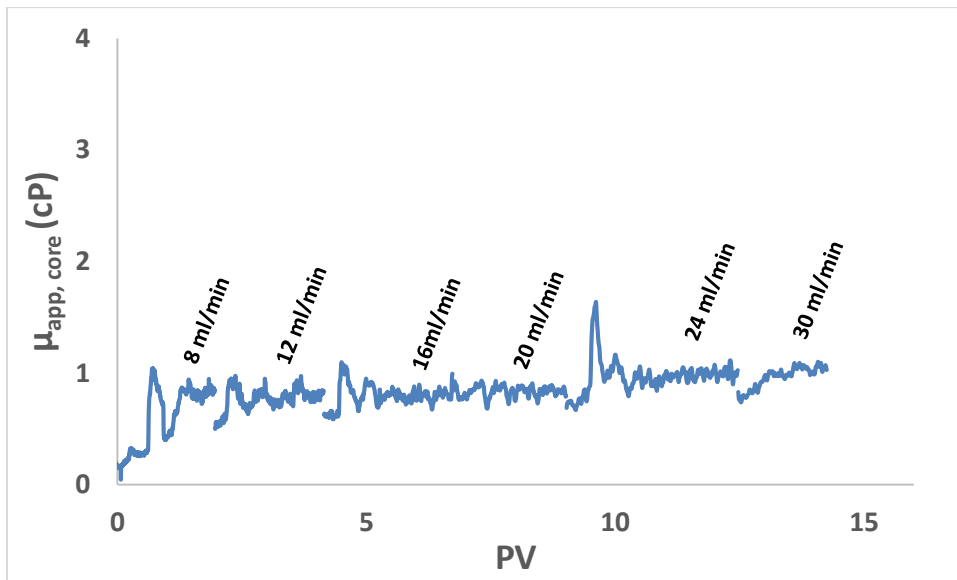


Figure A-14 Foam apparent viscosity measured across the core BS2 versus pore volume injected. The experiment was carried out using 1 wt% EOR-5xs nanoparticle dispersion in 2 wt% NaCl brine and CO₂ at 2200 psi and 80 °C. Foam quality was fixed at 0.5.

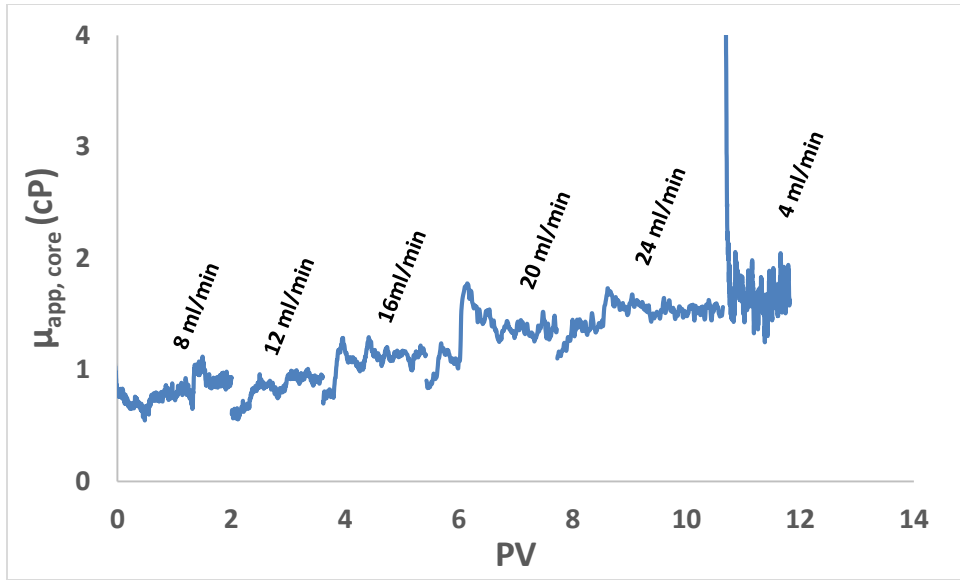


Figure A-15 Foam apparent viscosity measured across the core BS2 versus pore volume injected. The experiment was carried out using 1 wt% EOR-5xs nanoparticle dispersion in 3 wt% NaCl brine and CO₂ at 2200 psi and 80 °C. Foam quality was fixed at 0.5.

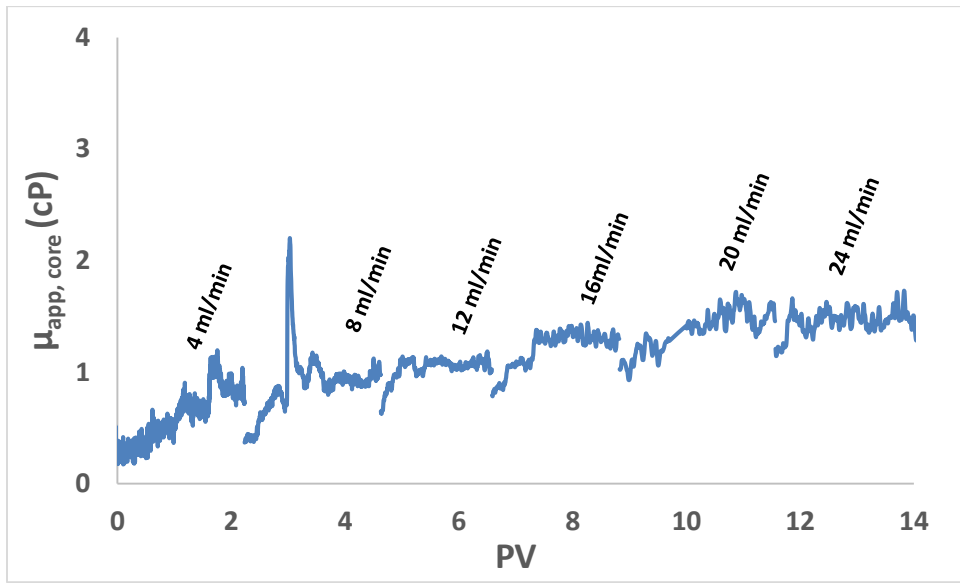


Figure A-16 Foam apparent viscosity measured across the core BS2 versus pore volume injected. The experiment was carried out using 1 wt% EOR-5xs nanoparticle dispersion in 4 wt% NaCl brine and CO₂ at 2200 psi and 80 °C. Foam quality was fixed at 0.5.

Boise sandstone coreflood BS4 (3360 mD)

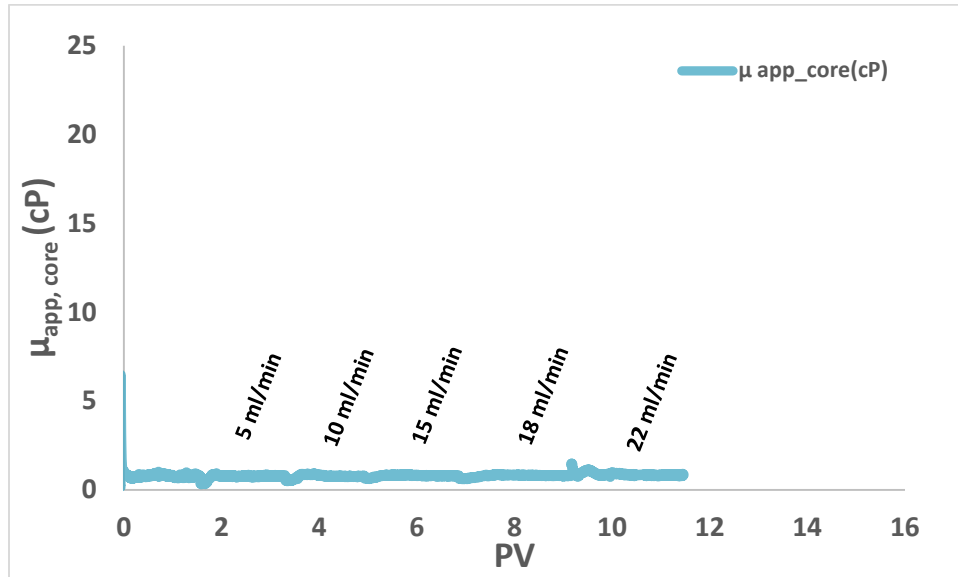


Figure A-17 Baseline apparent viscosity measured across the core BS4 versus pore volume injected. The experiment was carried out using 7.2 wt% TDS brine and CO₂ at 2200 psi and 57 °C. Foam quality was fixed at 0.75.

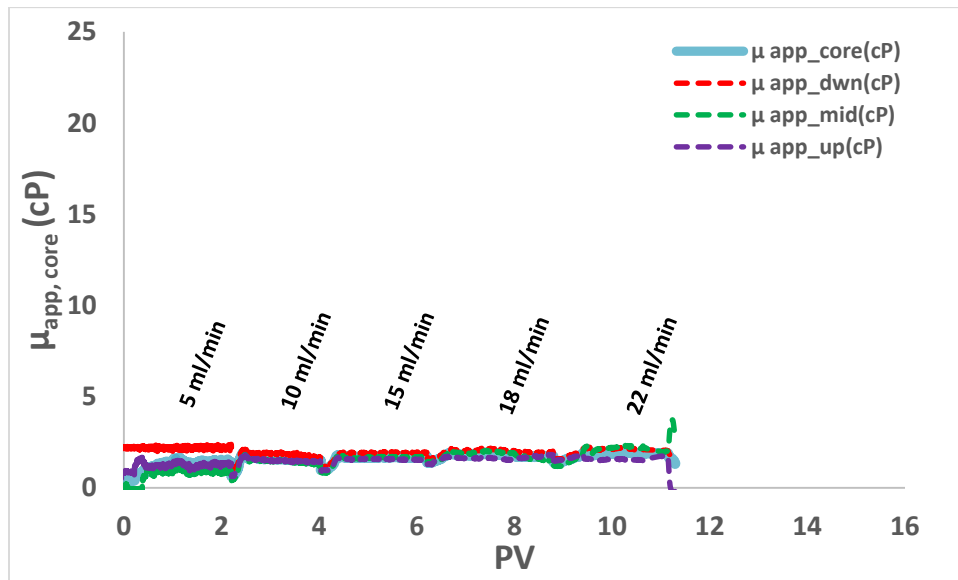


Figure A-18 Foam apparent viscosity measured across the core BS4 versus pore volume injected. The experiment was carried out using 0.1 wt% EOR-5xs nanoparticle dispersion in 7.2 wt% TDS brine and CO₂ at 2200 psi and 57 °C. Foam quality was fixed at 0.75.

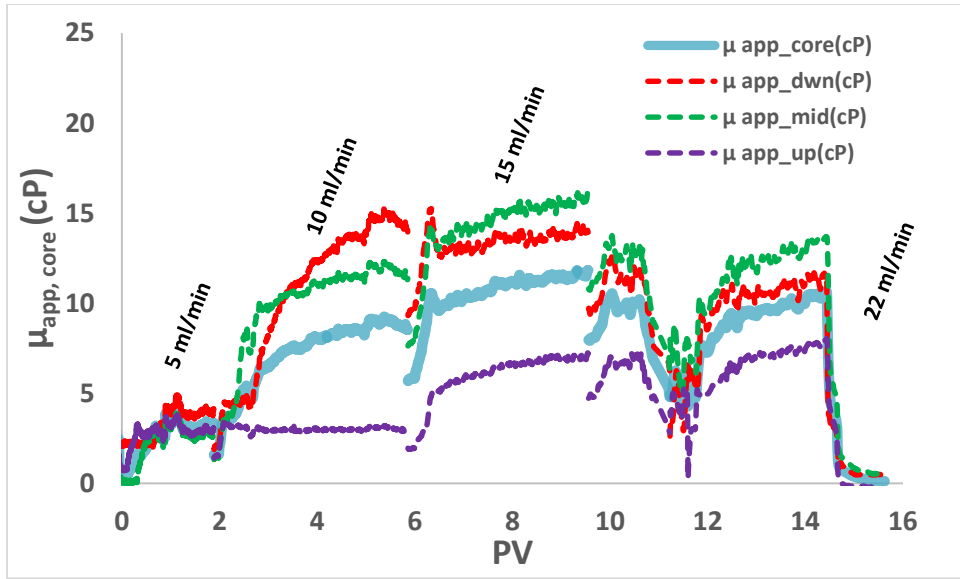


Figure A-19 Foam apparent viscosity measured across the core BS4 versus pore volume injected. The experiment was carried out using 0.5 wt% EOR-5xs nanoparticle dispersion in 7.2 wt% TDS brine and CO₂ at 2200 psi and 57 °C. Foam quality was fixed at 0.75.

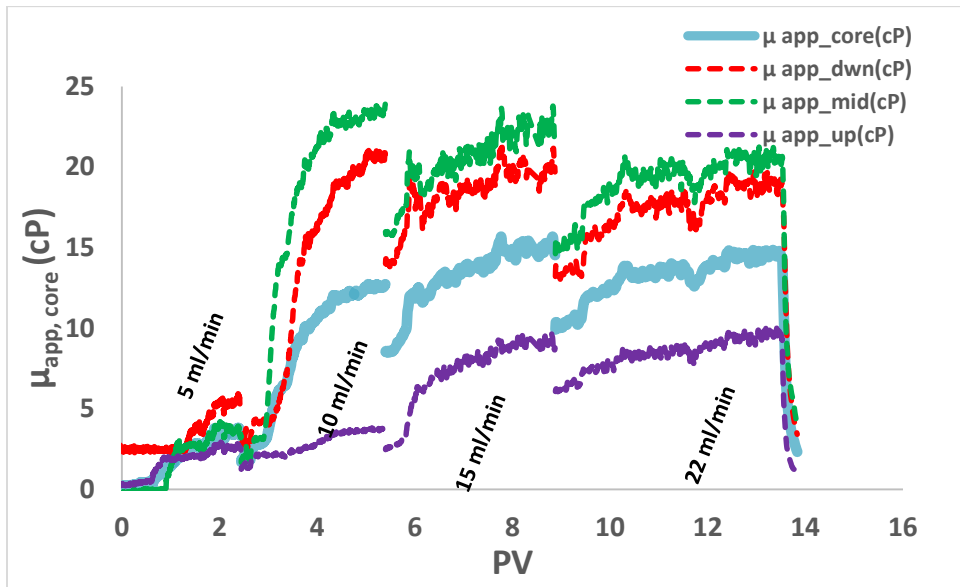


Figure A-20 Foam apparent viscosity measured across the core BS4 versus pore volume injected. The experiment was carried out using 1 wt% EOR-5xs nanoparticle dispersion in 7.2 wt% TDS brine and CO₂ at 2200 psi and 57 °C. Foam quality was fixed at 0.75.

Berea sandstone coreflood BRS1 (220 mD)

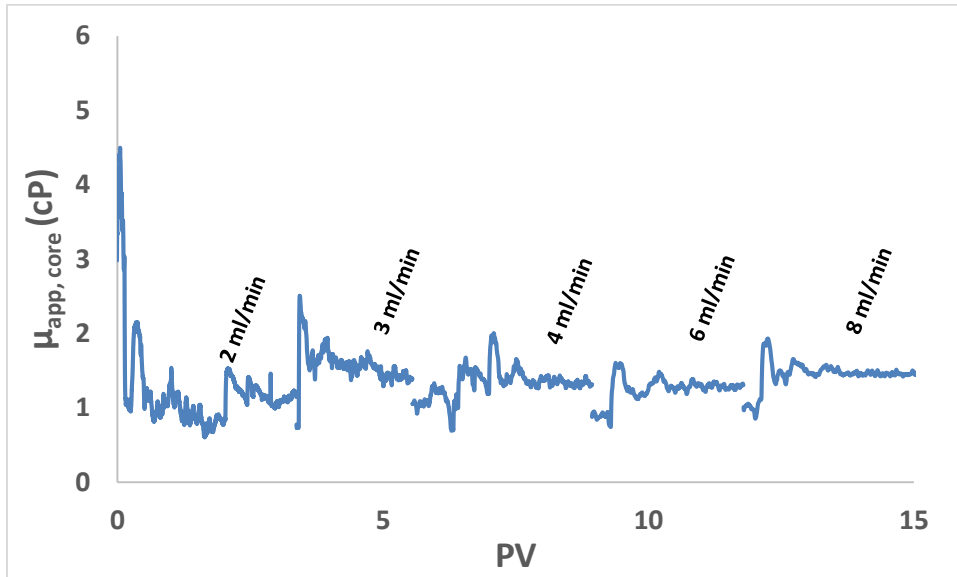


Figure A-21 Baseline apparent viscosity measured across the core BRS1 versus pore volume injected. The experiment was carried out using 4 wt% NaCl brine and CO₂ at 2200 psi and 80 °C. Foam quality was fixed at 0.5.

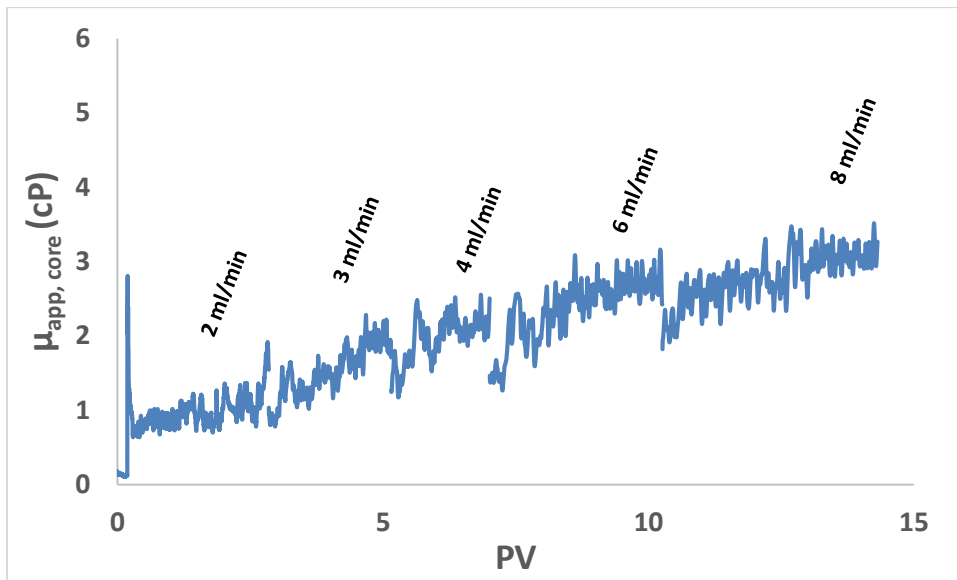


Figure A-22 Foam apparent viscosity measured across the core BRS1 versus pore volume injected. The experiment was carried out using 1 wt% EOR-5xs nanoparticle dispersion in 4 wt% NaCl brine and CO₂ at 2200 psi and 80 °C. Foam quality was fixed at 0.5.

Berea sandstone coreflood BRS2 (170 mD)

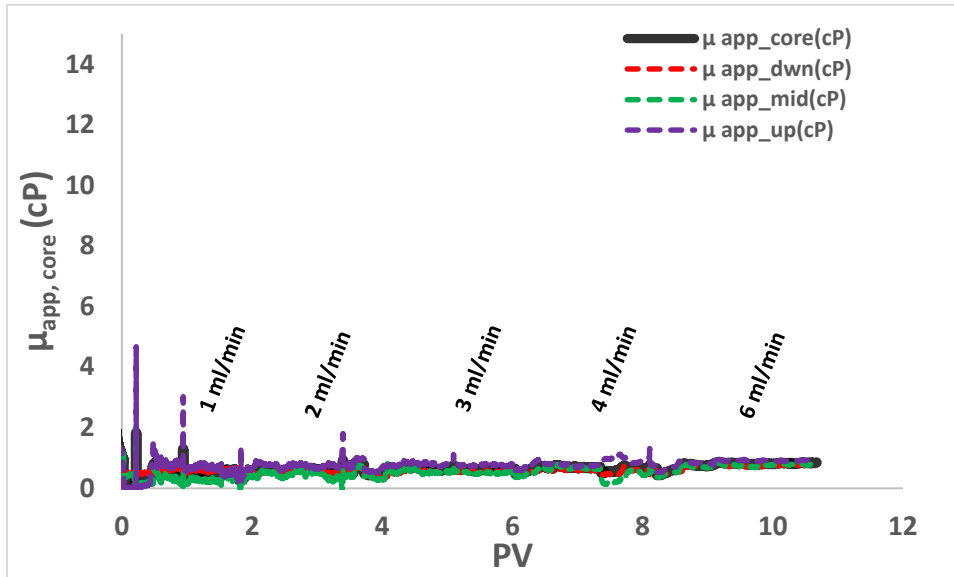


Figure A-23 Baseline apparent viscosity measured across the core BRS2 versus pore volume injected. The experiment was carried out using 7.2 wt% TDS brine and CO₂ at 2200 psi and 57 °C. Foam quality was fixed at 0.75.

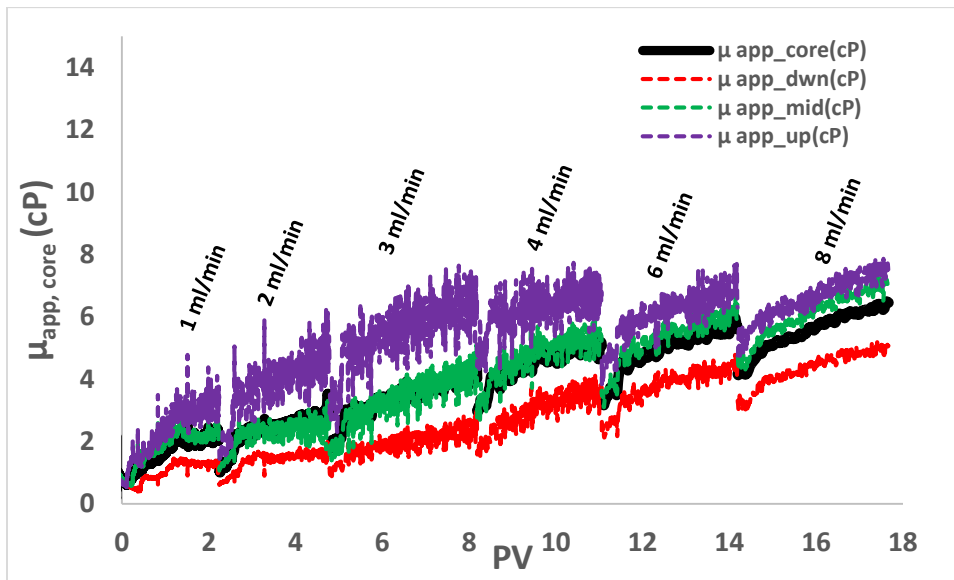


Figure A-24 Foam apparent viscosity measured across the core BRS2 versus pore volume injected. The experiment was carried out using 0.5 wt% EOR-5xs nanoparticle dispersion in 7.2 wt% TDS brine and CO₂ at 2200 psi and 57 °C. Foam quality was fixed at 0.75.

References

- Aroonsri, A., Worthen, A. J., Hariz, T., Johnston, K. P., Huh, C., and Bryant, S. L., 2013, Conditions for Generating Nanoparticle-Stabilized CO₂ Foams in Fracture and Matrix Flow, Society of Petroleum Engineers.
- Bachu, S., and Bennion, D. B., 2008, Interfacial Tension between CO₂, Freshwater, and Brine in the Range of Pressure from (2 to 27) MPa, Temperature from (20 to 125) °C, and Water Salinity from (0 to 334 000) mg·L⁻¹: *Journal of Chemical & Engineering Data*, v. 54, no. 3, p. 765-775.
- Bennion, B., and Bachu, S., Relative permeability characteristics for supercritical CO₂ displacing water in a variety of potential sequestration zones, *in* Proceedings SPE Annual Technical Conference and Exhibition 2005, Society of Petroleum Engineers.
- Binks, B. P., 2002, Particles as surfactants—similarities and differences: *Current Opinion in Colloid & Interface Science*, v. 7, no. 1, p. 21-41.
- Binks, B. P., Duncumb, B., and Murakami, R., 2007, Effect of pH and Salt Concentration on the Phase Inversion of Particle-Stabilized Foams: *Langmuir*, v. 23, no. 18, p. 9143-9146.
- Binks, B. P., Philip, J., and Rodrigues, J. A., 2005, Inversion of silica-stabilized emulsions induced by particle concentration: *Langmuir*, v. 21, no. 8, p. 3296-3302.
- Dickson, J. L., Binks, B. P., and Johnston, K. P., 2004, Stabilization of Carbon Dioxide-in-Water Emulsions with Silica Nanoparticles: *Langmuir*, v. 20, no. 19, p. 7976-7983.
- Enick, R. M., and Olsen, D., 2012, Mobility and Conformance Control for CO₂ EOR via Thickeners, Foams, and Gels—A Detailed Literature Review of 40 Years of Research.: National Energy Technology Laboratory, Department of Energy., DOE/NETL-2012/1540.
- Enick, R. M., Olsen, D. K., Ammer, J. R., and Schuller, W., 2012, Mobility and Conformance Control for CO₂ EOR via Thickeners, Foams, and Gels -- A Literature Review of 40 Years of Research and Pilot Tests, Society of Petroleum Engineers.
- Espinosa, D. A., Caldelas, F. M., Johnston, K. P., Bryant, S. L., and Huh, C., 2010, Nanoparticle-Stabilized Supercritical CO₂ Foams for Potential Mobility Control Applications, Society of Petroleum Engineers.
- Ettinger, R., and Radke, C., 1992, Influence of texture on steady foam flow in Berea sandstone: *SPE reservoir engineering*, v. 7, no. 1, p. 83-90.
- Falls, A., Hirasaki, G., Patzek, T. e. a., Gauglitz, D., Miller, D., and Ratulowski, T., 1988, Development of a mechanistic foam simulator: the population balance and generation by snap-off: *SPE reservoir engineering*, v. 3, no. 03, p. 884-892.

- Fridleifsson, I. B., Bertani, R., Huenges, E., Lund, J. W., Ragnarsson, A., and Rybach, L., The possible role and contribution of geothermal energy to the mitigation of climate change, *in* Proceedings IPCC scoping meeting on renewable energy sources, proceedings, Luebeck, Germany 2008, Volume 20, Citeseer, p. 59-80.
- Friedmann, F., Chen, W. H., and Gauglitz, P. A., 1991, Experimental and Simulation Study of High-Temperature Foam Displacement in Porous Media.
- Friedmann, F., and Jensen, J. A., 1986, Some Parameters Influencing the Formation and Propagation of Foams in Porous Media, Society of Petroleum Engineers.
- Habermann, B., 1960, The efficiency of miscible displacement as a function of mobility ratio.
- Hariz, T. R., 2012, Nanoparticle-stabilized CO₂ foams for potential mobility control applications [MS Master Thesis]: The University of Texas at Austin.
- Hirasaki, G., and Lawson, J., 1985, Mechanisms of foam flow in porous media: apparent viscosity in smooth capillaries: Society of Petroleum Engineers Journal, v. 25, no. 2, p. 176-190.
- Israelachvili, J. N., 1992, Intermolecular and Surface Forces: With Applications to Colloidal and Biological Systems (Colloid Science), Academic press London.
- Johnston, K. P., and da Rocha, S. R., 2009, Colloids in supercritical fluids over the last 20 years and future directions: The Journal of Supercritical Fluids, v. 47, no. 3, p. 523-530.
- Kovscek, A. R., and Radke, C. J., 1994, Fundamentals of Foam Transport in Porous Media, Foams: Fundamentals and Applications in the Petroleum Industry, Volume 242, American Chemical Society, p. 115-163.
- Kralchevsky, P. A., and Denkov, N. D., 1995, Analytical expression for the oscillatory structural surface force: Chemical Physics Letters, v. 240, no. 4, p. 385-392.
- Lake, L. W., 1989, Enhanced oil recovery, Englewood Cliffs, N.J., Prentice Hall, v. xxv, 550 p., xxv, 550 p. p.:
- Lee, S., and Kam, S. I., 2013, Chapter 2 - Enhanced Oil Recovery by Using CO₂ Foams: Fundamentals and Field Applications, *in* Sheng, J. J., ed., Enhanced Oil Recovery Field Case Studies: Boston, Gulf Professional Publishing, p. 23-61.
- Li, R. F., Yan, W., Liu, S., Hirasaki, G. J., and Miller, C. A., 2010, Foam mobility control for surfactant enhanced oil recovery: SPE J, v. 15, no. 4, p. 934-948.
- Mo, D., Yu, J., Liu, N., and Lee, R. L., 2012, Study of the Effect of Different Factors on Nanoparticle-Stablized CO₂ Foam for Mobility Control, Society of Petroleum Engineers.
- National Institute of Standards and Technology (NIST), 2011, Thermophysical Properties of Fluid Systems, <http://webbook.nist.gov/chemistry/fluid/>.
- Pickering, S. U., 1907, Cxcvi.—emulsions: Journal of the Chemical Society, Transactions, v. 91, p. 2001-2021.
- Rossen, W. R., 1990, Theory of mobilization pressure gradient of flowing foams in porous media: I. Incompressible foam: Journal of Colloid and Interface Science, v. 136, no. 1, p. 1-16.

- Rossen, W. R., 1995, Foam in Enhance Oil Recovery, *in* Prud'homme, R. K., ed., *Foams: Theory: Measurements: Applications*, Volume 57, CRC Press, p. 413 - 464.
- Rossen, W. R., and Renkema, W. J., 2007, Success of Foam SAG Processes in Heterogeneous Reservoirs, Society of Petroleum Engineers.
- Son, Y., 2007, Determination of shear viscosity and shear rate from pressure drop and flow rate relationship in a rectangular channel: *Polymer*, v. 48, no. 2, p. 632-637.
- Tambe, D. E., and Sharma, M. M., 1994, The effect of colloidal particles on fluid-fluid interfacial properties and emulsion stability: *Advances in colloid and interface science*, v. 52, p. 1-63.
- Worthen, A., Bagaria, H., Chen, Y., Bryant, S. L., Huh, C., and Johnston, K. P., 2012, Nanoparticle Stabilized Carbon Dioxide in Water Foams for Enhanced Oil Recovery, Society of Petroleum Engineers.
- Worthen, A. J., Bagaria, H. G., Chen, Y., Bryant, S. L., Huh, C., and Johnston, K. P., 2013a, Nanoparticle-stabilized carbon dioxide-in-water foams with fine texture: *J Colloid Interface Sci*, v. 391, p. 142-151.
- Worthen, A. J., Bryant, S. L., Huh, C., and Johnston, K. P., 2013b, Carbon dioxide-in-water foams stabilized with nanoparticles and surfactant acting in synergy: *AIChE Journal*, v. 59, no. 9, p. 3490-3501.
- Zhang, T., Davidson, D., Bryant, S. L., and Huh, C., 2010, Nanoparticle-Stabilized Emulsions for Applications in Enhanced Oil Recovery, Society of Petroleum Engineers.